HYPERFINE INTERACTION STUDIES USING PERTURBED ANGULAR CORRELATION AND MOSSBAUER EFFECT TECHNIQUES

A Thesis Submitted
in partial Fulfilment of the Requirements
for the Degree of

DOCTOR OF PHILOSOPHY

By

ASHOK KUMAR SINGHVI

to the

DEPARTMENT OF PHYSICS

INDIAN INSTITUTE OF TECHNOLOGY KANPUR

OCTOBER 1975

CERTIFICATE

This is to certify that the work presented in this thesis entitled "Hyperfine Interaction Studies Using Perturbed Angular Correlation and Mossbauer Effect Techniques" by Ashok Kumar Singhvi has been done under my supervision and it has not been submitted elsewhere for a degree.

G. N. Rao
Department of Physics
Indian Institute of Technology
Kanpur, India

October 9, 1975.

ACKNOWLEDGEMENTS

I, first of all, wish to express my deep sense of gratitude to all my teachers, at school, at college and here at IIT, who have indeed contributed generously and selflessly to this thesis.

I am highly indebted to Professor G. N. Rao for his continuing guidance and encouragement. I am much grateful to him for inspiring me to work on a broad spectrum of problems, ranging from the machine work to Mossbauer effect and PAC, which indeed has helped me immensely. I am also very thankful to him for giving me a rather free hand, which coupled to his patience with my mistakes, careful guidance and affectionate disposition, made my work a pleasant and a rewarding experience.

I wish to express my very sincere and grateful thanks to Professors K. Sri Ram and R. M. Singru for this kind encouragement and help throughout. My thanks are also due to Professors G. K. Mehta, Y. R. Waghmare and S. Mukherjee for their kind interest in my work. I thank Professors R. K. Ray, D. C. Khan and T. M. Srinivasan for their help and interest in the work. My sincere thanks are also due to Professor K.V.G.K. Gokhale for his collaboration in Mossbauer work.

Any experimental work is impossible without a proper technical assistance. It is indeed a great pleasure to

recognize the technical expertise of B. K. Jain, A. R. Korde, G. P. Mishra and K. M. L. Jha. I am indeed very thankful to them for their help. My very special thanks are due to B. K. Jain for his readiness to help me at all times and it indeed was a great pleasure to have his company throughout. My thanks are also due to the technical trio of Van de Graaff - K. Masood, M. M. Gupta and A. K. Khanna. I should also thank Shiv Prakash and Ramnath for their very efficient tea club.

My sincere thanks are due to Mr. Piar Singh of Glass Blowing Section for his everreadiness for doing my work with utmost efficiency. I also thank Mr. K. P. Mukherjee of Physical Metallurgy for his help in sample preparation. In this connection, I would also like to thank S. Kirtane and Professor M. N. Shetty for their kind help.

Working the Nuclear Laboratories was indeed a memorable and a rewarding experience. I wish to express my heartfelt thanks to Drs. D. K. Gupta, B. V. N. Rao, C. Rangacharyulu and D. N. Sanwal for their help in the initial phases of my work. My sincere thanks are due to Vijay Jadhao and T. Raman for many stimulating and useful discussions. My 'nearest neighbour interaction' with Dilip Kanhere, B. Krishnarajulu, B. M. Bahal, H. R. Prabhakara, K. R. Krishna Gandhi, Ali Akbar Bagwan and with Drs. Brajesh Srivastava, V. R. Prakash and Raghuvir Singh was indeed a very pleasant one. I shall certainly cherish my association with all of them and I am much thankful to them for their affectionate disposition.

My 'effective interaction' with Dr. Mahesh Prakash was indeed a nice experience, and I am thankful to him for his company. I take this opportunity to thank Drs. K. B. Lal, S. N. Chaturvedi and R. Prasad for their spirit of cooperation. My thanks are due to my hostel associates - Santosh, Ranjeet and Arvind - for their company during my stay.

I am extremely grateful to Professor G. Mehta for his kind help and for his sincere and thoughtful advice at all times. His affectionate behaviour was indeed a great asset. My very sincere thanks are due to Mrs. Ranjana Mehta for her kind and affectionate hospitality, which indeed made my stay at IIT as pleasant as it has been. I also thank Mr. & Mrs. M. M. Bhandari and Shri B. R. Kumbhat for their very affectionate and kind hospitality.

I gratefully thank my parents for their forebearance, sacrifice and their encouragement throughout my educational career. I earnestly wish to dedicate this small piece of my effort to them as a symbol of my gratitude and love for them. I am grateful to my sisters for their patience and encouragement throughout. I also wish to gratefully recall a 'great' who has indeed sacrificed a great deal for me.

Finally, I wish to thank Nihal Ahmad for patiently and tirelessly typing the thesis neatly and for his help in

correcting many technical mistakes. My thanks are also due to Shri B. B. Srivastava for neat tracings and to Shri Lallan Singh Rathaur for cyclostyling.

I hope and wish this thesis will symbolize my gratitude to all those who have given me their love and affection.

A K Singhvi

a. k. singhvi

CONTENTS

CHAPTER Page

LIST OF FIGURES

chapter I

HYPERFINE INTERACTIONS

A. INTRODUCTION

Hyperfine interactions in general deal with the interaction of the nucleus with the charge and current distribution of the surrounding electrons and ions. The electric charge and current distributions inside the nucleus can be expressed by means of a multipole expansion of electric and magnetic multipole moments. The interaction can be expressed as

1. The electric monopole term which is the interaction of nuclear charge distribution with the surrounding electrons giving rise to the isomer shift.
2. The interaction of the magnetic dipole moment with the effective magnetic hyperfine field at the site of the nucleus.

3. The electric quadrupole tensor interacting with the electric field gradients.

The isomer shift results because of the overlap of the nuclear charge distribution and the electron density at the nucleus. If one makes a reasonable theoretical estimate of one of the quantities the other can be obtained. The relative changes in the nuclear charge distribution for different excited states of the same nucleus can be measured rather accurately. More often one measures the changes in the electron densities at the nucleus for different chemical compounds.

The magnetic dipole moment measurements of the nuclear states are possible using external magnetic fields. If we know the magnetic dipole moment of the nuclear state, one can obtain the information about the induced hyperfine fields at the nuclear site due to the surrounding electrons and ions. Even the diamagnetic ions embedded in ferromagnetic hosts can experience large hyperfine fields. These large induced fields arise mainly from the s-type conduction electron polarization, core polarization of s-electrons by the polarized d or f electrons resulting in a net s-type contact spin density at the nucleus, large contributions from the unquenched orbital angular momentum and from the overlap of the 4s and 5s electrons with the polarized 3d, nf electrons of the neighbouring ion.

Lastly, the electric quadrupole splittings which arise because of the interaction of the electric quadrupole moment tensor with the electric field gradients can be used to obtain information about the electronic and ionic contributions to the electric field gradients at the nucleus. If the electric field gradients are known, the electric quadrupole moment of the nucleus can be measured.

Mossbauer effect and perturbed $(\gamma-\gamma)$angular correlation (PAC) techniques are used to measure the isomer shifts, magnetic splittings and quadrupole interactions. The high sensitivity of these techniques make them particularly suitable for the studies of the dilute impurity problems undertaken in the present thesis. The local environment of the probe nucleus plays an important role in all these interactions with the result that a proper source preparation is very important. In all the PAC measurements reported in this thesis, only time-differential measurements are carried out and a Fourier transform of the data were done so that the observed linewidths may be used to infer about the existence of non-unique impurity locations in the lattice and the satellite frequencies arising due to different lattice locations of the impurity ions.

It is my earnest hope that the new measurements reported here and as well as some of the measurements repeated along with the interpretation and discussions

given by me extends some of our understanding and/or remove some of the existing uncertainties and anomalies about the different mechanisms involved for the large induced internal magnetic hyperfine fields in particular, and the hyperfine interactions in general.

B. HYPERFINE INTERACTIONS

Hyperfine interactions [1-4] provide a single area of overlap between two rather diverse disciplines of physics, viz., the electronic structure of matter and the structure of nuclei. These interactions refer to deviations from Coulombic laws of interaction between a nucleus and surrounding electrons. Since a point charge yields, the Coulombic force field, the hyperfine interactions thus refer to and measure deviations of a nucleus from a point charge character. Such deviations are expressed in terms of a series of multipole moments. Parity considerations, then show that the systems with an axial symmetry have an alternating sequence of non-zero multipole moments, viz. electric monopole (E0), magnetic dipole (M1) electric quadrupole (E2) etc.

Any hyperfine interaction measurement yields a product of two quantities - one characteristic of a nuclear property and other signifying the electronic or solid state aspect. Thus, an a priori knowledge of one of these parameters is

essential as well as helps, determine the other. The interaction Hamiltonian of a nucleus embedded in a solid can be represented as:

$$H = H_N + [H_c + H_q + \ldots +] [H_M + \ldots] \qquad (1)$$

where H_N represents intra-nuclear interactions. H_N is approximately 10^{10} times stronger compared to the remaining contributions and is responsible in giving rise to the nuclear levels. The other terms, which act as a perturbation, arise due to the hyperfine interactions. The second term H_c in this expansion is the electric monopole term which represents the coulombic interaction of the nuclear charge and the surrounding electronic charge density. H_c is spherically symmetric and has no effect on the m-degeneracy of the eigenstates of H_N. The only effect H_c has is to produce a small shift in the energy eigen-values of H_N. H_Q represents the interaction of the nuclear quadrupole moment tensor with the electric field gradient at the nuclear site. Finally, H_M represents the interaction of nuclear magnetic dipole moment with the effective internal field at the nuclear site. Both H_M and H_Q lift the m-degeneracy of the eigen states of H_N. The general level splittings are schematically shown in Fig. (1) for the ground and first excited states of ^{57}Fe.

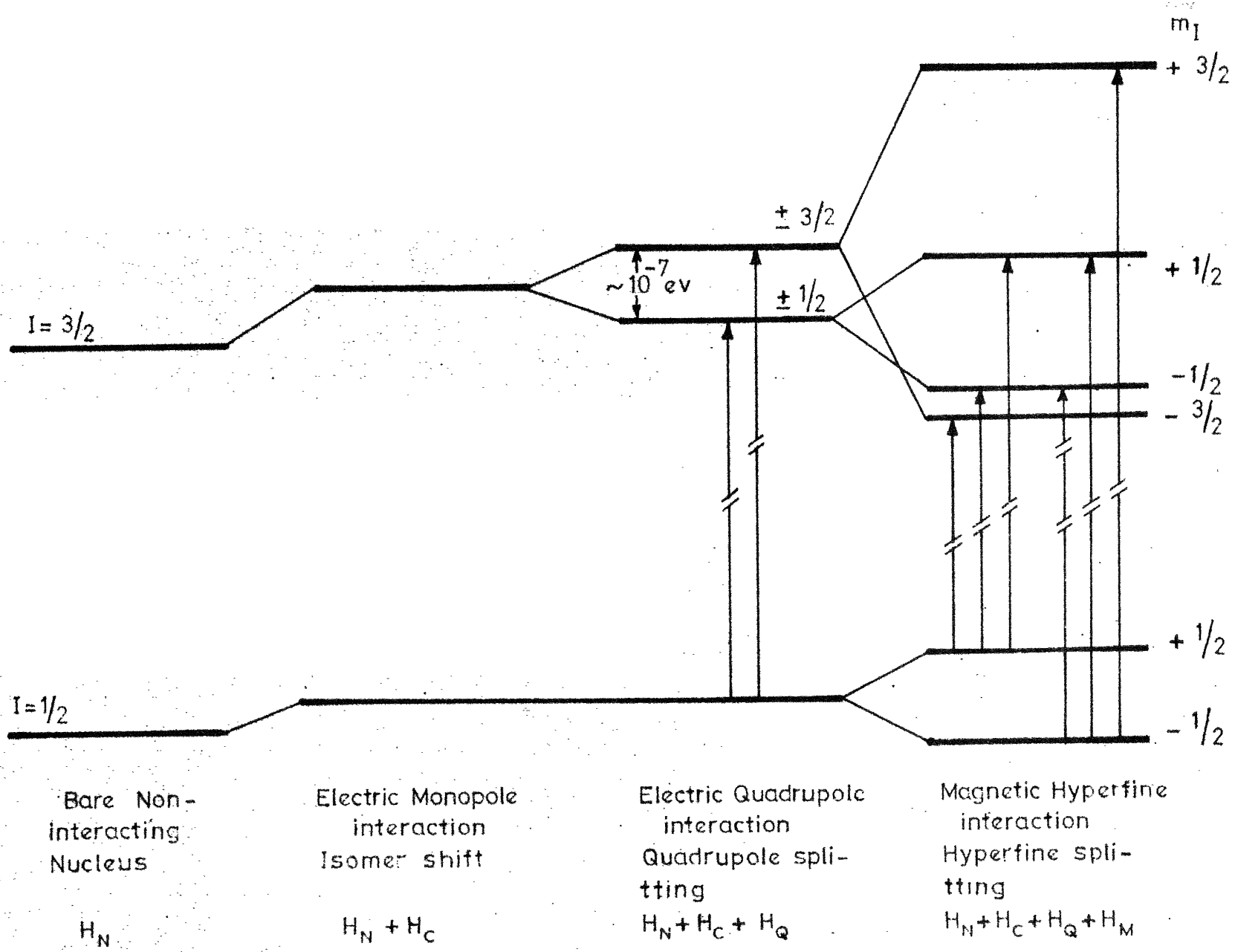

Fig. 1. Schematic representation of the effect of various components of hyperfine perturbation on the energy eigen states of H_N of ^{57}Fe.

1. Isomer Shift

The net change (ΔE) in the γ-ray energy due to electric monopole interaction can be expressed as,

$$\Delta E = \Delta E_e - \Delta E_g = \frac{2}{5}\pi Ze^2 |\psi(0)|^2 [\langle R_e^2 \rangle - \langle R_g^2 \rangle] \quad (2)$$

where ΔE_e and ΔE_g are the shifts in the energy of the excited and the ground states of the nuclei and R_e and R_g are the nuclear radii in the excited and the ground states respectively. Since the factor $(\langle R_e^2 \rangle - \langle R_g^2 \rangle)$ is constant for a given Mossbauer transition, an energy shift would occur, only if the source and the absorber nuclei experience different electronic charge distribution, i.e. different $|\psi(0)|^2$. This energy shift is called isomer shift (δ) and is given by,

$$\delta = \Delta E_a - \Delta E_s = \frac{2\pi Ze^2}{5} [\langle R_e^2 \rangle - \langle R_g^2 \rangle] [|\psi_A(0)|^2 - |\psi_S(0)|^2] \quad (3)$$

where the subscripts A and S refer to the absorber and the source respectively. If $R_e > R_g$, a positive isomer shift implies an increase in the s-electron density in going from source to absorber. However, if $R_e < R_g$, which is the case of ^{57}Fe, the same positive isomer shift shall signify a decrease in the s-electron density at the nuclear site in going from the source to the absorber. We shall defer a further discussion on isomer shifts to Chapter IV.

2. Electric Quadrupole Interactions

As the parity considerations exclude the possibility of nuclei having an electric dipole moment, the second non-vanishing term of the electrostatic part of the interaction, is a quadrupole interaction of the nuclear quadrupole moment with the electric field gradients produced at the nuclear site by the surrounding electronic charges in the crystal. The electric field gradient at the nucleus is defined as,

$$\nabla \cdot E = - \nabla^2 V = - \sum_{ij} \frac{\partial^2 V}{\partial x_i \partial x_j} \qquad (4)$$

With a proper choice of axes, this can be reduced to a diagonal form, with three principal components, i.e. $\frac{\partial^2 V}{\partial x^2}, \frac{\partial^2 V}{\partial y^2}$ and $\frac{\partial^2 V}{\partial z^2}$. These three components are however not independent, being connected through Laplaces equation, i.e.

$$\nabla^2 V = \frac{\partial^2 V}{\partial x^2} + \frac{\partial^2 V}{\partial y^2} + \frac{\partial^2 V}{\partial z^2} = 0 \qquad (5)$$

in the region where the charge density vanishes. It is important to note that although the s-electrons do have a finite probability of being at the nuclear site, however, being spherically symmetric, they do not participate in any quadrupole coupling. The electric field gradient is usually expressed in terms of V_{zz} and an asymmetry parameter defined as,

$$\eta = \frac{V_{yy} - V_{xx}}{V_{zz}} \qquad (6)$$

The interaction Hamiltonian is given by,

$$H_Q = \vec{Q} \cdot \vec{\nabla} E \tag{7}$$

$$= \frac{e^2 qQ}{4I(2I-1)} \left[3I_z^2 - I(I+1) + \frac{\eta}{2} (I_+^2 - I_-^2) \right] \tag{8}$$

The first order perturbation theory yields the energy eigen values as,

$$E_{m_I} = e^2 Q q \left(1 + \frac{\eta^2}{3}\right)^{1/2} \left[\frac{3I_z^2 - I(I+1)}{4I(2I-1)} \right] \tag{9}$$

In ^{57}Fe, since the ground state is a spin $1/2$ state, it is not affected by quadrupole interaction. The excited state however with a spin 3/2 gets split into two levels corresponding to $m_I = \pm 3/2$ and $m_I = \pm 1/2$.

The quadrupole splitting can be computed using equation (9) and accordingly,

$$2\varepsilon = E_{\pm 3/2} - E_{\pm 1/2} = \frac{1}{2} e^2 qQ \left[1 + \eta^2/3 \right]^{1/2} \tag{10}$$

Thus, we see that a pure quadrupole interaction is only partially successful in lifting the m-degeneracy, it being a quadratic operator in I_z.

3. Magnetic Hyperfine Interaction

The first magnetic term of the expansion is the well known nuclear Zeeman effect term. The interaction Hamiltonian is,

$$H_M = -\vec{\mu}_I \cdot \vec{H}_{eff} \tag{11}$$

where μ_I is the magnetic dipole moment of the nuclear state and $\vec{H}_{eff}$ is the effective magnetic field at the nuclear site. The magnetic perturbation in general completely lifts the m-degeneracy of the state. The energy separation of the two successive levels is,

$$\Delta E_m = \langle Im| -\vec{\mu}_I \cdot \vec{H}_{eff} |Im\rangle - \langle Im-1| -\vec{\mu}_I \cdot \vec{H}_{eff} |Im-1\rangle$$

$$= g_I \mu_N |\vec{H}_{eff}| m_I \qquad (12)$$

Since the ground state and the excited state magnetic moments are different, the splittings are different. Further, the transitions are governed by the selection rules, $\Delta m = 0, \pm 1$ (for ^{57}Fe, e.g.), depending on the nature of the transition. These two factors coupled together are responsible in giving rise to a six finger pattern in ^{57}Fe. The effective magnetic field $\vec{H}_{eff}$, seen by an impurity in a ferromagnetic host like Fe, Co and Ni was first discussed by Marshall [5]. He gave

$$\vec{H}_{eff} = \vec{H}_{ext} - D\vec{M}_s + \frac{4}{3}\vec{M}_s + \vec{H}_L' + \vec{H}_{hf} \qquad (13)$$

$\vec{H}_{ext}$, $D\vec{M}_s$ and $\frac{4}{3}\vec{M}_s$ are the external, demagnetizing and the Lorentz fields respectively. The origin of these contributions are well understood and can therefore be well accounted for. These are typically of the order of a few kOe. Demagnetization factors for various source shapes have been tabulated by Bozorth [6]. The saturation

magnetization is 7, 6, 2 for Fe, Co and Ni [7] respectively. $\vec{H}'$ is a small correction to the Lorentz field for materials having a symmetry other than cubic. Even for hexagonal symmetry (e.g., Co at room temperature), $\vec{H}_L'$ turns out to be about a thousandth of the Lorentz field [8] and hence can be altogether neglected. The last term represents the true hyperfine field and we shall discuss this in detail. The various contributions to $\vec{H}_{hf}$ can be given as [9],

$$\vec{H}_{hf} = \vec{H}_{ext} + \vec{H}_{orb} + \vec{H}_{dip} + \vec{H}_{core} + \vec{H}_{cond} + \vec{H}_{vol} \qquad (14)$$

$\vec{H}_{orb}$ represents the hyperfine field produced by the orbital current of the electrons and can be given as,

$$H_{orb} = - \Sigma_i \, 2\mu_B < \frac{\vec{l}_i \cdot \vec{I}}{r_i^3} > \qquad (15)$$

where $\vec{l}_i$ represents the angular momentum of the i^{th} electron having a position vector $\vec{r}_i$. Due to spherical symmetry, the orbital contribution is zero for the closed shells and for the half filled shells. Also, the orbital contribution is small when the orbital angular momenta is quenched by the crystal field gradient of the surrounding charge distribution. $\vec{H}_{dip}$ represents the spin dipolar interaction between the nuclear magnetic dipole moment and the magnetic moment of the electrons,

$$H_{dip} = 2\mu_B \sum_i < \frac{3(\vec{s}_i \cdot \vec{r}_i)(\vec{r}_i \cdot \vec{I}) - r_i^2 \, (\vec{s}_i \cdot \vec{I})}{r_i^5} > \qquad (16)$$

where $\vec{s}_i$ represents the spin of i^{th} electron with $\vec{r}_i$ as its position vector. This again vanishes for system with a cubic symmetry.

The other two contributions are the core polarization and the conduction electron polarization arising due to spin polarization of the core and conduction band electrons respectively. The exchange interaction between the 3d(4f) electron spins and the core s-electron spins causes a 'repulsion' of electrons with antiparallel spin and an effective 'attraction' with the electrons having a parallel spin. Such an interaction therefore results in a difference in the radial wave functions for electrons with opposite spin, thus resulting in spin polarization of the core, leaving a net down spin density at the nuclear site. This induces a negative hyperfine field at the nuclear site via a Fermi contact term given as,

$$H_{hf} \alpha \sum_{ns} [\, |\psi(0)|^2_{ns\uparrow} - |\psi(0)|^2_{ns\downarrow} \,] \qquad (17)$$

A similar exchange polarization of conduction electron spins is also produced via an exchange with host and as well as with the solute d(f)-electrons, which again results in a net hyperfine field at the nucleus.

Lastly, H_{vol} is a positive field arising due to valence ns-electrons, when the volume of the solute atoms is larger than the volume available to it on removal of a

host atom. The ns-like electrons overlap with the host matrix and get positively polarized by an amount proportional to the volume misfit of the solute atom. This contribution is however based somewhat on empirical reasonings. Chapter V deals in detail with the origin and the relative magnitudes of these contributions.

C. REFERENCES

1 V. I. Goldanskii and E. F. Makarov in Chemical Applications of Mossbauer Spectroscopy, Eds. V. I. Goldanskii and R. H. Herber (Academic, 1968), p.1.

2 G. K. Wertheim, Mossbauer Effect, Principles and Applications (Academic 1971), p. 47-106.

3 L. May, An Introduction to Mossbauer Spectroscopy (Plenum, 1971); N. N. Greenwood and T. C. Gibbs, Mossbauer Spectroscopy (Chapman and Hall, 1971) p. 46.

4 A. J. Freeman and R. B. Frankel, Hyperfine Interaction (Academic, 1971) (For a excellent general review on Hyperfine Interactions.)

5 W. Marshall, Phys. Rev. 110, 1280 (1958).

6 R. M. Bozorth, Ferromagnetism (Van Nostrand, 1951), p. 849.

7 American Institute of Physics Handbook (McGraw Hill, 1972), p. 5-144.

8 L. W. McKeehn, Phys. Revs. 43, 10251 (1951).

9 G. N. Rao and A. K. Singhvi, IIT/K Technical Report, Phys. 3/74 and also see Chapter V and the references cited therein.

chapter II

EXPERIMENTAL TECHNIQUES

A. INTRODUCTION

The methods employed in hyperfine interaction studies can be classified [1] into two categories depending upon whether the impurity is stable or radioactive. The methods used for stable nuclei are:

(a) Hyperfine structure of optical spectra

(b) Atomic and molecular beam methods

(c) Nuclear magnctic resonance

(d) Electron spin resonance

(e) Nuclear specific heat method

(f) Interaction of polarized neutrons with polarized nuclei.

The methods employing radioactive nuclei are:

(a) Mossbauer effect

(b) Perturbed angular correlation and its variants

(c) Nuclear orientation.

Besides these techniques, quite a few more methods employing hybrid principles of the above methods have been used. A typical example is NMR/PAC, the resonance destruction of angular correlation. The perturbed angular correlation and Mossbauer effect techniques used for the measurements presented in the present thesis are described in greater detail in the following sections.

B. PERTURBED ANGULAR CORRELATIONS

1. Introduction

In 1950, Brady and Deutsch [2] recognized the possibility of measuring the g-factors of excited nuclear states using an anisotropic angular correlation between gamma rays emitted in cascade. The first such measurement was reported by Aeppli et al.[3]. Since then the theory of extranuclear perturbations on angular correlations have been developed to a high degree of completeness and has been dealt with extensively in reviews by various authors [4-11]. In particular, the applications of PAC to solid state problems have been discussed in detail by Heer and Novey[9]. More recent reviews by Shirley and Haas [10] and by Deutch [11] discuss at length the present trends in PAC research, Fig. (1). In the following a brief and a self contained account of the theoretical formulation, relevant to the measurements presented in this thesis is given.

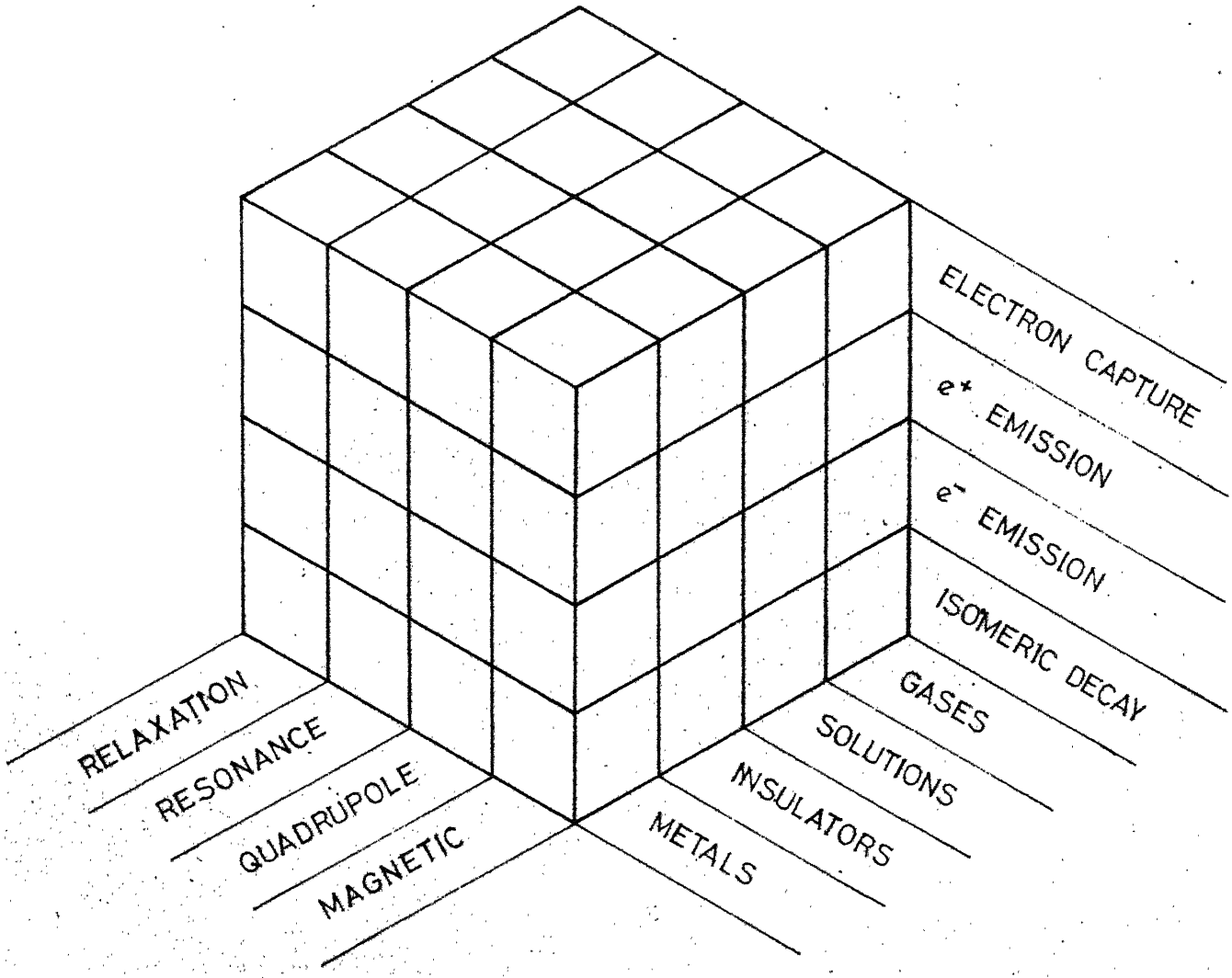

Fig. 1. Schematic characterization of PAC experiments based on (a) Mode of preceeding decay , (b) Physical state of the sample and (c) Type of extra-nuclear perturbation. Each box is described by three coordinates, corresponding to different permutations of the above three factors.

2. Theoretical formalism

In a radiative nuclear decay, through a three level system, via successive emission of two photons, an angular correlation in general exists between their (photons) propagation directions. Thus in an angular correlation experiment, one looks for the probability $W(\vec{k}_1,\vec{k}_2)d\Omega_1 d\Omega_2$, that a nucleus decaying through a cascade $I_i \xrightarrow{R_1} I \xrightarrow{R_2} I_f$, emits two radiations R_1 and R_2 in the direction $\vec{k}_1$ and $\vec{k}_2$ into solid angles $d\Omega_1$ and $d\Omega_2$ respectively, where $W(\vec{k}_1,\vec{k}_2)$ is the angular correlation function. For a system in a field-free space, i.e. for isolated nuclei, this correlation depends upon and yields information regarding the level spins and the transition multipolarities of the radiation fields. This angular correlation, however, is perturbed, if the intermediate state interacts with the environment. Physically, an extra nuclear perturbation lifts the m-degeneracy of the intermediate level and changes the m-sublevel population, consequently altering the angular correlation pattern.

Any angular correlation experiment can be described using the following three principal tools [12-14].

(a) The Density Matrix Formulation, which provides a conceptually simple and a mathematically elegant method to describe an incoherent mixture of impure

or mixed states, which is the case in a nuclear process like angular correlation. Impure states arise due to the fact that in an angular correlation experiment, we are often met with transitions of mixed multipolarities and that not all the quantum numbers are known. Incoherence in these states arise due to the fact that in a nuclear process, which is essentially a statistical phenomenon, each member of the nuclear ensemble develops in time in a statistical manner, totally independent of others.

(b) The Rotation Matrices, the usage of which gives one a freedom to calculate transition matrix elements in a convenient quantization frame of reference and then finally rotate them, with the help of rotation matrices, so that they correspond to actual experimental conditions, lastly

(c) Racah's Angular Momentum Algebra, which gives a convenient way to perform summation over various m-substates.

i. The unperturbed correlation function

A typical angular correlation cascade is shown in Fig.(2a). The initial nuclear state $|I_i m_i>$, described totally by the density matrix ρ_i, decays by emitting $R_1(L_1, L_1')$ in the direction $\vec{k}_1$, to the intermediate state

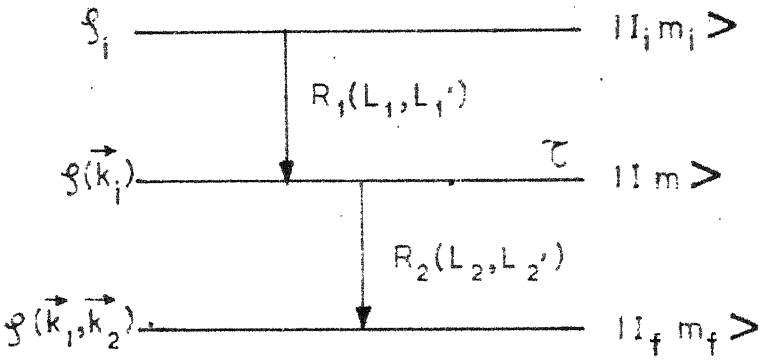

(a) Schematics of Unperturbed Angular Correlation

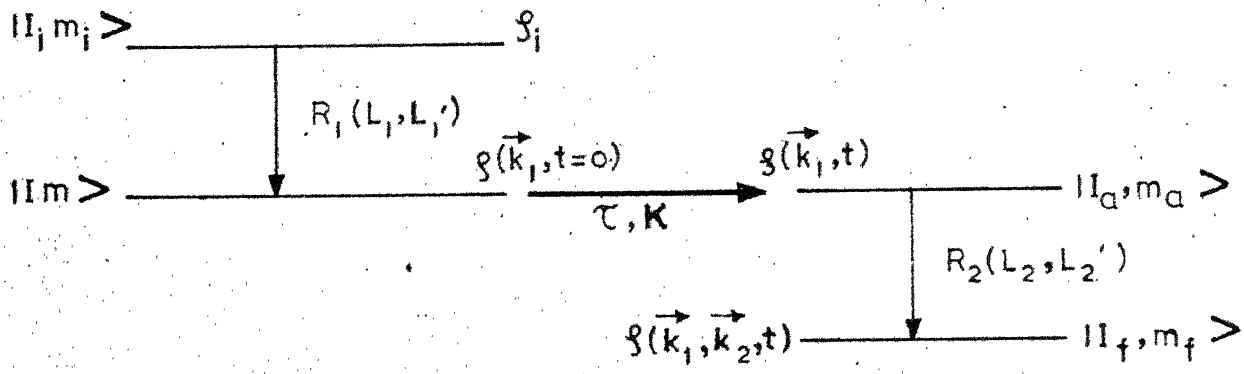

(b) Schematics of Perturbed Angular Correlation

Fig. 2. Schematics of (a) Angular Correlation and (b) Perturbed Angular Correlation.

$|Im>$ described by $\rho(\vec{k}_1)$. The intermediate state in turn decays by emitting $R_2(L_2, L_2')$ to the final state $|I_f m_f>$ described by $\rho(\vec{k}_1, \vec{k}_2)$. $\rho(\vec{k}_1, \vec{k}_2)$, thus contains all the information about the system and the radiation pattern. If H_1 and H_2, be the interaction Hamiltonian, causing the decays R_1 and R_2, we have,

$$<Im|\rho(\vec{k}_1)|Im'> = S_1 \sum_{m_i, m_i'} <Im|H_1|I_i m_i><I_i m_i|\rho_i|I_i m_i'> <Im'|H_1|I_i m_i'>^* \quad (1)$$

S_1 denotes a summation over all the unobserved properties like, e.g. the polarization. Similarly then for R_2, we can write,

$$<I_f m_f|\rho(\vec{k}_1, \vec{k}_2)|I_f m_f'> = S_2 \sum_{m, m'} <I_f m_f|H_2|Im><Im|\rho(\vec{k}_1)|Im'><I_f m_f'|H_2|Im'>$$

Using equation (1) we have,

$$<I_f m_f|\rho(\vec{k}_1, \vec{k}_2)|I_f m_f'> = S_1 S_2 \sum_{m_i, m_i'} \sum_{m, m'} <I_f m_f|H_2|Im><Im|H_1|I_i m_i><I_i m_i|\rho_i|I_i m_i'>^* <I_f m_f'|H_2|Im'>^* \quad (2)$$

For an isotropic initial state, the density matrix is diagonal, i.e.

$$<I_i m_i|\rho_i|I_i m_i'> = (2I_i + 1)^{-1} \delta_{m_i m_i'} \quad (3)$$

The correlation function is given by,

$$W(\vec{k}_1,\vec{k}_2) = \sum_{m_f} \langle I_f m_f | \rho(\vec{k}_1,\vec{k}_2) | I_f m_f \rangle \qquad (4)$$

where $\langle I_f m_f | \rho(\vec{k}_1,\vec{k}_2) | I_f m_f \rangle$ is the probability of finding the nucleus in the state $|I_f m_f\rangle$. Thus substituting equations (2) and (3) in equation (4) we get,

$$W(\vec{k}_1,\vec{k}_2) = S_1 S_2 \sum_{m_f} \sum_{m_i} \sum_{m,m'} \langle I_f m_f | H_2 | Im \rangle \langle Im | H_1 | I_i m_i \rangle$$

$$\langle Im' | H_1 | I_i m_i' \rangle^* \langle I_f m_f | H_2 | Im \rangle^* \qquad (5)$$

This is the unperturbed correlation function or the true correlation function, i.e. nothing happens to the intermediate nuclear spin, during the lifetime τ of the state.

ii. The perturbed correlation function

An extra-nuclear perturbation, in general, lifts the m-degeneracy of the intermediate level and changes the level densities during the lifetime τ . The density matrix $\rho(\vec{k}_1)$, therefore changes in time (Fig. 2b). Thus to obtain an expression for the perturbed correlation function, the time evolution of the density matrix has to be introduced in the formalism. The time evolution of the density matrix is described by the Heisenberg equation of motion, i.e.

$$\frac{\partial \rho}{\partial t} = -\frac{i}{\hbar} [\kappa , \rho]$$

which for static interactions has the solution,

$$\rho(\vec{k}_1,t) = \Lambda^{-1}(t)\ \rho(\vec{k}_1,t=0)\ \Lambda(t)$$

where κ is the interaction Hamiltonian, describing the extra nuclear perturbation and

$$\Lambda(t) = e^{-i\kappa t/\hbar}$$

The perturbed correlation function is then obtained by replacing $\rho(\vec{k}_1)$ by $\rho(\vec{k}_1, t)$ Fig.(2b)). Thus we have,

$$\langle I_f m_f | \rho(\vec{k}_1, \vec{k}_2, t) | I_f m_f' \rangle = S_2 \sum_{m_a, m_b} \langle I_f m_f | H_2 | I m_a \rangle \langle I m_a | \Lambda(t) \rho(\vec{k}_1, t=0) \Lambda^{-1}(t) | I m_b \rangle \langle I_f m_f' | H_2 | I m_b \rangle^*$$

$$= S_2 \sum_{\substack{m_a, \\ m_b}} \sum_{m, m'} \langle I_f m_f | H_2 | I m_a \rangle \langle I m_a | \Lambda(t) | I m \rangle \langle I m | \rho(\vec{k}_1, t=0) | I m' \rangle \langle I m' | \Lambda^{-1}(t) | I m_b \rangle^* \langle I_f m_f' | H_2 | I m_b \rangle^*$$

Using equations (1) and (4) and once again assuming the density matrix to be diagonal in the initial state, the perturbed correlation function can be written as,

$$W(\vec{k}_1, \vec{k}_2 t) = \sum_{m_f, m_i} \sum_{m, m'} \sum_{m_a, m_b} \langle I_f m_f | H_2 | I m_a \rangle \langle I m | H_1 | I_i m_i \rangle \langle I m' | H_1 | I_i m_i \rangle^* \langle I_f m_f | H_2 | I m_b \rangle^* \langle I m_a | \Lambda(t) | I m \rangle \langle I m_b | \Lambda(t) | I m' \rangle \quad (7)$$

A comparison of equations (5) and (7) indicates that the effect of extra nuclear perturbation is contained in the

matrix elements,

$$\langle Im_a m_b | G(t) | Im\, m' \rangle = \langle Im_a | \Lambda(t) | Im \rangle \langle Im_b | \Lambda(t) | Im' \rangle^* \quad (8)$$

Using rotation matrices and the Racah algebra, the PAC function can be written in the conventional form, i.e.

$$W(\vec{k}_1, \vec{k}_2, t) = \sum_{\substack{k_1,k_2 \\ N_1,N_2}} \frac{A_{k_1}(L_1,L_1',I_i,I)\, A_{k_2}(L_2,L_2',I_f,I)}{\sqrt{(2k_1+1)(2k_2+1)}} G_{k_1k_2}^{N_1N_2}\, Y_{k_1}^{N_1}(\vec{k}_1)\, Y_{k_2}^{N_2}(\vec{k}_2) \quad (9)$$

where the 'rotated' perturbation factor is related to the original perturbation factor through the relation,

$$G_{k_1k_2}^{N_1N_2} = \sum_{m,m_a} (-)^{2I+m_a+m_b} [(2k_1+1)(2k_2+1)]^{1/2} \begin{pmatrix} I & I & k_1 \\ m'-m & N_1 & \end{pmatrix} \begin{pmatrix} I & I & k_2 \\ m_b-m_a & N_2 & \end{pmatrix} \langle Im_a m_b | G(t) | Imm' \rangle \quad (10)$$

In the above L and L' are the angular momenta carried by the γ-rays. For mixed multipole transition, both L and L' are non-zero. The summation indices k and N are determined by the selection rules $|\vec{L}-\vec{L}'| \leq k \leq |\vec{L}+\vec{L}'|$ and $N_1 = m'-m$ and $N_2 = m_b-m_a$ and the coefficients,

$$A_{k_1}(L_1,L_1',I_i,I) = \frac{1}{1+\delta^2} F_k(L_1,L_1,L_i,I) + (-)^{L_1+L_1'} 2\delta F_k(L_1,L_1',I_i,I) + \delta^2 F_k(L_1',L_1',I_i,I)$$

and the mixing ratio

$$\delta = \frac{\langle I \| L_1' \pi_1' \| I \rangle}{\langle I \| L_1 \pi_1 \| I \rangle}$$

The F-coefficients are tabulated by Frauenfelder and Steffen [4]. Chosing the axis of quantization to be the symmetry axis, we have,

$$G^{N_1 N_2}_{k_1 k_2}(t) \Longrightarrow G^{NN}_{k_1 k_2}(t) = \sum_{m,m'} [(2k_1+1)(2k_2+1)]^{1/2} \begin{pmatrix} I & I & k_1 \\ m'-m & N & \end{pmatrix} \begin{pmatrix} I & I & k_2 \\ m'-m & N & \end{pmatrix} e^{-i(E_m - E_{m'})t/\hbar} \quad (11)$$

For static magnetic perturbation,

$$E_m - E_{m'} = \langle Im | -\vec{\mu}_I . \vec{H} | Im \rangle - \langle Im-1 | -\vec{\mu}_I . \vec{H} | Im-1 \rangle = \hbar w_L$$

the perturbation factor reduces to a simple form,

$$G^{NN}_{k_1 k_2}(t) = [(2k_1+1)(2k_2+1)]^{1/2} e^{-iw_L t} \sum_m \begin{pmatrix} I & I & k_1 \\ -m & m' & N \end{pmatrix} \begin{pmatrix} I & I & k_2 \\ -m & m' & N \end{pmatrix}$$

$$= e^{-iw_L t} \delta_{k_1 k_2} \quad (12)$$

Substituting (12) in (9) we get,

$$W(\vec{k}_1, \vec{k}_2, H, (t) = \sum_{\substack{k_1 k_2 \\ N_1 N_2}} A_{k_1}(R_1) A_{k_1}(R_2) e^{-iw_L t} Y^{N_1}_{k_1}(\vec{k}_1) Y^{N_2}_{k_2}(\vec{k}_2) \delta_{k_1 k_2} \quad (13)$$

The 'observed' correlation pattern is finally obtained by multiplying the above equation by the probability that the

radiation R_2 will be emitted at all, at time t, after the emission of R_1. This is given by a Poisson distribution $\frac{1}{\tau} e^{-t/\tau}$, where τ is the mean life of the intermediate state.

Equation (13) describes the correlation pattern that would have been observed experimentally, if the correlation apparatus had a 'perfect' time response. In practice, however, as the experimental system has a finite resolving time, the observed angular correlation pattern depends on the relative magnitudes of the resolving time τ_o of the detectors and the lifetime of the intermediate state τ. Thus, if $\tau_o >> \tau$, one can then measure only a time integrated correlation pattern (IPAC), i.e.

$$W(\theta, \infty, H) = \frac{\int_0^\infty W(\theta, t, H)\, e^{-t/\tau} dt}{\int_0^\infty e^{-t/\tau} dt} \qquad (14)$$

which is independent of the apparative constants. On the other hand, if the apparatus has a resolving time such that $\tau_o << \tau$, we get a time differential pattern (TDPAC), i.e. the pattern can be described by equation (13), and hence one is able to observe the rotation of the angular correlation pattern with time. Thus, a TDPAC measurement directly 'senses' the motion of the nuclear spin as a function of time, i.e.

$$W(\theta, t, H) = \frac{\int_{t_1}^{t_2} W(\theta, H, t)\, e^{-t/\tau} dt}{\int_{t_1}^{t_2} e^{-t/\tau} dt} \quad \text{where } \min(t_2 - t_1) \gtrsim \tau_o .$$

3. Experimental geometries

It is often possible to select the propagation direction in such a way that facilitates the extraction of the perturbation information from the experimental data. There are three variants of PAC set-ups employed mostly.

i. Perpendicular geometry

In this most widely used geometry, the magnetic field is perpendicular to the plane of the detectors. Thus, referring to Fig.(3),

$$\theta_1 = \theta_2 = \pi/2 \quad \text{and} \quad \Theta = \phi_1 - \phi_2$$

In such a case, the correlation pattern reduces to a particularly simple form,

$$W_{\perp}(\ , t, H) = \sum_{\substack{k=0 \\ \text{even}}}^{k_{max}} A_k(R_1)\, A_k(R_2)\, P_k[\cos(\theta \pm w_L t)] \quad (15)$$

or equivalently,

$$W_{\perp}(\theta, t, H) = \sum_{\substack{k=0 \\ \text{even}}}^{k_{max}} b_k \cos k(\theta \pm w_L t) \quad (15)$$

Interpreted on the basis of vector model, equation (15) offers a simple picture, that is, that a magnetic interaction results in a Larmor precession of the nuclear spin by an angle $w_L t$ and thus alters the angular correlation pattern appropriately. The direction of precession is determined

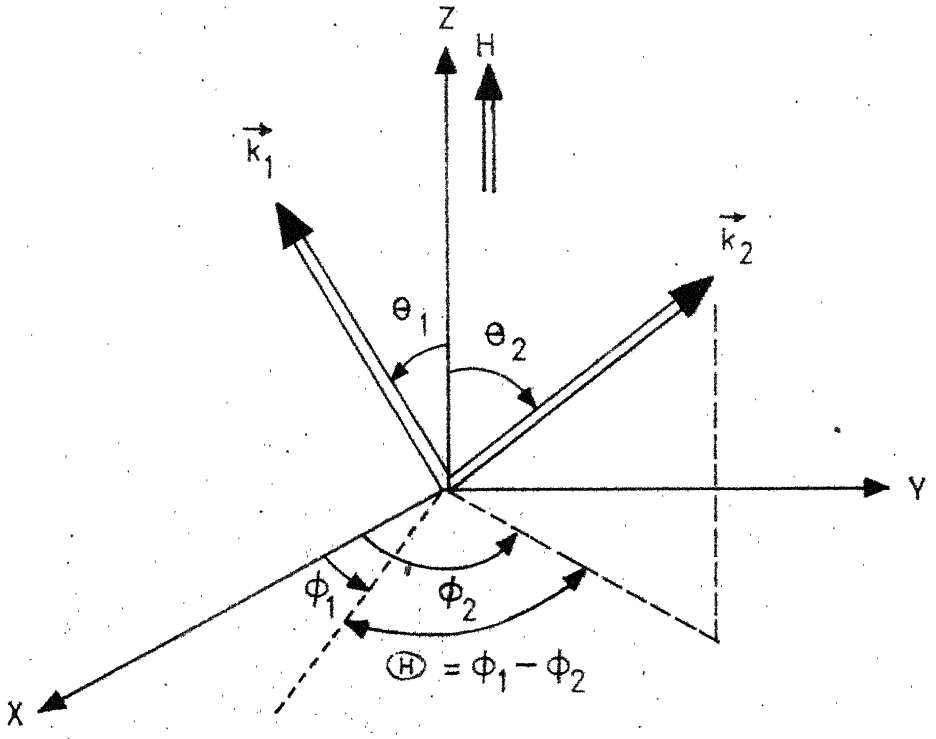

Fig. 3. Schematic representation of angular coordinates of propagation directions. The external magnetic field is in the Z direction.

by the requirement that the energy $E = -\vec{\mu}\cdot\vec{H}$ and the torque $\vec{T} = \vec{\mu} \times \vec{H}$. Figure (4) elucidates this point clearly. Thus, in a fixed angle (θ) geometry, the experimental data is a decay curve superimposed with a harmonic part. The modulation frequency in such a time differential method is $2w_L$. The method further allows a determination of the sign of the field, by observing the sense of rotation.

The time integrated correlation (IPAC) in such a geometry is given by

$$W_{\perp}(\theta, \infty, H) = \frac{1}{\tau}\int_0^{\infty} W_{\perp}(\theta, t, H)\, e^{-t/\tau}\, dt$$

$$= \sum_{k=0}^{k_{max}} \frac{b_k}{\sqrt{1 + (kw_L\tau)^2}} \cos k(\theta - \Delta\theta) \qquad (16)$$

where $\Delta\theta = \tan^{-1}(kw_L\tau)$.

It is therefore obvious that in an integral perturbed angular correlation, the angular correlation pattern is both rotated and attenuated. Further, it is worthwhile to note that a time differential measurement does not require an a priori knowledge of nuclear decay parameters, while an IPAC measurement does assume an a priori knowledge of these parameters. The perpendicular geometry DPAC was used in the measurement of hyperfine field on ScCo and TaNi and in the g-factor measurements on ^{181}Ta.

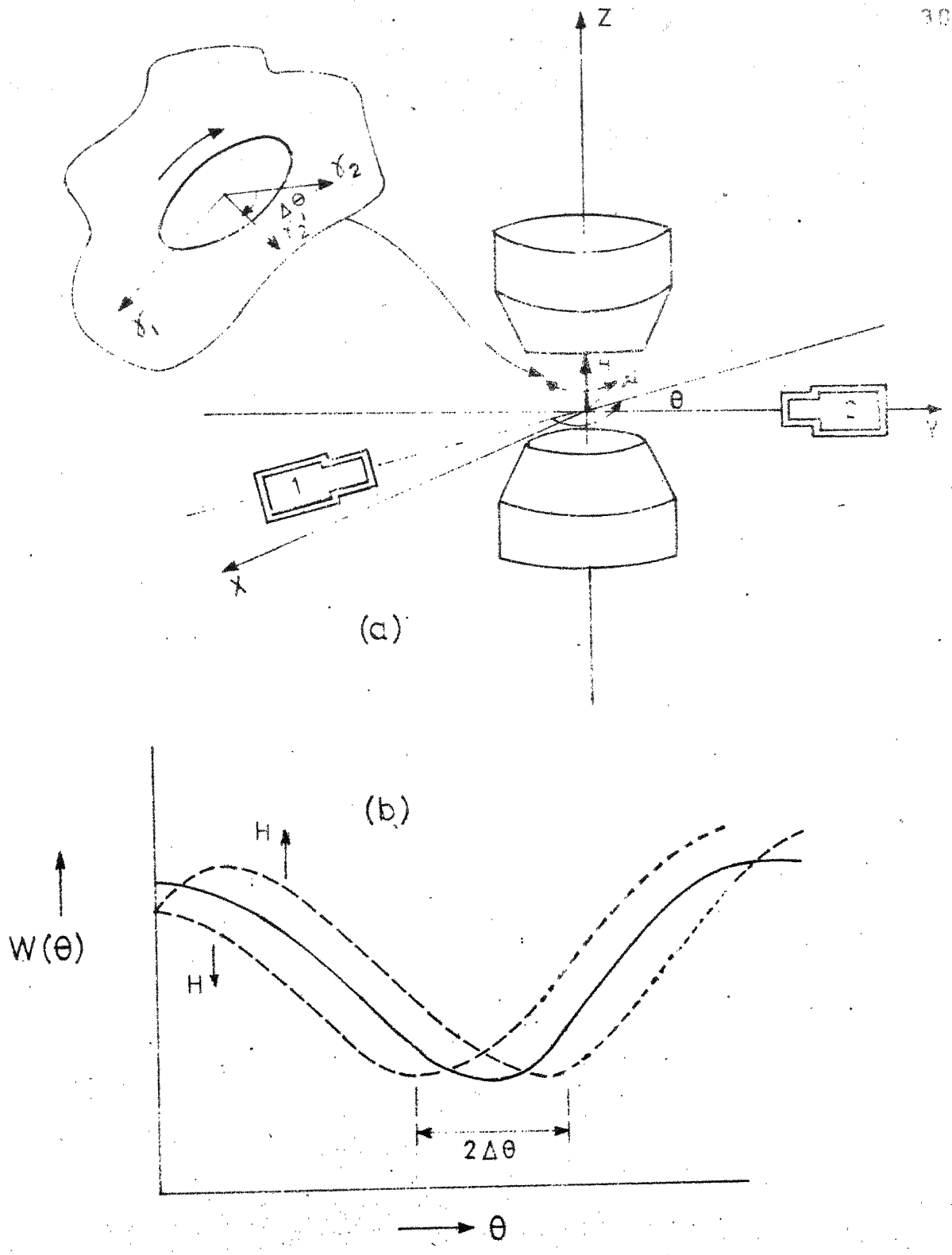

Fig. 4. (a) Schematic representation of the Larmor precession of nuclear spin in a magnetic field.
(b) The shift of W(θ) due to Larmor precession

ii. Randomly oriented domains technique

It was pointed out by Matthias et al.[15], that PAC could also be observed in a randomly oriented domain sample, i.e. when no external polarizing fields are employed. Here, therefore, although,

$$\theta_1 + \theta_2 = \pi \quad \text{and} \quad \Theta = \phi_1 - \phi_2 = \pi$$

are fixed, however, θ_1 may take any value. Accordingly then to get the correlation function, an integration over all the possible values of θ_1, has to be carried over. The correlation pattern in such a case is a superposition of k frequencies, weighted equally, i.e.

$$W(\theta, H, t) = \sum_k A_k(R_1)\, A_k(R_2) \left[\frac{1}{2k+1} \sum_N \cos N w_L t \; P_k(\cos\theta) \right] \qquad (17)$$

which for k=2, takes the form,

$$W(\ , H, t) \quad \alpha \; [1 + 2 \cos w_L t + 2 \cos 2w_L t]$$

The integral correlation pattern, however, remains the same as in perpendicular geometry. This TDPAC/randomly oriented domains method was used in hyperfine field measurement on Ta in Co matrix.

iii. Raghavan and Raghavan's geometry

Raghavan and Raghavan[16] pointed out two geometries that emphasize a modulation frequency of w_L rather than $2w_L$.

The method, however, is not capable of giving the sign of the field. This geometry is characterized by,

$$\theta_1 = \theta_2 = \frac{\pi}{4} \left(\frac{3\pi}{4}\right) \text{ and } \phi_1 - \phi_2 = \pi, \pi/2.$$

The polarizing field now lies in the plane of the detectors. This technique was used in the measurements on Re in Ni (not presented in the thesis).

4. Data Reduction

In the data reduction the first part is to extract the frequency content of the observed TDPAC spectra. This is easier after correcting for the exponential decay of the nuclear excited state. This in most cases is accomplished by forming a reduced counting rate ratio R(t) defined as, e.g., for the perpendicular geometry one has,

$$R(\theta, t_i H) = 2 \frac{W(\theta, t_i, H\uparrow) - W(\theta, t_i, H\downarrow)}{W(\theta, t_i, H\uparrow) + W(\theta, t_i, H\downarrow)} \simeq \frac{3A_{22} \sin 2w_L t_i}{4 + A_{22}} \tag{18}$$

The two correlation patterns corresponding to the $H\uparrow$(up field) and $H\downarrow$ (down field) are phase shifted with respect to each other by π.

Equivalently in Raghavan and Raghavan's geometry one calculates the reduced counting rate by computing the ratio

$$R(t) = 2 \frac{W(\pi) - W(\pi/2)}{W(\pi) + W(\pi/2)} \simeq \frac{\frac{3}{2} A_{22} \cos w_L t}{1 + 1/16\ A_{22} + 3/16\ A_{22} \cos 2w_L t} \quad \text{for } A_{22} \ll A_{44} \tag{19}$$

Alternatively, one could also form a ratio C(t) defined as,

$$C(t) = \frac{W(\theta, H, t) - A e^{-t/\tau}}{A e^{-t/\tau}}$$

which would eliminate the exponential decay factor.

From these ratios giving the reduced counting rates R(t) and C(t)'s, the frequency content could be directly computed by an extremely elegant and powerful method, suggested by Matthias et al.[17], who observed that 'except for the details of the line shape, the fourier transform of the correlation spectra, decay part taken out is essentially analogous to the free precession version of an NMR line (i.e., no R.F.) with a line width τ^{-1}.' Thus to extract the frequency content, one just has to calculate the Fourier transform of the reduced counting rate defined as,

$$\begin{aligned} A(w) &= \int_0^\infty R(t) \sin 2\pi w_L t \, dt \\ B(w) &= \int_0^\infty R(t) \cos 2\pi w_L t \, dt \\ F(w) &= [A^2(w) + B^2(w)]^{1/2} \end{aligned} \qquad (20)$$

Lastly, the range of the applicability of a TDPAC experiment is determined by the relation

$$\tau_o \leq \tau_{w_L} \leq \tau$$

where τ_{w_L} represents the time period corresponding to the

Larmor frequency. The presently available time resolutions give the lower limit of 1 nsec and accordingly TDPAC is applicable to the lifetime range

$$10^{-9}\,s \leq \tau \leq 10^{-2}\,s$$

The upper limit however for conventional off-beam coincidence methods is 1 sec, because of poor true to chance ratios. However, the upper limit can be considerably larger for in-beam experiments. The uncertainties in most favourable cases are ~0,1%.

C. MOSSBAUER EFFECT

1. Introduction

The discovery of recoilless gamma resonance fluorescence by Mossbauer [18] brought with it a diversity of applications, diffused practically in all the domain of natural sciences. Although, in principle, the effect originally belonged to nuclear physics, its solid state applications are now dominant, to the extent that it has become one of the standard tools in the investigation of solids. Such a multitude of applications have arisen essentially due to extreme energy precision offered by Mossbauer effect with relative simple experimental equipment. Probably no other technique offers so much of a wealth of information with so great an ease. Various aspects of

Mossbauer effect, its principles and applications, have been extensively reviewed [19-24] and accordingly we shall briefly outline the underlying principles and indicate the variety of information that can be gained by a typical Mossbauer study.

2. Theory

Mossbauer showed that the nuclei that are embedded in a solid can emit and absorb low energy gamma rays in a recoil-free manner. A free nucleus, while deexciting from an excited state E_o, by emitting a gamma ray of energy E_γ, recoils with an energy $E_R = E_\gamma^2/2mc^2$, where m is the mass of the recoiling nucleus. Conservation of energy gives the gamma ray energy $E_\gamma = E_o - E_R$. Analogously for the absorption process, it follows that in order to excite nucleus from its ground state to the same excited state E_o, a gamma ray with an energy $E_\gamma = E_o + E_R$ is necessary. Thus, there is a net deficit of $2E_R$, for the resonant absorption of the gamma ray. Resonance absorption can still occur if $2E_R \leq \Gamma$, the width of the nuclear state E_o (determined by its life-time). Typically for ^{57}Fe, $E_o = 14.4$ keV, $E_R \sim 2 \times 10^{-2}$ eV and $\Gamma \sim 5 \times 10^{-9}$ eV and obviously enough it is impossible to get a resonance under such conditions. Things, however, are different when the nucleus is rigidly bound in a lattice. The recoil momentum is now taken by the lattice as a whole. In such a case, the inevitable recoil energy is drastically

reduced, and is now given by $E_R = E_o^2/2\,Mc^2$ where M is the mass of the lattice instead of m, the mass of the nucleus. Under such conditions the recoil energy is not adequate to excite the solid to any higher phonon states so that the condition $2E_R << \Gamma$ is amply satisfied and accordingly resonant emission and absorption occurs. Here, in principle, most of the emission and absorption processes occur recoil-free, i.e. the fraction (f) of the gamma ray emitted recoil free can be almost close to one, while for a free nucleus f=0. A real crystal however does not provide an infinite binding to a nucleus and accordingly the internal degrees of freedom of the lattice may be excited by the emission and the absorption processes. In these cases, f may be between the two extremes, i.e. $0 \leq f \leq 1$, depending on the energy E_o of the transition and the 'rigidity' of the lattice. This may be summarized by the Lipkin's sum rule [25]

$$\sum_{n_f} [E_{n_f} - E_{n_i}]\; P(n_f \cdot n_i) \;=\; E_R \qquad (21)$$

where E_{n_i} and E_{n_f} are the energies of the lattice in the initial and final states (n_f & n_i) and $P(n_f, n_i)$ is the corresponding transition probability, representing the fraction of events inducing a lattice transition from a state n_i to state n_f. Clearly then, the transitions of interest in Mossbauer effect are identified by the probability $P(n_i, n_i)$, which is, in fact, the recoil free fraction. For a Debye solid [4],

$$P(n_i, n_i) = f = \exp[-k^2 \langle x^2 \rangle] = \exp\left[-\left(\frac{3}{2}\frac{E_R}{k_B\theta_D} + \frac{2}{3}\frac{\pi^2 T^2}{\theta_D^2}\right)\right] \quad (22)$$

where θ_D is the Debye temperature and k_B is Boltzmann constant. Thus, the conditions necessary to observe recoil free transition and hence the Mossbauer effect are given by equation (22): 1) E_R and i.e., E_o should be small, 2) lattice temperature should be small, 3) the Debye temperature of the solid should be large.

To summarize, therefore, under these conditions, the emitted gamma ray has the full energy E_o of the nuclear transition and has a natural width (Γ) (which is indeed the key to high energy resolution offered by Mossbauer effect) and accordingly have the right energy to be reasonantly absorbed by a similar nucleus under similar conditions. One is then able to study small perturbations in the nuclear energy levels arising due to, e.g., hyperfine interactions, by observing the change required in the gamma ray energy for it to be resonantly absorbed. Such changes are afforded by an appropriate Doppler shift.

A typical Mossbauer spectrum is characteristic of the atom under study and depends critically on the valency and the symmetries of the surroundings of Mossbauer atom. When several phases are present, the resultant Mossbauer spectrum is a linear superposition of the constituent spectra of different phases. Further, for thin samples,

the intensity of Mossbauer spectrum is proportional to the concentration of Mossbauer nuclei. In the following, we shall briefly discuss the information that could be derived from a Mossbauer spectrum.

A study of the nuclear hyperfine splittings directly reveal nuclear electromagnetic coupling coefficients both in the ground state and in the excited state. Then, the isomer shift, which can be measured only by Mossbauer effect is given by the shift in the centre of gravity of the spectra with respect to zero velocity. The isomer shift directly reflects on the s-electron density at the nucleus and consequently yields information regarding the chemical bondings and site symmetries. There is yet another contribution to the centroid shift, which is strongly temperature dependent, viz., the second order Doppler shift. The second order Doppler shift could be understood as follows. The relativistic energy of the source as seen by a moving absorber is

$$= E_o \left(1 + \frac{v}{c} + \frac{v^2}{2c^2} + \ldots \right)$$

arising due to the fact that both the emitting and absorbing nuclei are vibrating inside the lattice with very high frequencies ($\sim 10^{12}$ Hz). In such cases, although the average displacement during a spectroscopic event ($\frac{v}{c}$ term) averages out to zero, the term $\frac{v^2}{c^2}$, however, does not. This

results in a small perturbative addition to E_o and accordingly results in a centroid shift, depending upon the mean square velocity of the nucleus. The temperature dependence of such a term is obvious.

The next information which once again relates to lattice vibration is the recoil free fraction. It was seen in equation (22), that for a Debye solid, where all the nuclei occupy equal sites, the recoil free fraction f is

$$f = \exp(-k^2 \langle x^2 \rangle)$$

where k is the wave vector of the nuclear radiation. The recoil free fraction of a nucleus is directly related to the area of a Mossbauer spectrum corresponding to the resonance absorption, i.e.

$$A = f \int_{-\infty}^{\infty} [1 - \frac{I(v)}{I(\infty)}] dv = f \int_{-\infty}^{\infty} [1 - e^{-nf'\sigma(E)}] dE$$

where $(1 - \frac{I(v)}{I(\infty)})$ simply denotes the intensity of absorption. f and f' are the recoil-free fraction in the source and the absorber. n is the number of nuclei/cm^3 in the absorber.

The inference about the recoil free fraction is drawn from the temperature dependence of the area of the spectrum. It is important to note that the recoil free fraction is dependent upon the mean square displacement of the nuclei, while the second order Doppler shift is a measure of the mean square velocity. Indeed therefore the f-factor and

the second order Doppler shifts provide complementary ways of studying the lattice vibrations. The former is dominated by the low frequency vibrations whilst the latter depends on higher frequency modes.

The above expression for f is valid only if the lattice vibration of the Mossbauer nuclei are isotropic. In such cases, f is independent of the propogation direction of the radiation. An anisotropy of vibration can exist, which in turn results in an anisotropic recoilless fraction. For an axially symmetric case, it is given by [21],

$$f(\theta) = \exp\left[-k^2 \langle X^2_{\perp} \rangle + \left[\langle X^2_{\parallel} \rangle - \langle X^2_{\perp} \rangle \right] \cos^2 \right] \qquad (24)$$

where θ is the angle between the symmetry directions and the direction of propogation of the gamma rays. Such an anisotropic f leads to an asymmetry in the intensity of quadrupole splittings in polycrystalline samples. Conversely therefore an unequal intensity of quadrupole lines may reflect the anisotropy of f and hence about the crystal binding, which is known as Goldanskii - Karayagin effect.

Intensity differences in different hyperfine components can arise from two other sources as well. The first one is due to the difference in the relative transition probability of different hyperfine components and the second one is due to the difference in the angular dependence

of radiation intensity of different components. This, however, averages out for polycrystalline samples. Thus the intensity difference of different hyperfine components may give useful information regarding the relative transition probabilities.

Lastly, the information regarding the electronic spin relaxation effects can be inferred from the line shapes and line widths.

Thus, it is by now very clear that every bit, every minutest detail of a Mossbauer spectra carries significant information and this indicates that an extremely careful analysis is absolutely essential for exploiting the latent information.

3. Experimental

In Mossbauer spectroscopy a precision Doppler velocity spectrometer is required to produce small shifts in the gamma ray energies. The nuclear absorption at resonance is detected in terms of decreased transmission of gamma rays through the sample containing the absorber nuclei.

Now, since the natural line width of the 14.4 keV excited states of $^{57}Fe \simeq 5 \times 10^{-9}$ eV, corresponding to a velocity ~ 0.1 mm/sec, the accuracy of Doppler velocity required is much higher, so as to avoid any instrumental broadening of the spectral lines. This puts stringent

requirements on the frequency and the amplitude stability of the Doppler drive signal. In the following, we shall describe the sinusoidal drive spectrometer [26] which was used for the measurements presented in this thesis (Chapter IV).

Sinusoidal drive spectrometers are probably closest to an ideal system for two reasons [27], (i) that they do not put any mechanical stress on the transducer, ii) with a sinusoidal waveform, one could measure even small isomer shifts more accurately compared to the constant acceleration systems. The only disadvantage of such a drive system is that the spectra obtained have to be linearized since in this case, the time spent/channel is not constant. However, such a linearization can be afforded by a simple computer programme.

A schematic block diagram of the spectrometer is given in Fig. (5). The drive signal was derived from an 100 kHz, crystal controlled oscillator so as to get an frequency stability of one part in 10^5. The 100 kHz signal after proper level shifting is scaled down by 10 to get 10 kHz output which is used to advance the memory. For such channel advance pulse, the velocity reference signal is required to have a frequency (10/512) kHz for a 512 channel MCA. This was achieved by scaling down the 10 kHz output by 512 (= 4 x 32 x 2 x 2) using TTL-JK flip-flops. The

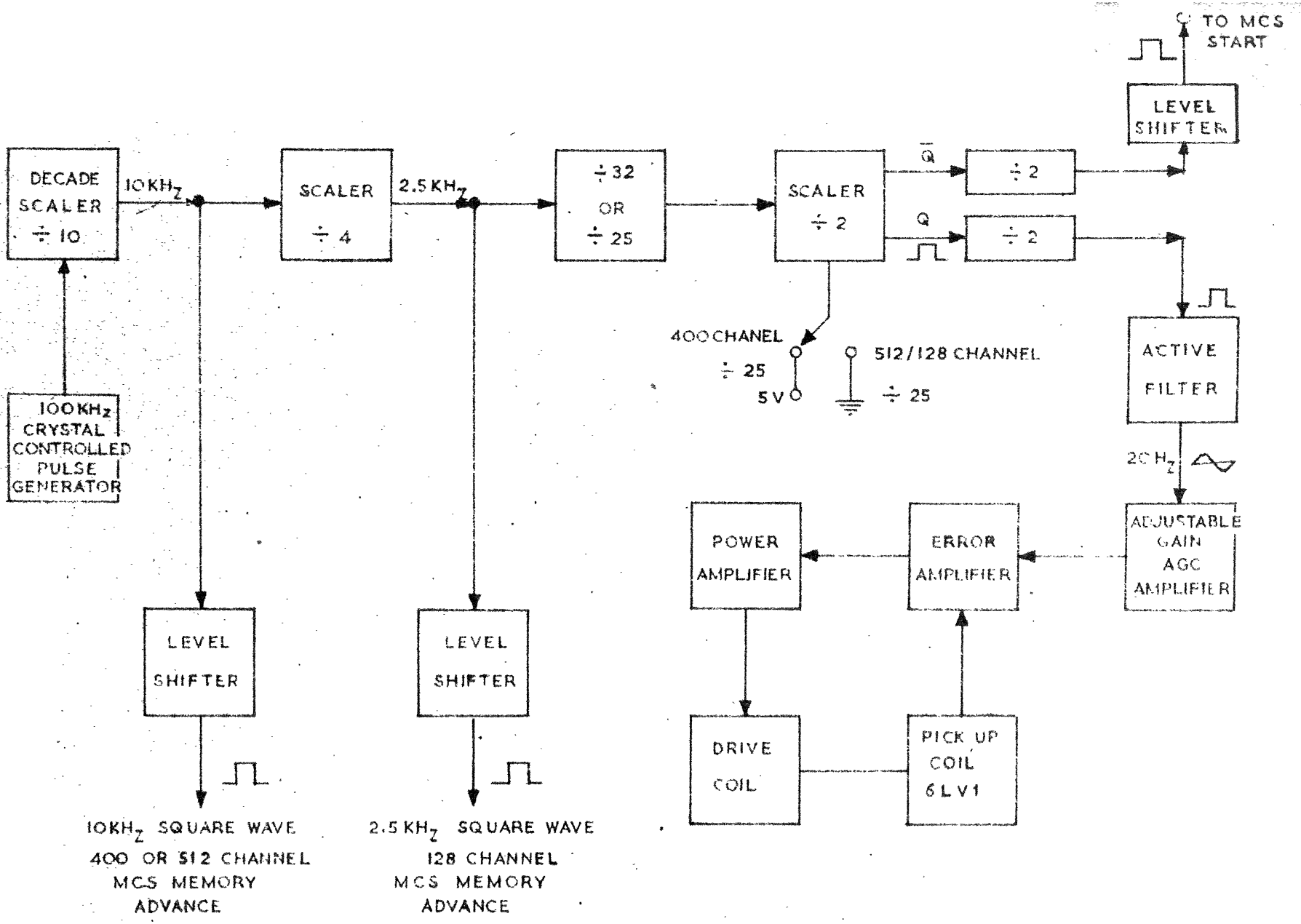

Fig. 5. Block diagram for Mössbauer spectrometer.

last stage in this chain is deliberately taken to be ÷2, so as to get square wave at the output of the divider chain. The reference sine wave for the velocity drive signal is finally obtained by extracting the fundamental component of the square wave through an active filter. A square wave input to the active filter minimizes the distortion in the sine wave as the square wave does not contain any second harmonic. In this case the rising and falling edge of the square wave then corresponds to zero of the sine wave and hence to zero velocity. Thus if multiscaling is started using this sine wave the initial channel (zeroth channel) would automatically correspond to zero velocity. It is however preferable to have the display with zero velocity in the centre. This in turn requires a delay of T/4 between MCS start and the filter input. Such a phase shift of $\pi/2$ is achieved by triggering a flip-flop using a complementary output of ÷2 counter.

A high amplitude stability in the amplitude of the sine wave is achieved by using a variable gain amplifier with an automatic gain control. The output of the amplifier is precision peak detected and is fed to the error amplifier. The error amplifier compares this voltage, with the reference voltage and the difference provides the AGC voltage. When the peak of the sine wave goes above or below this reference d-c voltage, the gain of the amplifier is appropriately

changed. The amplifier is a difference amplifier, whose gain is controlled by varying the base voltage of the current source. This peak stabilized - sine wave was used as a velocity reference signal. This signal is fed to the drive coil of the transducer through a power amplifier. The transducer converts the electrical signals into mechanical motion via the drive coil. A second coil, the pick up coil (we used Sanborn 6LV1 coil) then measures the instantaneous velocity of the system. The pick up signal is generated by the motion of a pencil magnet rigidly connected to the drive coil and this moves in the centre of the pick up coil. The pick up signal is compared with the reference signal by an error amplifier and such a feed back configuration ensures that the actual velocity waveform of the transducer is the same as that of the input signal. The error amplifier used was a push-pull type class AB amplifier using a complementary symmetry circuit. The above circuit was found to have an amplitude stability of better than 0.1%.

4. Data Reduction

Since we scan the full sine wave in 512 channels, we get in the MCA memory, two spectra, mirror images of each other. The symmetry lies around the folding point, which is a velocity extremum point and cannot be calculated in a straightforward manner. Now, as the full wave corresponds

to 512 channels, the zero velocity point would be 128 channels off from velocity extremum point and hence an addition and/or subtraction of 128 channels from the channel number corresponding to the velocity extremum point would yield zero velocity point. In this way, the zero velocity is unambiguously fixed up without using any external calibration standard. The zero velocity fixed in this way compared favourably with the zero velocity obtained using standard sources and absorbers. The channel number counted from the zero velocity channel, is then linearized by a simple programme.

D. SOURCE PREPARATION

The basic requirement in dilute impurity hyperfine interaction studies is a dilute source with impurity mostly in substitutional sites. This indeed requires a careful source preparation.

One of the standard and fairly reliable methods of source preparation is by alloying. The usual criterion is that the solid solubility of the solute in the host should exceed the impurity concentration desired. The solubility is usually good, if the ionic volumes are not too different. A rough guide to the solid solubility is provided by the Darken-Gurry plot (Fig. 6). However, alloying is not feasible when the melting points of the

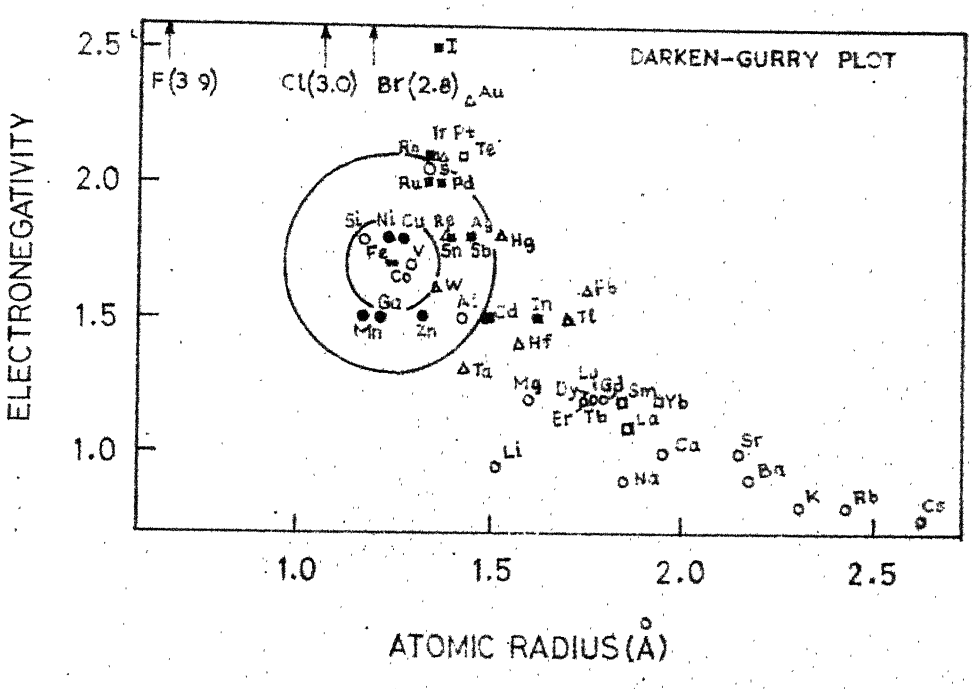

6. Darken-Gurry plot providing a rough estimate of solubility of elements in each other. The larger the distance between two points in this plot, lesser is the solubility, i.e. solid solution is expected to exist for points not too far. Such a plot, however, has only a qualitative significance and hence provides only a rough estimate.

solute and the host are too different. The other alternative method of source preparation is by high temperature diffusion, after electroplating the impurity on the host metal. Yet another method is a brute force technique when grinded samples are thoroughly mixed up and then solidified under a high pressure with a subsequent annealing. In such methods, however, the impurity position is always quite uncertain and a variety of lattice sites may be attained.

One of the recent and most promising techniques of source preparation is by implanting the impurity atoms into the host matrix by means of an isotope seaparator [28] or through a recoil after a nuclear reaction or Coulomb excitation. Here, one can, in principle, and under suitable experimental conditions can implant any impurity in any desired lattice. Subsequent ion channelling experiment can help to determine the exact impurity location in the host lattice.

E. REFERENCES

1 P. Inia, Ph.D. Thesis, University of Groningen, The Netherlands (Unpublished, 1971) p. 3.

2 E. L. Brady and M.Deutsch, Phys. Revs. 18, 558 (1950).

3 H. Aeppli, H. A. Schonberg, A. S. Bishop, H. Frauenfelder and E. Heer, Phys. Revs. 84, 370 (1951).

4 R. M. Steffen and H. Frauenfelder in α, β, γ ray Spectroscopy, eds. K. Siegbahn (North Holland, 1966) p. 997, and in Perturbed Angular Correlations, Eds. E. Karlsson, E. Matthias and K. Siegbahn (North Holland, 1964) p. 1.

5 R. M. Steffen, Phil. Mag. 4, 293 (1955); R. M. Steffen, University of Purdue Lecture Notes (1965-66); R. M. Steffen, Tata Institute of Fundamental Research, Lecture notes prepared by R. M. Singru (1965).

6 K. Alder and R. M. Steffen, Ann. Rev. Nucl. Sci. 14, 403 (1964).

7 L. Grodzins, Ann. Rev. Nucl. Sci. 18, 291 (1968).

8 E. Recknagel in Nuclear Spectroscopy and Reactions, Eds. J. Cerny (Academic Press, 1974), p. 93.

9 E. Heer and T. B. Novey, Solid State Physics, Eds. F. Seitz and D. Turnbull (Academic Press, 1959), p. 199.

10 D. A. Shirley and H. Haas, Ann. Rev. Phys. Chem. 23, 385 (1972), and H. Haas and D. A. Shirley, J. Chem. Phys. 58, 3339 (1973).

11 B. I. Deutch, Atomic Energy Reviews, IAEA (Vienna) 12(4), 605 (1974).

12 P. Inia, Ph.D. Thesis, Groningen University, The Netherlands (Unpublished, 1971) p. 20.

13 M. Levanoni, Ph.D. Thesis, California Institute of Technology (Unpublished, 1970) p. 6.

14 S. S. Rosenblum, Ph.D. Thesis, Lawrence Radiation Laboratory, University of California, UCRL-18675 (Unpublished, 1969) p. 4.

15 E. Matthias, S. S. Rosenblum and D. A. Shirley, Phys. Rev. Lett. 14, 46 (1965).

16 R. S. Raghavan and P. Raghavan, Nucl. Instrum. Meth. 92, 435 (1971).

17. E. Matthias and D. A. Shirley, Nucl. Instrum. Meth. 45, 309 (1966); G. N. Rao, E. Matthias and D. A. Shirley, Phys. Rev. 18A, 325 (1969).

18 R. L. Mossbauer, Z. Physik 151, 124 (1958).

19 G. K. Wertheim, Mossbauer Effect : Principles and Applications (Academic Press, 1971).

20 L. May: An Introduction to Mossbauer Spectroscopy (Plenum, 1971).

21 V. I. Goldanskii and E. Makarov, in Chemical Applications of Mossbauer Spectroscopy, Eds. V. I. Goldanskii and R. H. Herber (Academic, 1968) p. 1.

22 H. Frauenfelder: The Mossbauer Effect,(Benjamin Inc., 1962).

23 N. N. Greenwood and T. C. Gibbs, Mossbauer Spectroscopy (Chapman and Hall, 1971).

24 Mossbauer Effect Methodology Series (Vols. 1-9) Eds. I. J. Gruverman (Plenum Press). Also, R. L. Mossbauer and M. J. Clauser in Hyperfine Interactions, Eds. A. J. Freeman and R. B. Frankel (Academic, 1968), p 497.

25 H. J. Lipkin, Ann. Phys. 9, 332 (1960).

26 A. K. Gupta, K. R. Sarma, J. J. Huntzicker and G. N. Rao, Rev. Sci. Instrum. 45, 1423 (1974).

27 G. M. Kalvius and E. Kankeleit in Mossbauer Spectroscopy and its Applications (IAEA Panel Proceedings, Vienna, 1971) p. 9.

28 H. de Waard and S. A. Drentje, Physics Letters 20, 38 (1968).

chapter III

DILUTE IMPURITY HYPERFINE FIELD MEASUREMENTS USING PERTURBED ANGULAR CORRELATION TECHNIQUE

A. HYPERFINE FIELD MEASUREMENTS ON SCANDIUM IN COBALT MATRIX*

1. Introduction

The spin rotation of 1^+, 68 keV state was used to measure the hyperfine field on scandium as a dilute impurity in cobalt matrix. The 78 keV-68 keV (γ-γ) cascade populated in the decay of ^{44}Ti to ^{44}Sc was used for this measurement. The relevant part of the level structure of ^{44}Sc is given in Fig. (1) [1]. Using time differential perturbed (γ-γ) angular correlation technique, we earlier reported [2] the g-factor of the 68 keV state to be g = 0.342 $\pm$ 0.002. The half-life of this state was measured to be $T_{1/2}$= 158.8$\pm$2.0 nsec [2].

2. Source Preparation

For the hyperfine field measurement a TiCo alloy

*Published in Phys. Lett. 47A, 319 (1974).

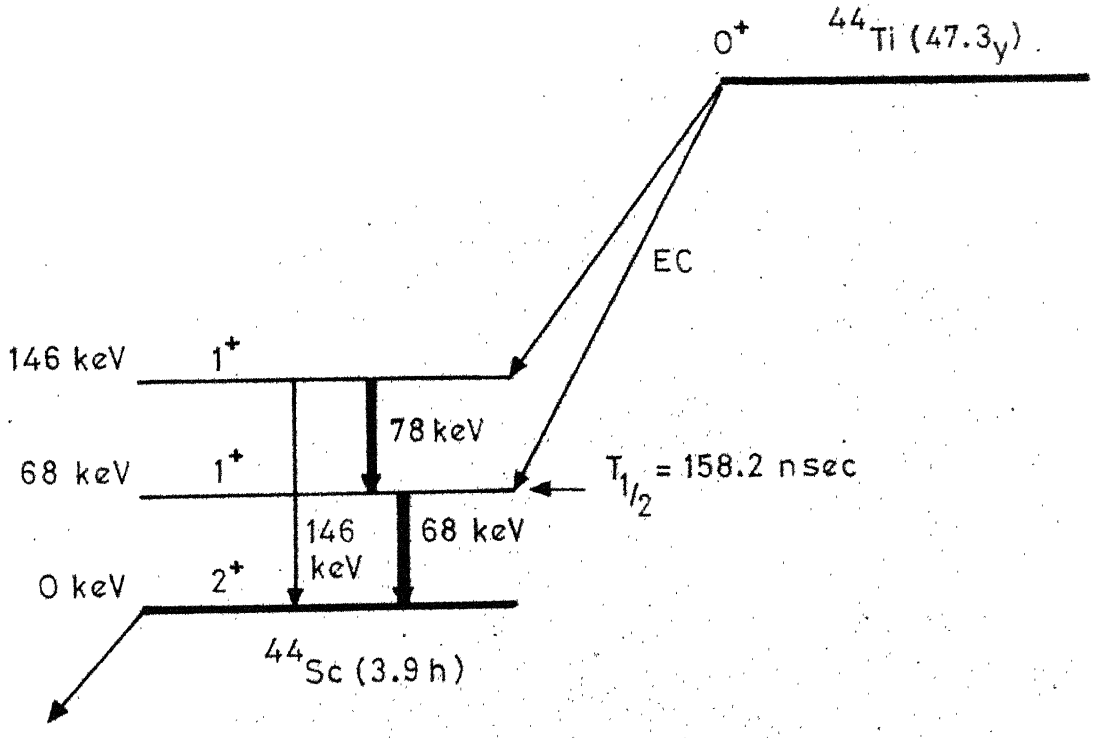

Fig. 1. Level structure of ^{44}Sc. The 78-68 keV cascade is indicated by thick arrows.

containing traces of Ti activity was prepared. The ^{44}Ti activity, produced through a $^{45}Sc(p,2n)^{44}Ti$ reaction, was procured in a solution form (as chloride) from Nuclear Science and Engineering Corporation (USA). The liquid activity was evaporated on to a thin cobalt foil (99.99%). This foil was then melted in an inert argon atmosphere, using a radio frequency induction furnace. The molt was then gradually cooled down to room temperature. The resulting shining ball was rolled into a thin foil, which was then annealed for 24 h, and finally cooled down to room temperature over a period of 3 h.

The solid solubility of Ti in Co has been reported to be about~ 8 at % [3]. The atomic radii of Ti and Co are 1.47 Å and 1.25 Å respectively and therefore we expect that we have a solid solution with Ti ions occupying substitution positions.

3. Experimental Details

The spectrometer used for the measurement was a conventional delayed coincidence set up comprising of two 2" x 2" NaI(Tl) scintillators coupled to RCA-56AVP photomultiplier tubes, kept at an angle 135°. The fwhm of the prompt curve was 6 nsec with the gates set at ~70 keV energy in both the channels. The source to detector distance was kept at~ 7 cms. The block diagram of the electronics (mostly an ORTEC system) is given in Fig. (2).

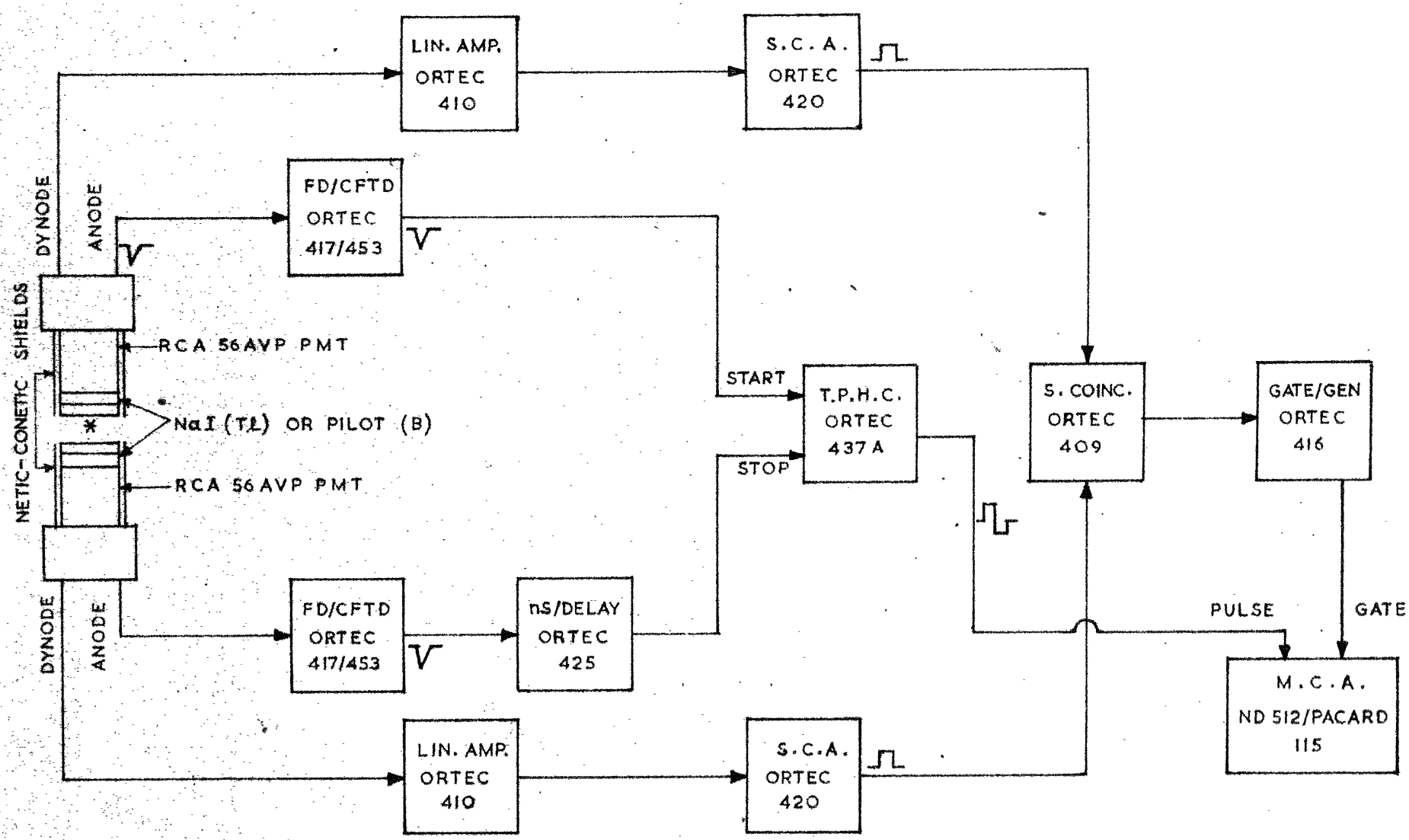

Fig. 2. Block diagram of the set up used for PAC measurements.

A magnetic field of 7 kOe was applied to polarize the host matrix, perpendicular to the plane containing the detectors. A small electromagnet was used for this purpose (Atomic Laboratories Inc. U.S.A.). The magnetic field was measured accurately with a Hall probe, which in turn was calibrated using proton resonance. The photomultiplier tubes were adequately shielded from stray magnetic fields using a series of Netic-CoNetic magnetic shields [4].

4. Measurement

Approximately 16 K counts were collected for each of the field directions. A typical time spectrum for ^{44}Sc<u>Co</u> in an external polarizing field is given in Fig. (3). The Fourier transforms of the reduced counting rate R(t), defined in Chapter II, are plotted in Fig. (4).

The measured hyperfine field H_{meas} is given by the relation

$$\vec{H}_{meas} = \vec{H}_{ext} + \vec{H}^{true}_{hf} - D\vec{M}_s + \vec{H}_L$$

as defined in Chapter I, The hyperfine field value after correcting for the external and demagnetizing field is H_{hf} Sc<u>Co</u> (RT) = -58 $\pm$ 4 kOe. The field is not corrected for Lorentz field [5].

The sign of the hyperfine field was determined by the usual method, i.e. from the sense of rotation of the angular correlation pattern. The approximate uncertainties

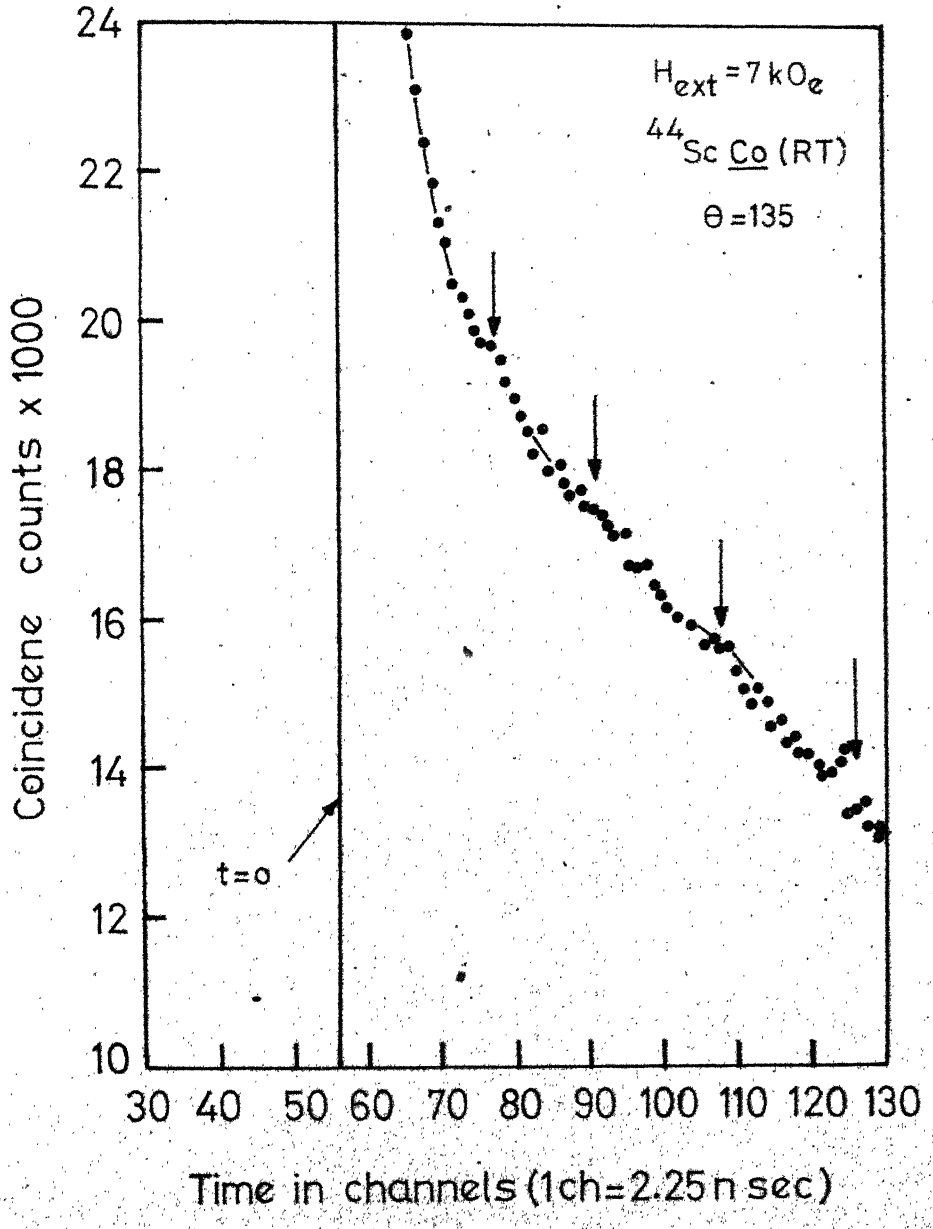

Fig. 3. TDPAC time spectra of ^{44}Sc Co in a external polarizing magnetic field of 7 kOe.

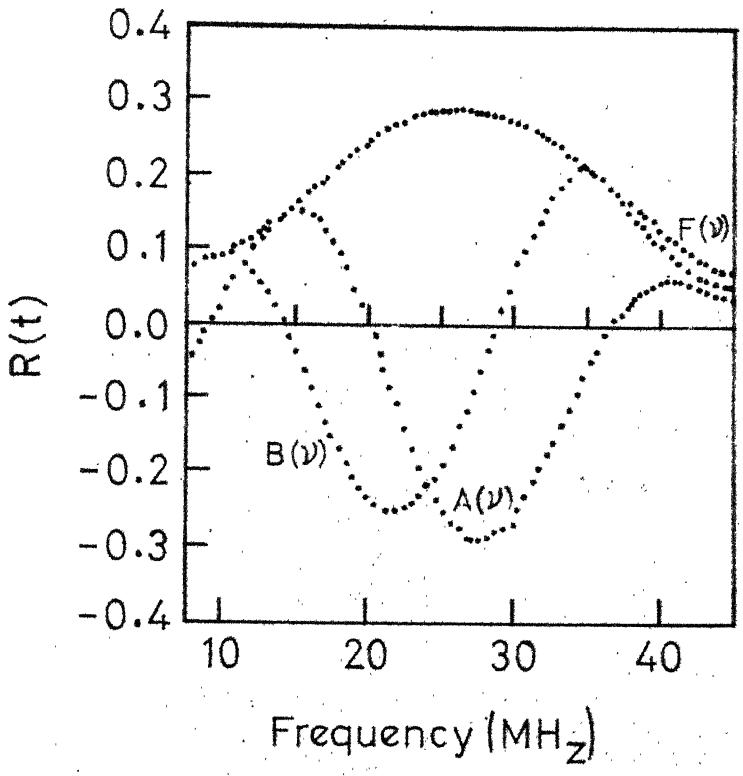

Fig. 4. Sine, cosine and the absolute transforms of the reduced counting rate R(t) for CoCo in an external polarizing magnetic field of 7 kOe.

are, 4% in the frequency determination from the experimental data, 2% in the magnetic moment value and 1% in the time calibration, which gives an error of 7% in the measured hyperfine field.

5. Discussion

After the present measurement was published, Colley et al. [6] reported hyperfine field measurements on Sc<u>Co</u> using TDPAC technique. They however have reported a series of values for the hyperfine field, ranging from -91 kOe to + 13 kOe, depending upon the method they used for source preparation. They prepared their samples by melting cobalt plates containing evaporated ^{44}Ti activity, covered by thin layers of Li and Ca. Li and Ca were used as reducing agents to prevent any internal oxidation of Ti to TiO_2 [7]. The positive field was attributed to an internal oxidation of $Ti \rightarrow TiO_2$. This was further confirmed, when they annealed their sample 5, which indeed showed a change in sign of hyperfine field from a negative to positive. We, however, took all the care to prevent any possible internal oxidation of the activity and we accordingly did not observe any oxidation effects in either of our measurement on Sc<u>Fe</u> and Sc<u>Co</u>. Benski and Hohenhemser [8] prepared their samples in hydrogen atmosphere and in vacuum for the hyperfine field measurement on Sc in Ni and they did not observe any oxidation effects either.

The observed amplitude is ~ 2.5%. The observed large width ($6\Gamma_n$) of the absolute Fourier transform may be from 1) HCP structure of the cobalt host with unresolved quadrupole interactions, 2) all the Sc ions are not in the same well defined lattice positions resulting in unresolved hyperfine frequency components. However, further experiments are necessary to understand this problem.

Should we expect a smooth variation of the hyperfine field values around Sc impurity in the cobalt host, the expected hyperfine field for Sc<u>Co</u> from the systematics [9] is H_{hf} Sc<u>Co</u> = -60kOe, which compares well with the present experimental value of -58 kOe.

The dilute impurity hyperfine fields in the ferromagnetic hosts are often assumed to be proportional to their host moments at least when there are no locald-moments. The hyperfine field on Sc ($3d^1 4s^2$) in Fe and Ni hosts have been reported to be -129±4 kOe [2] and -25.7±0.3 kOe [8] respectively. The ratios of the reduced hyperfine fields (H_{hf}/μ_h) in Co and Ni hosts, normalized to the reduced hyperfine field in Fe host, turns out to be 0.8:1.0 indicating thereby that the fields are proportional to the host moments to within 20%. Later in Chapter V, it has been shown that such a conjecture, as expected, is valid only very approximately and indeed the hyperfine field depends on many other contributions arising due to impurity host interactions and due to impurity itself.

Scandium has a configuration $3d^1 4s^2$. The orbital angular momentum for a transition impurity like Sc in a cobalt host is expected to be largely quenched and therefore the orbital contribution to the hyperfine field may be neglected to a first approximation. Because of the configuration, $3d^1 4s^2$, the d-moment contributions are expected to be small. Therefore the major contribution to the hyperfine field should come from the conduction electron polarization. Sc with its $3d^1 4s^2$ configuration would have rather a small contribution due to core polarization, because the magnitude of local d-moment in the beginning of the transition series are expected to be small.

With the recently available accurate data, we have recalculated the polarization 'p' defined in Shirley et al's model [5] (discussed in detail in Chapter V) and the values obtained are 0.026 for Fe host, 0.02 for Co host and 0.023 for Ni host. Using these values and the free atomic hyperfine field value of 1 MOe, we get the conduction electron polarization contribution $H_{CEP} = -\mu p H_{ns} = -35$ kOe. Therefore, the contributions from the core polarization is ~ -23 kOe. Using Freeman and Watsons [10] estimates for the hyperfine field per polarized d-spin (H_{hf}/3d spin = -125 kOe), local d-moment at the scandium impurity site turns out to be $0.2\mu_B$.

The atomic volume of Sc is 18 $\AA^3$ and accordingly from the Stearns model, one would expect a large positive contribution to the hyperfine field from the volume overlap effect, which is not observed. Therefore this model is not successful in explaining the experimental field **[11]**.

Finally Balabanov and Delyagin [12], approximated the observed hyperfine field across a period to a parabola of the type,

$$H_{hf} = \mu_h \; Z_o^{1.3} \; [-2.48 + 0.113 \; (\nu - 9)^2]$$

For scandium, $\nu = 3$ and $Z_o = 18$. This model predicts a value +113 kOe, much too different both in magnitude and sign of the observed field.

The model due to Shirley et al. therefore seems to explain the experimental value both in sign and magnitude. However, a further check of this model would be to measure the local d-moment using neutron diffraction techniques. The volume overlap effect suggested by Stearns and the model due to Balabanov and Delyagin are not successful in explaining the observed field. It is, however, quite clear that conduction electron polarization is a major contributor to the field on Sc in Co host.

B. HYPERFINE FIELD MEASUREMENTS ON TANTALUM IN COBALT AND NICKEL HOSTS

1. Introduction

The spin rotation of 10.8 ns, $5/2^+$, 482 keV state of ^{181}Ta was used to measure the hyperfine field of Ta in Ni and Co hosts. The 133-482 keV cascade in ^{181}Ta, populated in the β^-decay of ^{181}Hf was used for this purpose. The decay scheme is given in Fig.(5) [13].

2. Source Preparation

The 42.4 day, ^{181}Hf activity was produced through an (n,γ) reaction of Hf metal powder (99.9%). The neutron irradiation was carried out at the CIRUS reactor, BARC (India). For g factor measurements, active Hf was dissolved in 26 N hydrofluoric acid. In this form the quadrupole interactions are expected to be small. The liquid sample containing HfF_4 was then sealed in a thin walled polythene tube and was used as such for the measurements.

The Ta<u>Co</u> sample was prepared by a radio frequency induction melting of cobalt plates (99.99%) with traces of finely powdered Hf activity in an inert argon atmosphere. The molt was gradually cooled to room temperature. The resulting shining ball was used as such for the measurements.

The Ta<u>Ni</u> sample was prepared by thermally diffusing the ^{181}Ta activity into a thin nickel foil (99.99%). The

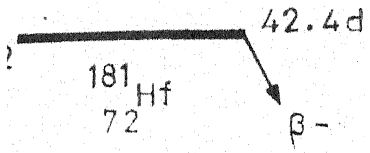

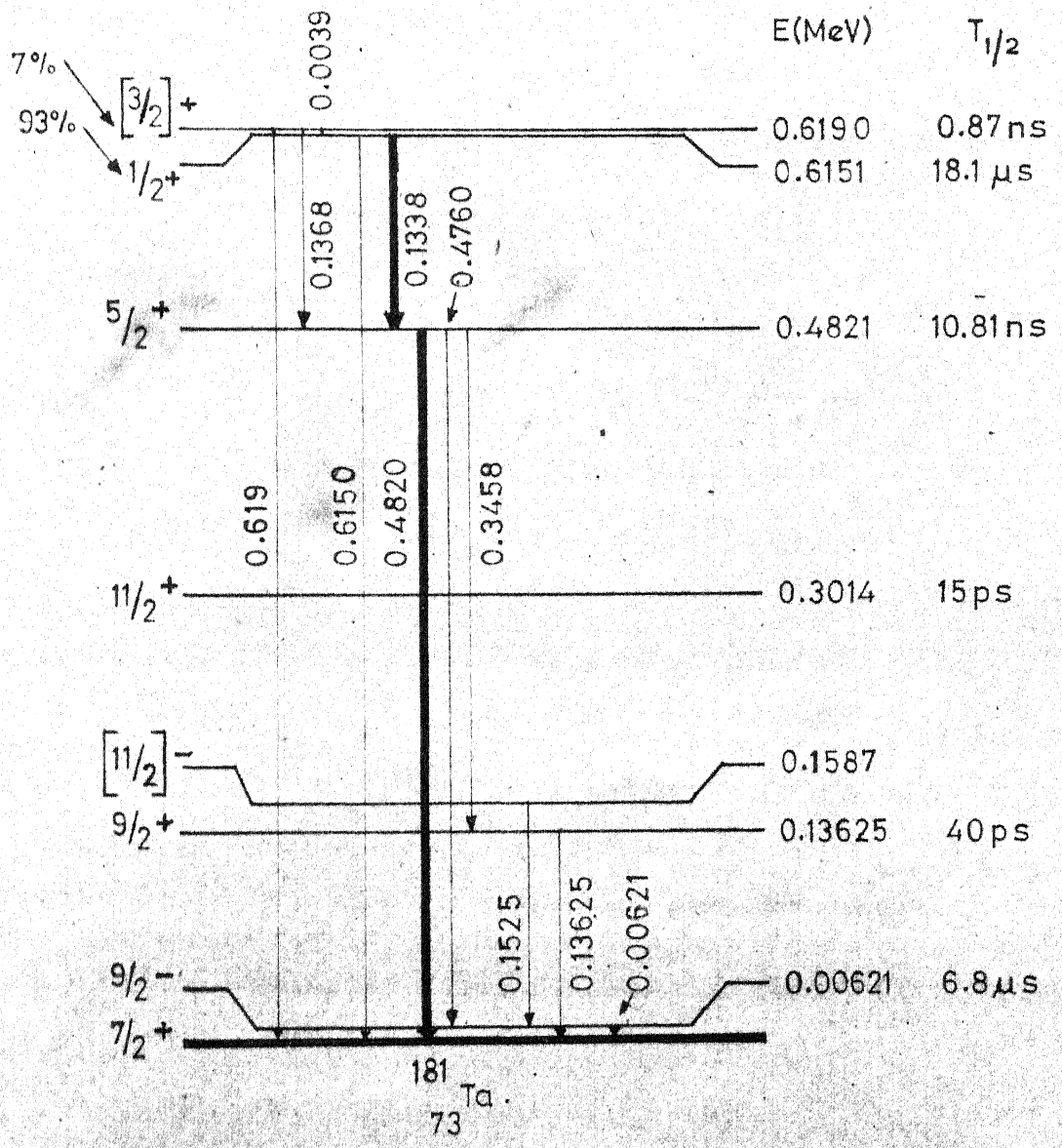

Fig. 5. Level structure of ^{181}Ta. The 133-482 keV cascade is indicated by thick arrows.

radioactive Hf in the form of $HfCl_4$ (prepared by heating the metal Hf activity in a chlorine atmosphere) was sandwiched between Ni foil and then sealed in a quartz tube in vacuum (10^{-6} cm). The diffusion was carried out at 1100°C for 80 h. The active foil was then thoroughly cleaned with distilled water to ensure a complete removal of the undissolved surface activity and was then used as such for the measurements. Another sample of Ta<u>Ni</u> prepared by induction melting was also studied to see the source preparation effects. The procedure adopted for the sample preparation was similar to the one used for Ta<u>Co</u>.

3. Experimental Details

The spectrometer consisted of two 2" x 2" NaI(Tl) scintillators coupled to 56 AVP photomultipliers. The detectors were kept at an angle of 135°. The system had a fwhm of ~ 2.5 nsec for the energy gates set at 133-482 keV energies. The g factor measurement was carried out in an external polarizing field of 7 kOe. The hyperfine field measurements on Ta<u>Ni</u> was also carried out using the same set up in an external polarizing field of 2 kOe. The other experimental details are discussed in part A.

The spectrometer for the hyperfine field measurements on cobalt host consisted of ½" x 2" NaI(Tl) and 1" x 1" lead loaded plastic (Pilot B) scintillators. The system

had a fwhm resolution of ~ 1.7 nsec for the 133-482 keV energy gate settings. The measurements was carried out using randomly oriented domain technique (Chapter II, eqn. (17)), with the two detectors kept at an angle 180°.

4. Measurement

Typical TDPAC time spectra obtained for g-factor measurements in an external field of 7 kOe is given in Fig. (6) and the reduced counting rate R(t) is given in Fig. (7). The TDPAC time spectra obtained for Ta<u>Ni</u> samples (both induction melting and diffusion samples) along with the corresponding reduced counting rates R(t) and C(t) respectively are given in Figs. (8) and (9). Finally, the TDPAC spectra along with the reduced counting rate C(t) obtained for Ta<u>Co</u> sample is given in Fig. (10). Figure (11) gives the absolute Fourier transform plot of C(t) for Ta<u>Co</u>. sample.

The g-factor of 482 keV state is measured to be $g = 1.3 \pm 0.1$. The hyperfine field value in the nickel host after correcting for the external and the demagnetizing fields is H_{hf} Ta<u>Ni</u> (RT, Diffusion)= -77 ± 5 kOe and H_{hf} Ta Ni (RT, Induction melting) = -75 ± 5 kOe. For Ta<u>Co</u>, the data reduction was done by forming the ratio C(t), defined earlier. As shown earlier in Chapter II, the TDPAC spectra in a randomly oriented domain sample is in general modulated

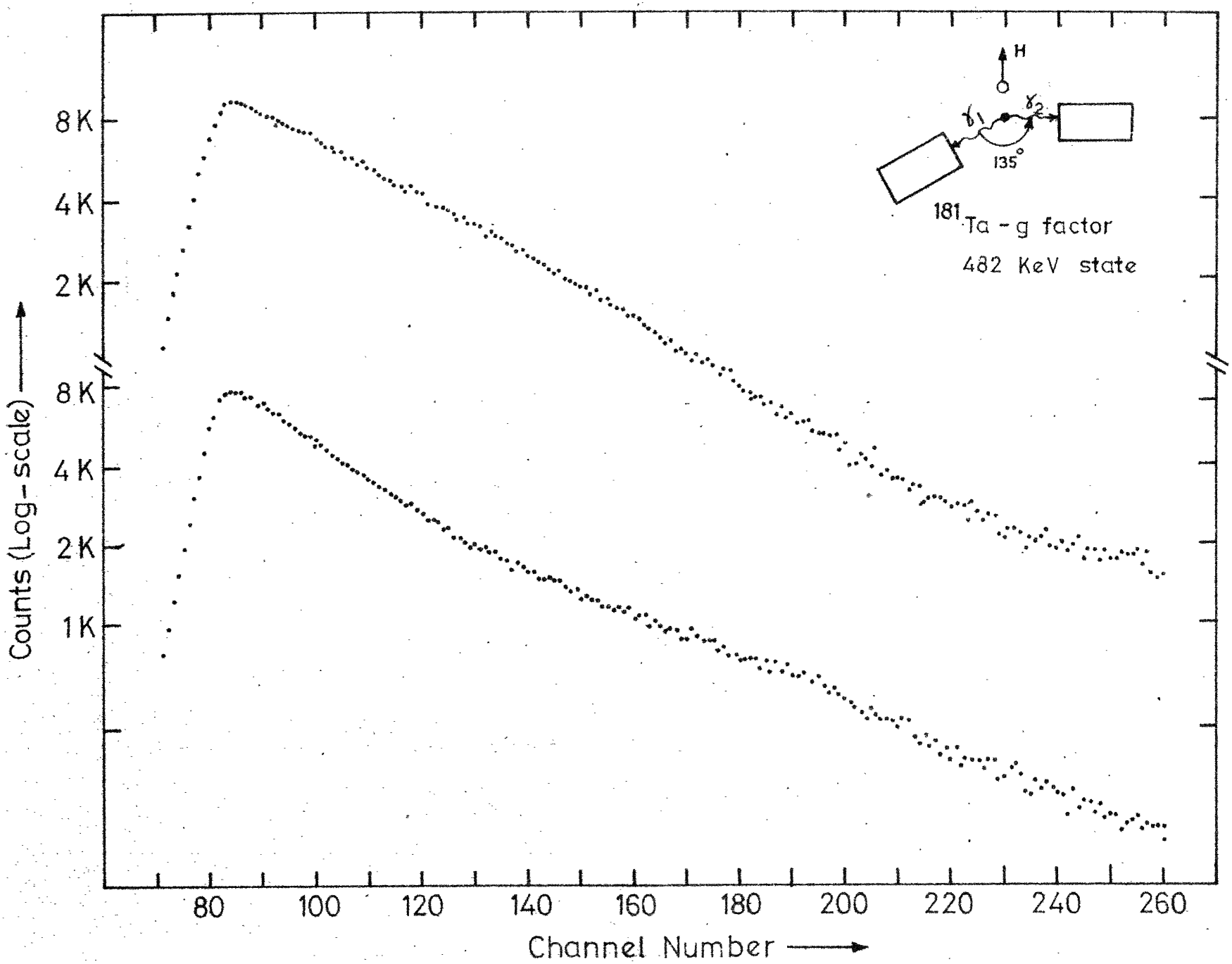

Fig. 6. TDPAC time spectra of ^{181}Ta (Source HfF_4 as solution) in an external magnetic field of 7 kOe (raw data).

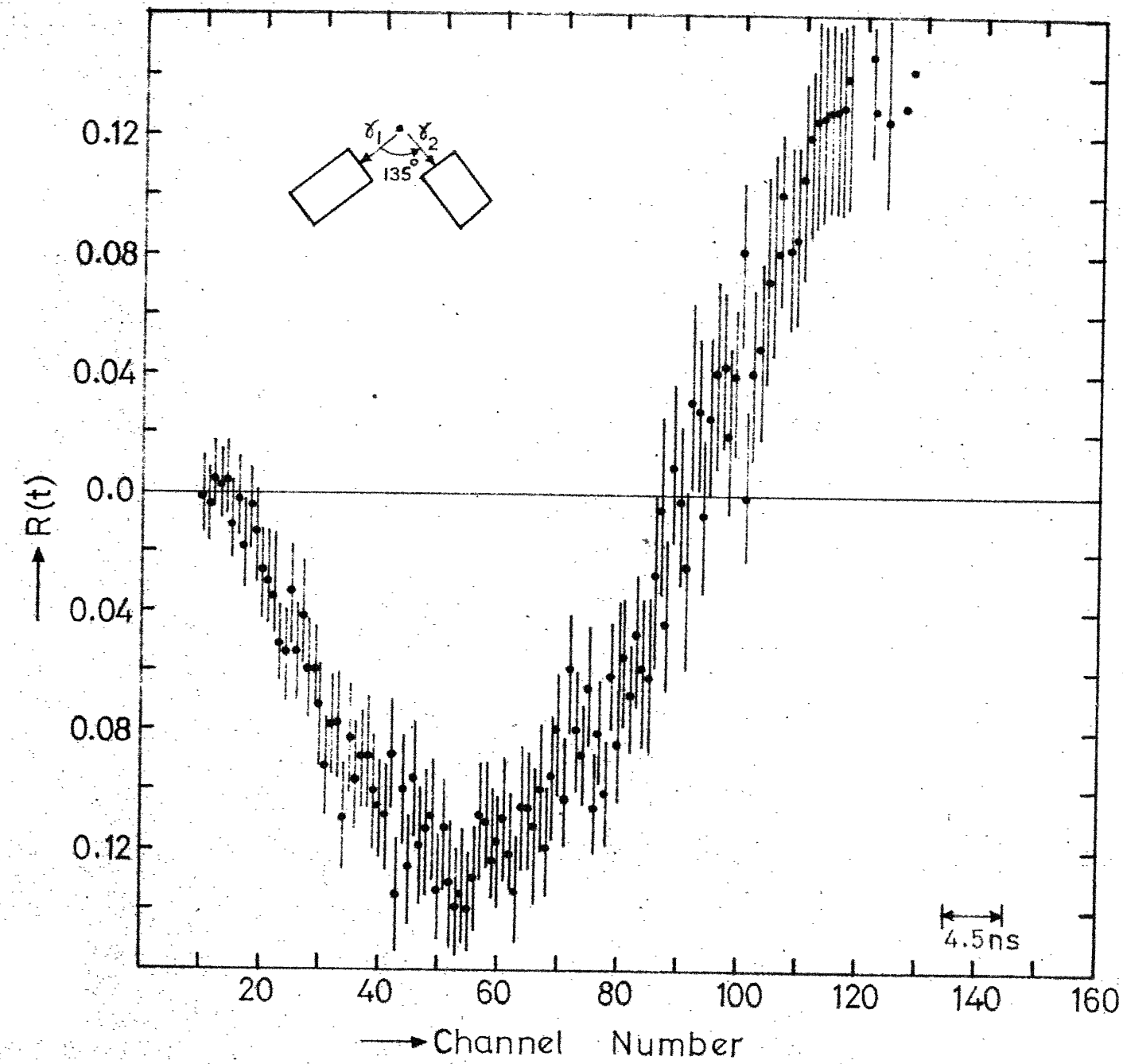

Fig. 7. Reduced counting rate R(t) for ^{181}Ta (source HfF_4 as solution)

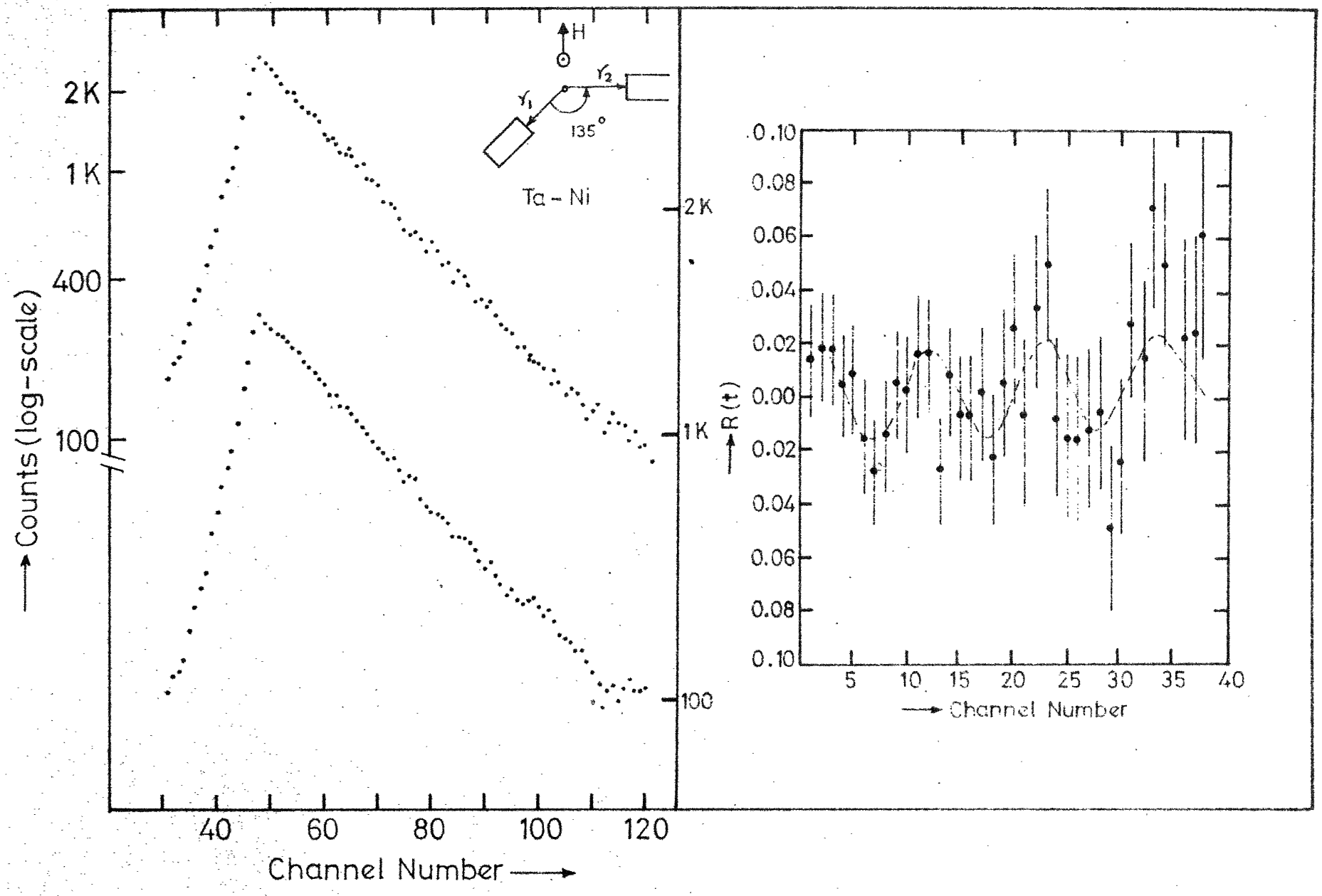

Fig. 8. TDPAC time spectra along with the reduced counting rate R(t) of ^{181}Ta in Ta (induction melting sample) in an external polarizing field of 2 kOe (raw data).

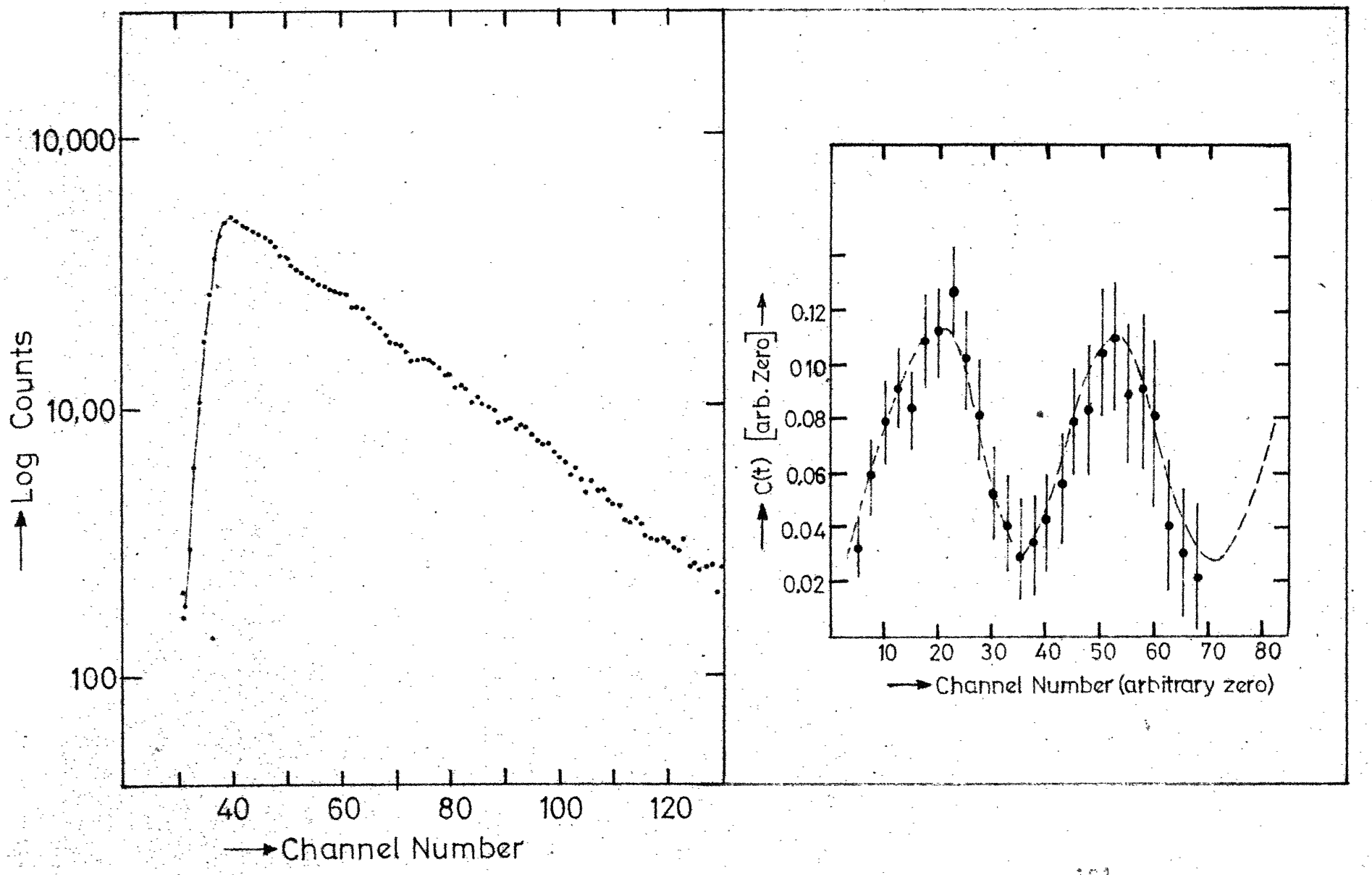

Fig. 9. TDPAC time spectra along with the reduced counting rate C(t) of ^{181}TaNi (diffusion) sample in an external polarizing field of 2 kOe (raw data).

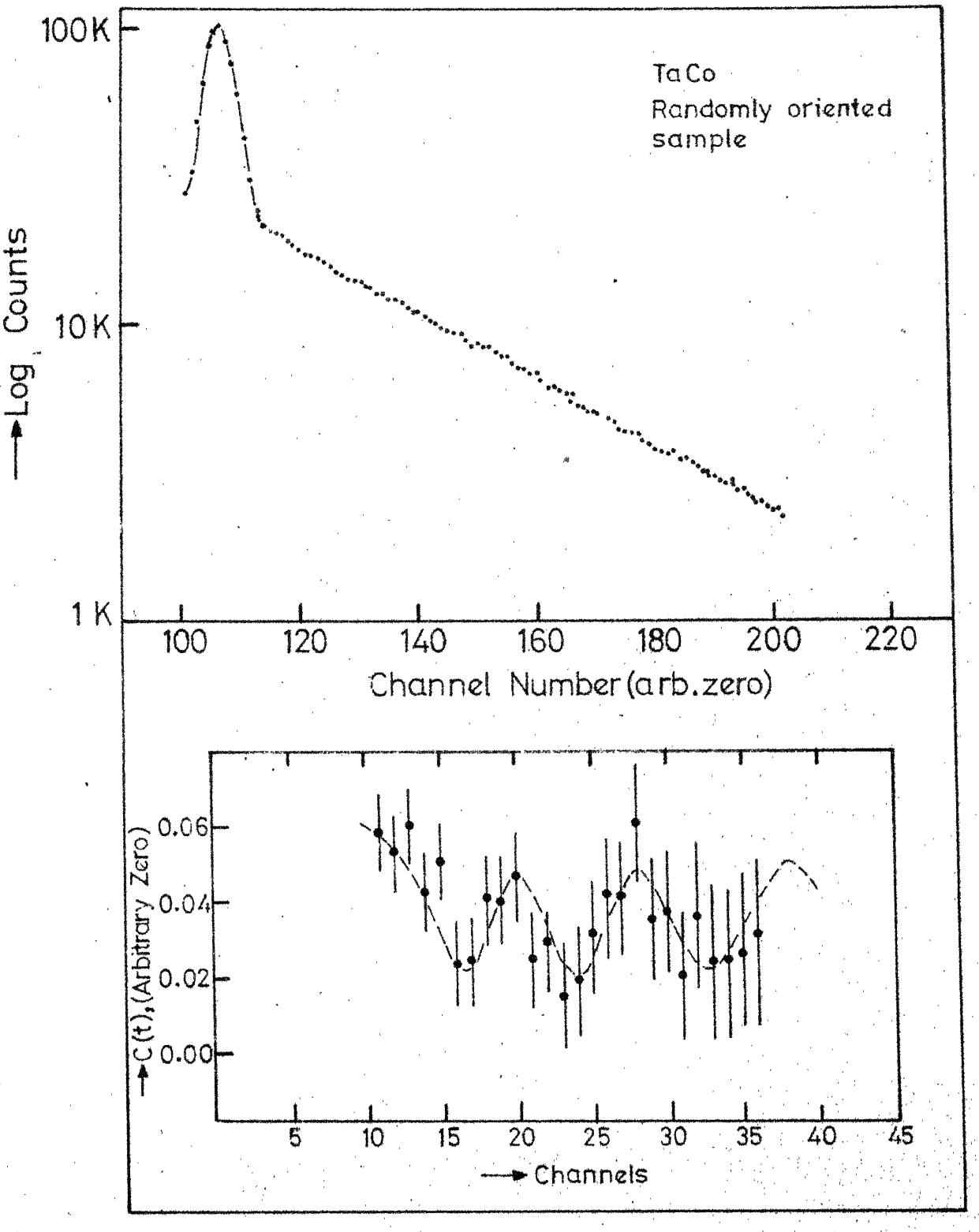

Fig. 10. TDPAC time spectra along with reduced counting rate C(t) of TaCo sample. No external polarizing field was applied (raw data).

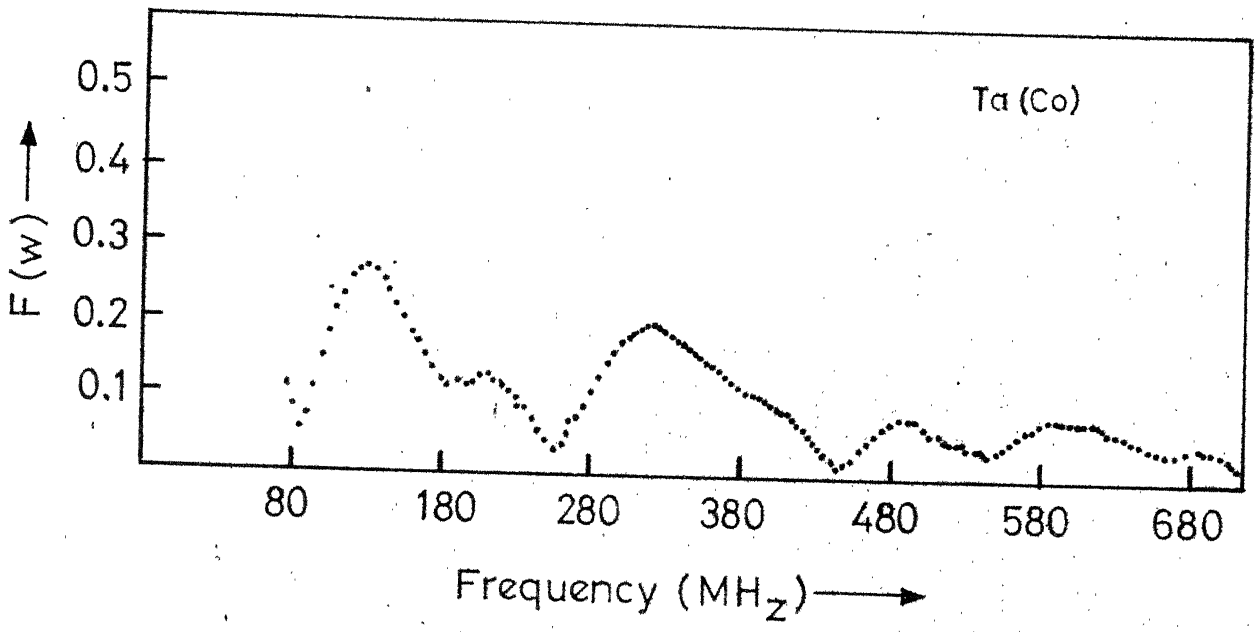

Fig. 11. Fourier transform of the reduced counting rate C(t) for TaCo.

by two frequencies w_L and $2w_L$. In the present study, however, the $2w_L$ modulation could not be observed because the corresponding time period of modulation (T_{2w_L}) was comparable to the fwhm resolution of the system. From the Fourier transform, which indicated two distinct and broad frequency distributions, the hyperfine field value of H_{hf} Ta<u>Co</u> (RT) is deduced to be = (-)347±7 kOe. The sign is not measured in this experiment, but is expected to be negative, based on systematic trends. The basis of error estimation has been the same as detailed in part A.

5. Discussion

In the g-factor measurement only one Larmor precession frequency could be observed. Our value is in agreement with the previously reported value of g = 1.29 ± 0.02 by Matthias et al. [14] and by Agarwal et al. [15]. The observed amplitude is 12%, which is close to the value expected from the unperturbed correlations.

Hyperfine field on Ta in Ni has been very extensively studied [16-23]. The results reported so far along with the present values are detailed in Table I. A restudy was however undertaken with the objective of probing into the composite nature of the field in the Ni matrix, as was pointed out by Bozek et al.[22]. Further Vanderledeen [17] reported an amplitude of 0.3%, while Cameron et al. [18] obtained an amplitude 7.5%. The measurements reported by

Table I

S.No.	Source Preparation	T°K	Solute concentration	H_{hf} (kOe)	Method	Reference
1.	Ni-Hf alloy	1.4	1 at. %	98 (2)	SE	Kontani and Itoh 16
2.	Ni-Hf alloy	-	1 at. %	87.9(25)	DPAC	Vanderledeen 17
3.	Hf-implanted in Ni	RT	0.04 at. %	89.9(10)	DPAC	Cameron et al. 18
4.	Ni-Hf alloy (Single Crystal)	RT	0.07 at. %	90 (4)	DPAC	Oddon et al. 19
5.	Ni-Hf alloy (Single Crystal)	4	3-120 ppm	96.2 (3)	DPAC	Oddon et al. 20
6.	Ni-Hf alloy	RT	-	89.6(10)	Moss	Kaindl and Soloman 21
7.	Thermal diffusion $HfCl_4$ (10 h)	RT	1 at. %	82.6(11)	DPAC	Bozek et al. 22
8.	Ni-Hf alloy	RT	0.025 wt %	87.8(16)	DPAC	Livi et al. 23
9.	Ni-Hf alloy	RT	T	75 (5)	DPAC	Present
10.	Thermal diffusion $HfCl_4$ (10 h)	RT	T	77 (5)	DPAC	Present

Bozek et al. [22], indicated a steep fall in the amplitude of R(t), which lead them to conclude that the hyperfine field has a composite nature, much in contrast to the observation by Cameron et al. More recently Livi et al. [23] reported their measurement on TaNi using an induction melting sample.

We in the present measurement studied two samples made by diffusion of Hf activity and by induction melting. The sample prepared by diffusion did not indicate any observable attenuation in R(t). The method followed by us was exactly similar to the one employed by Bozek et al, except that we carried out the diffusion for 80 h and they did it for 10 h only. Although we did not observe any fall in the amplitude of C(t), the Fourier transform did indicate a broad frequency distribution with its centroid around 150 MHz. It therefore appears that longer diffusion times are necessary to get an appreciable fraction of Hf atoms in substitutional lattice sites. The measurement with TaNi induction melted sample also indicated a similar behaviour. It, therefore, based on the present observations, is concluded that all the observed discrepancies may be explained in terms of rather low solubility of Hf ions in the Ni matrix, which in turn results in a variety of lattice sites occupied by the Hf impurity and thus results in a broad spectrum of hyperfine fields observed by sources

prepared by different methods. The implanted sample used by Cameron et al. with very dilute Hf concentration did indicate a unique hyperfine field, showing that most of the Hf ions came to rest in substitutional lattice sites after implantation. This may lead us to conclude that we do not yet completely understand the source preparation problems and each system should be treated independently.

Concurrent to the present measurement in cobalt matrix, Soares et al.[24] have recently reported the field on TaCo to be H_{hf} TaCo (RT) = 362.4 (5.0), employing e^{-}-γ TDPAC. Their sample was prepared by isotope separator implantation. It is however interesting to note that in both the measurements two distinct frequencies were observed, which as has been pointed out by Soares et al. allows for the possibilities of two different lattice sites acquired by Hf ions in cobalt host. The almost one to one correspondence in the results obtained by contrasting methods of source preparation indeed supports such a point of view. From the intensities of the different frequency components it can be concluded that ~ 30-40% of Hf ions do acquire unique lattice sites. The weak sattellite peaks in Fourier transform show that the Hf ions occupy different lattice sites as well. However, sharper frequency distribution observed by Sores et al corroborate well with the results of Cameron et al. indicating that that in implantation, most of the ions come to rest at unique lattice sites

(probably substitutional). It, therefore, appears that for Hf in Co and Ni hosts ion implantation method is more favourable compared to metallurgical methods.

Expecting a smooth variation in the hyperfine field values around Ta impurity, the expected field on Ta, from the systematics (Fig. (1-3); Chapter V) are -325 kOe and -75 kOe for the cobalt and nickel hosts respectively. These values compare reasonably well with the experimental values. A comparison of the ratios of the reduced hyperfine fields (H_{hf}/μ_h) in the cobalt and nickel hosts normalized to the reduced field in Fe host indicates that the fields are proportional to the host moment only within 30%.

The orbital contribution for a transition series impurity like Ta ($5d^3 6s^2$) is expected to be largely quenched. The major contribution for such a transition series is expected to arise mostly through conduction electron polarization (H_{CEP}). The other significant contributions are the core polarization field (H_{CP}) and the volume overlap polarization (H_v).

Using Shirley et al.'s prescription [5], the conduction electron polarization is expected to be H_{CEP} (Ta$\underline{Co}$) = -290 kOe and H_{CEP} (Ta$\underline{Ni}$) = -110 kOe, where the free electron hyperfine field for Ta is taken to be H_{ns} = 8.3 MOe. Such a H_{CEP} contribution leaves behind a contribution of -60 kOe (cobalt host) and +30 kOe (nickel host) to be explained by

a sum of core polarization and volume overlap polarization. The atomic volume of Ta is 10.3 $\mathring{A}^3$ and therefore a finite volume overlap contribution may be expected. Using our recent estimates presented later in Chapter V, the volume overlap contribution turns out to be H_v^{Co} = +72 kOe and H_v^{Ni} = +53 kOe. This in turn would imply a core polarization field of $H_{CP}^{Co} \simeq$-130 kOe and H_{CP}^{Ni} = -25 kOe, for the two hosts respectively. Using Freeman and Watson's [10] estimates of H_{CP} = 1200 kOe/5d, unpaired spin, the deduced core polarization fields indicate that Ta impurity in cobalt and nickel host develop a d-moment of ~0.1 μ_B and ~0.02 μ_B in cobalt and nickel hosts respectively. However, if we do not take volume overlap contribution the expected d-moments are obviously smaller. Such small values of d-moments are indeed supported by the temperature dependence of the hyperfine field measurements on Ta<u>Ni</u>, reported by Barret et al. [25]. More sensitive and direct probes like diffuse neutron scattering experiments which directly yield the d-moment value and hence H_{CP} are expected to be useful in determining the validity of various hyperfine field models and as well as in understanding the detailed breakdown of various contributions to the hyperfine field on Ta in Co and Ni hosts.

The Balabanov and Delyagin [12] model predicts H_{hf} Ta<u>Co</u> = -295 kOe and H_{hf} Ta<u>Ni</u> = -96 kOe in good agreement with the measured value. The model however does not offer

any microscopic details on the origin of the hyperfine fields.

From the above measurement, it could be concluded that

(1) Conduction electron polarization gives the dominant contribution to the hyperfine field on Ta in Ni and Co.

(2) All the observed discrepancies on H_{hf} Ta Ni could be understood on the basis of the low solubility of Hf atoms in Ni host.

A similar behaviour is also seen from the measurements on Ta in Co host.

C. REFERENCES

1 I. Bergstrom and P. Thieberger, Ark. Fysik. 22, 307 (1962); R. A. Ristinen and A. W. Sunyar, Phys. Rev. 153, 1209 (1967)

2 D. K. Gupta, A. K. Singhvi, D. N. Sanwal and G. N. Rao, Phys. Revs. 7B, 2942 (1973), and references cited therein.

3 W. Koster and E. Wagner, Z. Mettallkunde, 29, 189 (1937), cited in Constitution of Binary Alloys by M. Hansen (McGraw Hill, 1958) p. 511; E. K. Zakharov and B. G. Linshitz, Russ. Met. Fuels, 5, 88 (1962) cited in Constitute of Binary Alloys, Suppl. 2, by I. A. Shunk (McGraw Hill) p 365.

4 Perfection Mica Company, Magnetic Shields Division, Manuals 101-122, 128-129, 176 (USA).

5 D. A. Shirley, S. S. Rosenblum and E. Matthias, Phys. Rev. 170, 363 (1968).

6 M. G. Colley, D. H. Chaplin, D. E. Swan and G. V. H. Wilson, Phys. Lett. A48, 227 (1974).

7 D. H. Howling, Phys. Revs. 155, 642 (1967).

8 H. C. Benski and C. Hohenemser in International Conference on Hyperfine Interaction in Excited Nuclei, Eds. G. Goldring and R. Klish (Gordon and Breach, 1971), p 495.

9 G. N. Rao and A. K. Singhvi, IIT/K Tech. Rep. Phys. 3/74.

10 A. J. Freeman in Hyperfine Structure and Nuclear Radiation, Eds. E. Matthias and D. A. Shirley (North Holland, 1971) p. 427.

11 M. B. Stearns, Phys. Lett. 34A, 146 (1971); M.B. Stearns, Phys. Revs. 8B, 4383 (1973).

12 A. E. Balabanov and N. N. Delyagin, Sov. Phys. JETP 27, 752 (1968).

13 Nuclear level schemes A = 45 through A = 257 from Nuclear Data Sheets, Editors Nuclear Physics Group (Academic, 1973).

14 E. Matthias et al. Nucl. Phys. 40, 656 (1963).

15 Y. K. Agarwal, C. V. K. Baba and S. K. Bhattacharjee, Nucl. Phys. 58, 651 (1964).

16 M. Kontani and J. Itoh, J. Phys. Soc. Japan 22, 345 (1967).

17 J. C. Vanderledeen in Hyperfine Structure and Nuclear Radiation, Eds. E. Matthias and D. A. Shirley (North Holland, 1968) p. 495.

18 J. A. Cameron, P. R. Gardner, W. V. Prestwich, Z. Zamora and D. C. Santry, Can. J. Phys. 48, 2725 (1970).

19 J. L. Oddou, J. Bertheir, P. Pretto and M. Robin, Phys. Stat. Sol. 45b, K139 (1971).

20 J. L. Oddou et al. Phys. Lett. 45A, 445 (1973).

21 G. Kaindl and D. Soloman, Phys. Lett. 6, 1 (1973).

22 E. Bozek, A. Z. Hrynkiewicz, J. Golczewiskii, R. Goss and J. Styczen, Phys. Stat. Sol. 52B, 659 (1972).

23 R. P. Livi, F. P. Livi, J. D. Rodgers and F. C. Zawislak, Phys. Revs. B8, 3098 (1973).

24 J. Soares, K. Krien and K. Freitag, Hyperfine Interactions, 1, 45 (1975).

25 J. Barret et al. Can. J. Physics 50, 619 (1972).

chapter IV

HYPERFINE INTERACTION STUDIES ON ILMENITES AND MAGNETITE ORES USING MOSSBAUER EFFECT

Here, we discuss the Mossbauer effect studies on natural iron ores viz. ilmenites ($FeTiO_3$) and magnetites (Fe_3O_4). Mossbauer effect studies on mineralogical samples is interesting mainly for two reasons: (1) presence of sufficient amount of iron in most of iron ores of the earth and hence quantitative estimates of iron could be obtained using Mossbauer effect, (2) the ability of Mossbauer effect to distinguish between the different oxidation states of Fe, i.e., e.g., Fe^{2+} and Fe^{3+}, which in turn reflects on the geochemical genetics and the subsequent weathering history of the sample under perview.

---

* Published in Phys. Stat. Solidi (a) 23, 321 (1974).

A. ILMENITES

1. Introduction

Ilmenite is common in nature as an accessory mineral in basic igneous rocks, notably the gabbross. Its structure is similar to that of hematite (Fe_2O_3), except that the octahedral voids are occupied by Ti^{4+} and Fe^{2+} ions [1]. It is also an ubiquitous mineral in beach sands, concentrated by weathering process. The beach sands of Kerala (India) and Florida (U.S.A.) are important members of this category. During weathering and concentration, the alteration process includes oxidation and leaching. The resulting structure is disordered and resembles pseudo-brookite [2], however, the arrangement of oxygen atoms as well as their relative composition is preserved in this process. Ilmenites from beach sands have dominant Fe^{3+} compared to others [3]. Such an enrichment of Fe^{3+}, indicates the extent of weathering the mineral has undergone. From a comparison of measured transmission through the sample, with the transmission of another sample of known stoichiometry, it is possible to make an estimate of iron content of the sample.

2. Experimental

The details of the Mossbauer spectrometer and its performance are given elsewhere [4]. A Nuclear-Data 512 multichannel analyzer in a multiscaling mode was used for

data acquisition. A Xe-CH_4, proportional counter with an fwhm of 14% was used for the detection of 14.4 keV -rays. The samples used were finely powdered and the absorbers were prepared by sandwiching the samples between thin paper sheets. All the spectra were recorded at room temperature. Since we used a sinusoidal drive, the spectra were linearized by fitting the data to a sine function with the help of a computer program.

3. Measurement

The Mossbauer spectra obtained for ilmenite samples from Kishengarh, Bihar, Kodaikanal, Kerala and Nellore (India) and from Florida (USA) along with a spectrum of a synthetic sample (Temp-Press Inc., USA) are given in Figs. (1) and (2). The Mossbauer parameters are detailed in Table I. The errors are the uncertainties in locating the peak positions. The statistical uncertainties are somewhat less.

Quantitative estimates of iron was obtained using the areas under the peaks. The recoil-free fractions were assumed to be same in all the cases. The samples were also chemically analyzed and the results are also presented in Table I.

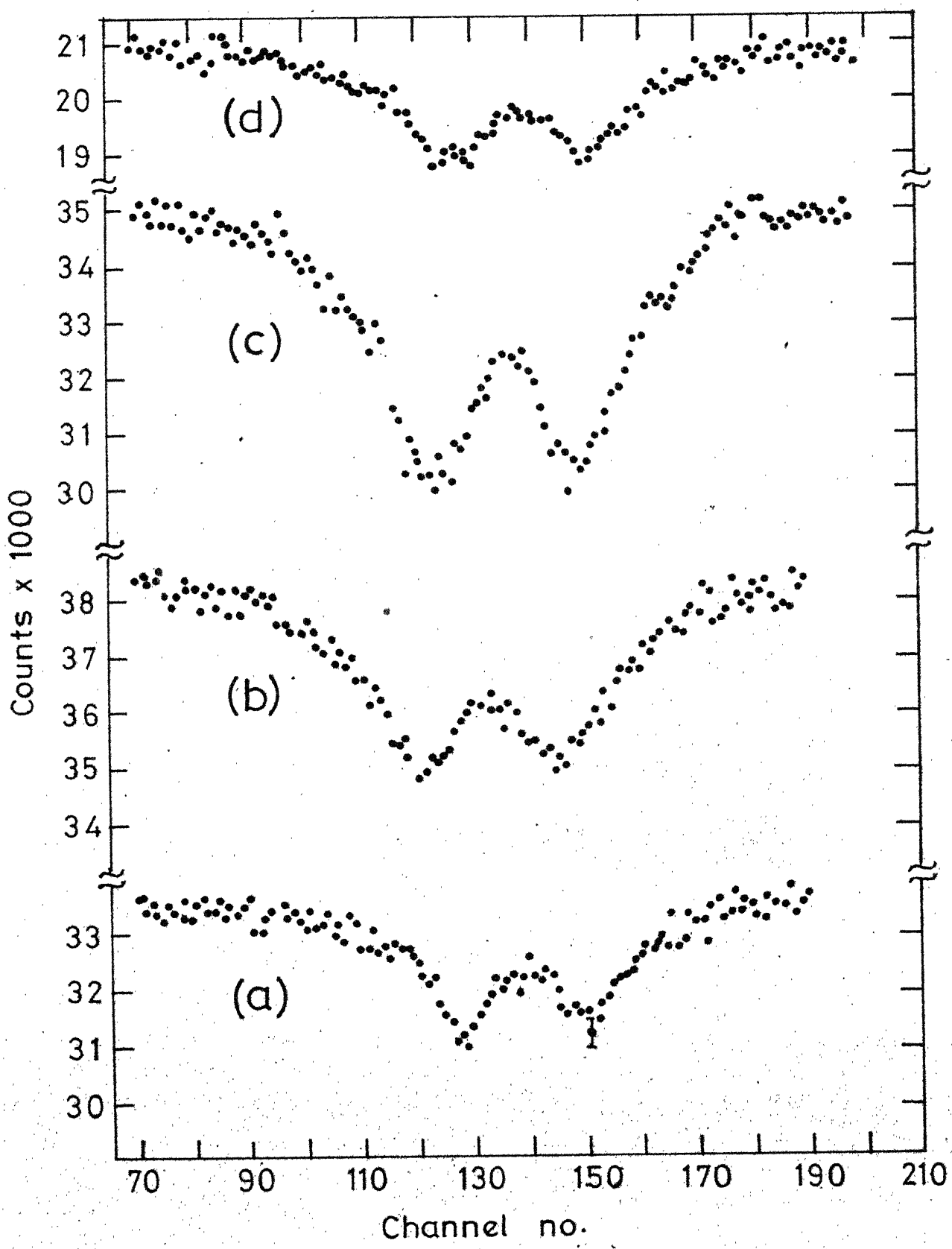

Fig. 1. Mossbauer spectra of Ilmenites from primary high temperature origin, a) Synthetic, b) Kishangarh, c) Kodaikanal, d) Other.

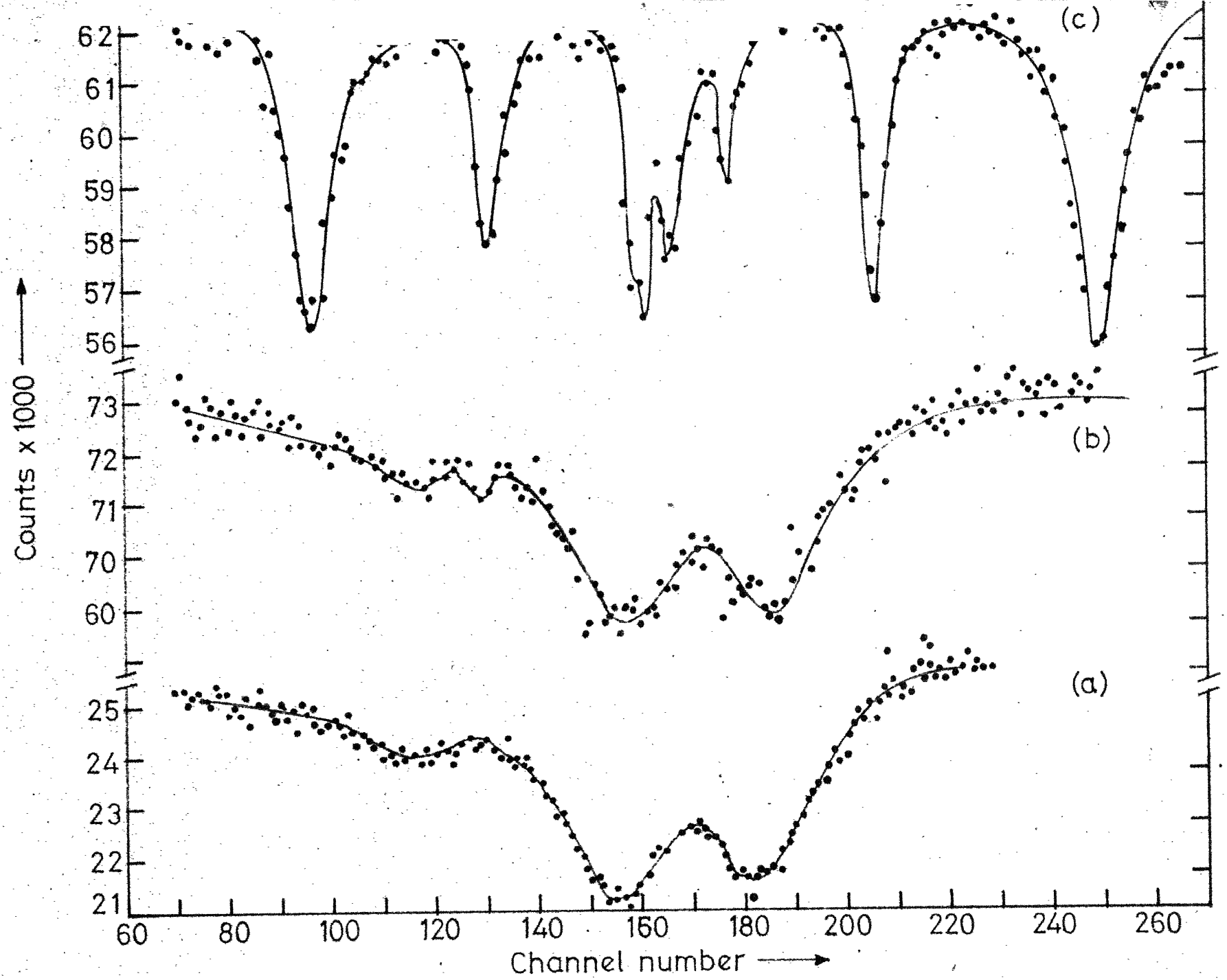

Fig. 2. Mossbauer spectra of ilmenites from placer secondary sources a) Florida, b) Kerala, c) Seidapuram.

Table I: Mossbauer Parameters of Ilmenites of Different Geochemical Origins

S.No.	Sample	Mossbauer Parameters			Fe^{2+}/Fe (%)	% Iron content (Mossbauer)	% Iron content (Chemical)
		Isomer shift[1] (mm/sec)	Quadrupole splittings (mm/sec)	Hyperfine field (kOe)			
1.	Synthetic	1.23±0.02	0.71±0.02	-	100	36.8	36.8
2.	Kishengarh	1.34±0.02	0.73±0.02	-	100	25	36
3.	Bihar	1.20±0.02	0.71±0.02	-	100	36	36.5
4.	Kodai Kanal	1.29±0.02	0.73±0.02	-	100	31	36.8
5.	Kerala	0.61±0.02	0.77±0.02	-	23	36	36.8
		1.54±0.02	0.28±0.02	-			
6.	Florida	0.67±0.02	0.62±0.02	-	13.5	5.5	7.5
		1.78±0.02	< 0.2				
7.	Saidapuram (Nellore)	0.90±0.2	0.3 ±0.2	540±5	10	9.6	9.7
		1.27±0.2	0.8 ±0.2				

[1] w.r.t. sodium nitro prusside.

4. Discussion

Various phases present in the samples under study may be identified using the fact that the different oxidational states of Fe have different isomer shift. The isomer shift was shown to be

$$\delta = \frac{2\pi Ze^2}{5} \left[|\psi(0)|_A^2 - |\psi(0)|_S^2 \right] \left[\langle R_{ex}^2 \rangle - \langle R_{gnd}^2 \rangle \right]$$

The isomer shift is proportional to the difference in the s-electron density at the source and at the absorber nuclei. The isomer shift changes by a sizeable amount for different oxidation states of Fe. Such a difference arises because of difference in the shielding of 3s electrons by 3d electrons. Physically, the 3s-electrons spend a part of time, farther from the nucleus compared to the 3d-electron. The electrostatic potential experienced by them therefore depends on the screening effect of inner electrons. Addition of a 3d-electron reduces the attractive Coulomb potential and this causes the 3s wave function to expand, thereby reducing its density at the nucleus. Thus, a removal of 6th d-electron in going from ferrous to ferric state, would result in an increased charge density at the nucleus. Further since $\delta R/R$ is negative for ^{57}Fe, an increase in charge density would consequently imply a proportionate decrease in isomer shift for ^{57}Fe: i.e.

$$|\psi_{3+}(0)|^2 > |\psi_{2+}(0)|^2 \longrightarrow \delta_{3+} < \delta_{2+}$$

Systematic measurements of the Mossbauer spectra of various iron compounds coupled to theoretical calculations by Walker et al.[5] and Danon et al. [6], have established that the range of values of isomer shifts is distinct for various oxidation states of Fe. In such conditions, it has been possible to identify the different oxidation states of iron from the measured isomer shift and this has been the basis of present investigation. Table II below gives typical ranges of the isomer shifts referred to sodium nitropursside standard [7].

Table II

Oxidation state	Fe^{2+}	Fe^{3+}	Fe^{4+}	Fe^{6+}
Isomer shift (mm/sec)	+1.0- +1.8	+0.4- +0.9	+0.3	-0.6
Typical example	FeF_2	$FePO_4$	$SrFeO_3$	K_2FeO_4

The ilmenites chosen for the present study may be grouped into two categories, viz.,

i. Ilmenites of primary high temperature origin, and

ii. Secondary ilmenites of placer origin.

i. Ilmenites of primary high temperature origin

Four ilmenites viz., synthetic, Kishengarh, Bihar and Kodaikanal fall in this category. The synthetic sample was

chosen for its high purity and ideal stoichiometry. The Mossbauer spectrum of the synthetic sample is a doublet with an isomer shift of +1.23 mm/sec (w.r.t. SNP), which is typical of Fe^{2+}. The quadrupole splitting is 0.71 mm/sec. These values are in fair agreement with the earlier reported values [8]. The existence of two small satellite peaks reported by Ruby and Shirane [8] is also confirmed in the present studies. These peaks may be due to atmospheric oxidation of ferrous iron to a slight extent. The isomer shift of the ilmenite samples from primary igneous association, viz., Bihar, Kishengarh and Kodaikanal, cluster around 1.3 mm/sec, showing that these samples have a near stoichiometric composition, with iron mostly in Fe^{2+} state. The observed quadrupole splittings are also nearly the same as that observed for the synthetic sample. The possible oxidation of these samples leading to Fe^{3+} is seemingly low and an upper limit of 5% is obtained for Fe^{3+} out of the total Fe content.

ii. Secondary ilmenites of placer origin

The major source of these ilmenites are beach sands (placer) deposits, which have been formed by accumulation of heavy minerals (with higher specific gravity) due to continuous weathering and wave action. The samples from the beaches of Kerala, Florida and Saidapuram fall into this category. The Mossbauer spectra of Kerala and Florida

and Saidapuram fall into this category. The Mossbauer spectra of Kerala and Florida samples clearly indicate the coexistence of Fe^{2+} and Fe^{3+} ions. The dominance of Fe^{3+} in both these spectra clearly establish that these samples have undergone considerable weathering and that the Florida sample has undergone relatively through more cycles of weathering. The ratio of the Fe^{2+} to Fe^{3+} for ilmenite ore of Florida origin was measured previously [2] using the Mossbauer effect and our result is in agreement with theirs.

In addition the Saidapuram sample shows a doublet superimposed on a magnetic hyperfine structure pattern, which is typical of a solid solution $(1-x)\ FeTiO_3-(x)\ Fe_2O_3$. The spectra thus revealed that the sample contains a substantial fraction (90%) of hematite with about 10% ilmenite.

Thus the ilmenites of primary high temperature origin could be unambiguously distinguished from the secondary type on the basis of isomer shift. Further, the relative intensities of Fe^{2+} and Fe^{3+} in the sample indicates the geochemical genetics and as well as the subsequent weathering the sample has undergone. The quantitative estimates obtained using the Mossbauer spectroscopy are given in Table I. From these data one finds that these values are comparable to the values obtained from the chemical methods.

B. MAGNETITES

1. Introduction

Magnetite is one of the most abundent oxide minerals of iron and has its occurrence in igneous and in sedimentary sources. In igneous rocks it is commonly of late stage magmatic seggregation origin and is associated with the basic magma. Because of its high temperature genesis, titanium enrichment in its composition is frequently observed. For magnetites in sedimentary formations, many theories have been put forth [9-13].

Since the conditions of formation of magnetites differ, it is expected that compositional variations should also exist. As pointed out earlier, a study of such variations, would enable us to understand the genetic history of the sample. Structurally, magnetite is an inverse spinel. From its structure, composition for this mineral should contain 68.97% Fe_2O_3 and 31.03% FeO. However, this ratio varies in a natural sample, which may be interpreted as due to a varience in oxygen supply during its formation. In the present studies two samples from Bihar (India) (one of igneous origin and the other from banded iron formations), and two samples (one from Karnataka and another from Tamilnadu (India)), associated with banded iron formations [14] were taken up. For comparison, one synthetic sample (Temp-Press Research Inc. USA) was also studied.

2. Experimental

The experimental conditions were essentially similar to those described in part A.

3. Measurement

The Mossbauer spectra obtained for these magnetite samples are given in Figs. (3) and (4). The Mossbauer parameters are provided in Table III. The errors are the errors in the peak positions. The statistical uncertainties are however somewhat less.

4. Discussion

The magnetites chosen for the present study may be classified into two categories, viz.,

i. Magnetites of high temperature origin

ii. Magnetites of possible low temperature origin

i. Magnetites of high temperature origin

a. Synthetic magnetite

The spectrum given in Fig. (3(a)) is clearly a superposition of two iron spectra with different isomer shifts and different hyperfine fields corresponding to sites A (tetrahedral) and sites B (octahedral), having ferric and ferric + ferrous ions respectively. The analysis was done by separating the spectra following the procedure suggested by Bauminger et al. [15]. The present values compare well with the earlier reported values [15-17].

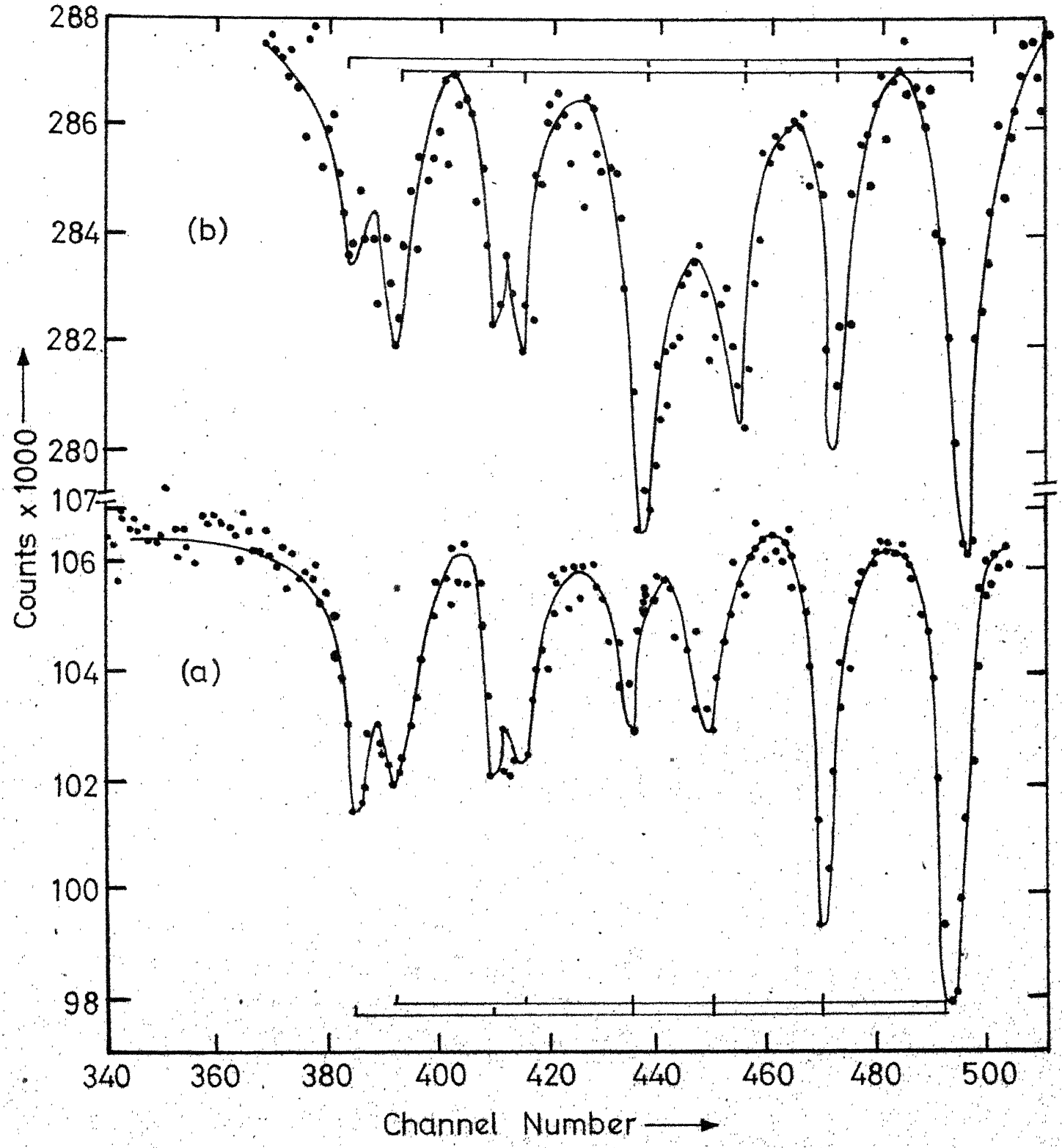

Fig. 3. Mossbauer spectra of magnetites of high temperature origin a) Synthetic, b) Massive magnetite (Diher).

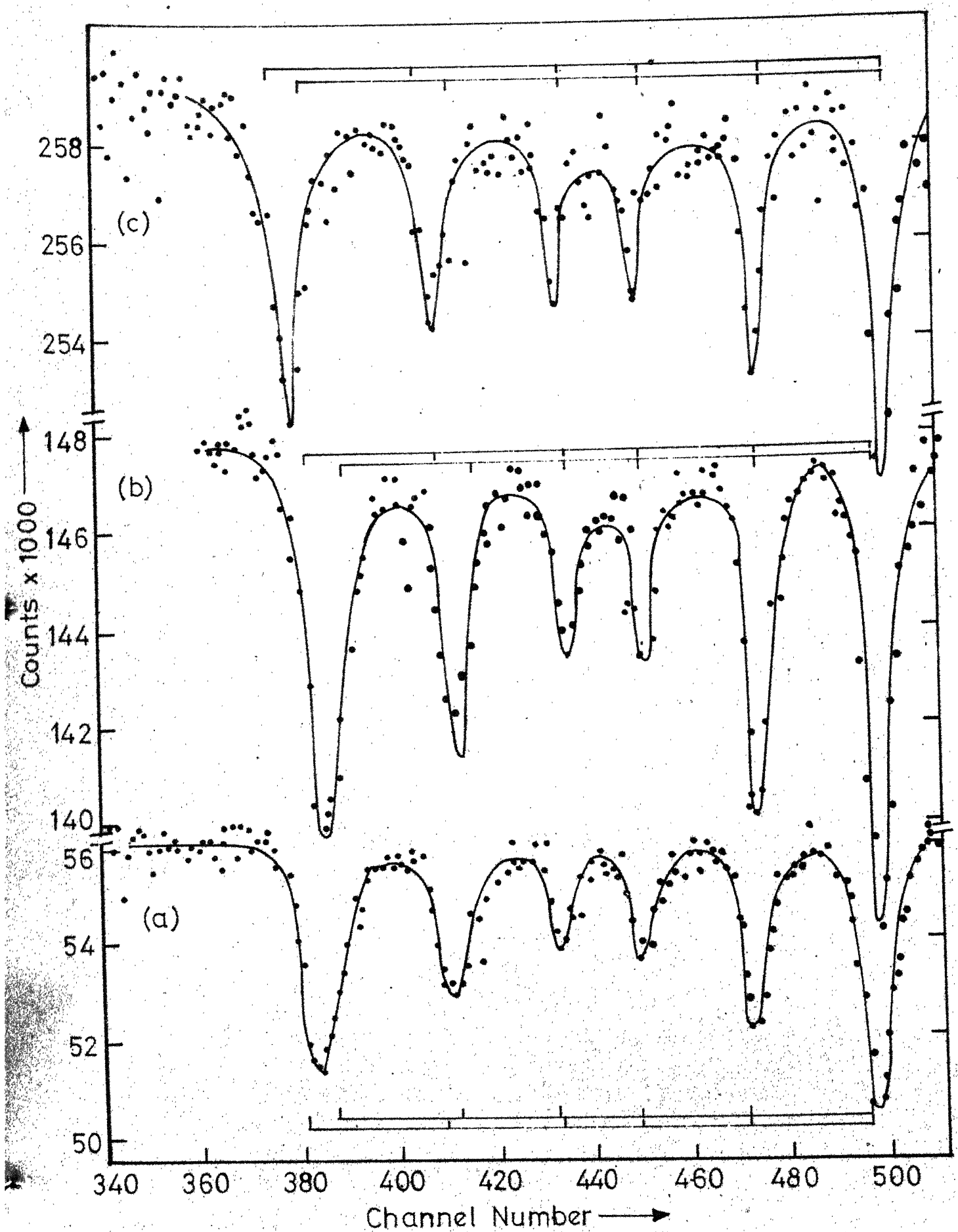

Fig. 4. Mossbauer spectra of magnetites of sedimentary origin
a) Magnetite (BMQ) Karnataka, b) Magnetite (BMQ) Tamilnadu,
c) Magnetite (BHQ) Bihar.

Table II. Mossbauer Parameters of Magnetites of Different Geochemical Origins.

S.No.	Sample	Mossbauer Parameters			
		Site	Isomer shift* (mm/sec)	Hyperfine field (kOe)	Quadrupole splittings (mm/sec)
1	Synthetic Magnetite	Tetra.(A)	0.5±0.1	487±4	0.1±0.1
		Octa. (B)	1.1±0.1	441±4	0.1±0.1
2	Igneous Magnetite (Bihar, India)	Tetra.(A)	0.6±0.1	483±4	0.1±0.1
		Octa. (B)	1.0±0.1	453±4	0.0±0.1
3	Magnetite, BMQ (Karnataka, India)	Tetra.(A)	0.5±0.2	497±8	0.0±0.2
		Octa. (B)	0.8±0.2	480±8	0.1±0.2
4	Magnetite, BMQ (Tamilnadu, India)	Tetra.(A)	0.5±0.2	497±8	0.1±0.2
		Octa. (B)	0.9±0.2	476±8	0.1±0.2
5	Magnetite, BHQ (Bihar, India)	Tetra.(A)	0.4±0.2	526±8	0.0±0.2
		Octa. (B)	0.8±0.2	508±8	0.2±0.2

* w.r.t. Sodium Nitro Prusside.

b. Magnetites from igneous associations of Bihar

The similarity of Mossbauer parameters with those obtained for the synthetic sample indicate a near stoichiometric composition of the sample, which is expected from a sample of high temperature origin. Further, there is a clear indication of a quadrupole doublet, Fig.(3(b)), which is possibly due to the titanium enrichment in the sample. This sample was chosen from an igneous association in nature and microscopic investigations in fact indicated the presence of thin lamallae of titanium-rich portions along the cleavage planes in magnetite. These observations further confirmed the titanium enrichment, as evidenced in the Mossbauer spectra.

ii. Magnetites of possible low temperature origin

The samples from Karnataka, Tamilnadu and Bihar fall into this category. Of these, the samples from Karnataka and Tamilnadu are from banded magnetite silica formations, and the Bihar sample is from banded haematite quartzite formations. The Tamilnadu sample is, however, an enrichment of magnetite within these banded magnetite formations due to a near complete leaching of silica.

The spectra of these three samples - Fig. (4) are once again a superposition of two spectra. The isomer shift obtained, however, indicated the presence of iron in ferric state only. Further the magnetic hyperfine field on the

two sites were found to be almost equal. These observations suggest a possible oxidation of magnetite to hematite. These banded magnetite quartzite formations are typical metamorphosed horizons and although initially magnetite was one of the dominant iron oxide mineral, much of it got oxidized to hematite during metamorphism, which thus explains the indication of Fe^{3+} in the spectra. A comparative study of these spectra with that of the synthetic sample clearly brings out the near absence of ferrous iron phase, thus supporting above explanation.

The sample taken from the banded hematite-quartzite formation of Bihar also indicated the presence of a ferric phase, which again should be due to near complete oxidation of magnetite.

Thus it is possible to differentiate magnetites of igneous origin from those of low-temperature origin. In the former a near stoichiometric structure is evidenced, while in the latter, a dominance of ferric phase over ferrous phase occurs. Indication of titanium enrichment in the magnetites of high-temperature origin could be very clearly observed in the spectrum.

C. REFERENCES

1 W. A. Deer, R. A. Howie and J. Zussman, Rock Forming Minerals, Vol. 5, Ed. 4 (Longmans, 1965).

2 G. Teufer and A. K. Temple, Nature, 211, 179 (1966).

3 T. C. Gibbs, N. N. Greenwood and W. Twist, J. Inorg. Nucl. Chem., 31, 947 (1969).

4 A. K. Gupta, K. R. Sarma, J. J. Huntzicker and G.N. Rao, Rev. Sci. Instrum. 45, 1423 (1974).

5 L. R. Walker, G. K. Wertheim and V. Jaccarino, Phys. Rev. Letts. 6, 98 (1961).

6 J. Danon, Rev. Mod. Phys. 36, 459 (1964).

7 J. Danon, in Chemical Applications of Mossbauer Spectroscopy, Eds. V. I. Goldanskii and R. H. Herber (Academic, 1968), p. 159; V. G. Bhide, Mossbauer Effect and its Applications (Ta McGraw Hill, 1973); G. K. Wertheim, Mossbauer Effect: Principles and Applications (Academic, 1971).

8 S. L. Ruby and G. Shirane, Phys. Revs. 123, 1239 (1961).

9 H. L. James, Econ. Geol., 49, 235 (1954).

10 D. L. White, Minn. Geol. Sur. Bull. 38 (University of Minnessotta, 1954).

11. J. L. Hough, J. Sed. Petrol. 28, 414 (1958).

12 N. K. Huber, Econ. Geol. 53, 123 (1958).

13 N. K. Huber, Econ. Geol. 54, 82 (1959).

14 K.V.G.K. Gokhale and T.C. Rao, Ore Deposits of India (Thomson, 1974).

15 R. Bauminger, S. G. Cohen, A Marinov, S. Ofer and E. Segal, Phys. Revs. 122, 1447 (1961).

16 J. M. Daniels and A. Rosencwaig, J. Phys. Chem. Sol. 30, 1961 (1969).

17 R. S. Hargrove and W. Kundig, Sol. St. Commun., 8, 303 (1970).

chapter V

DILUTE IMPURITY HYPERFINE FIELDS IN FERROMAGNETIC Fe, Co AND Ni MATRICES -THEIR ORIGINS AND COMPARISONS OF THE BEST EXPERIMENTAL VALUES WITH THE EXISTING MODELS

A. INTRODUCTION

Samoilov et al. [1], first reported that non-magnetic impurities dissolved in ferromagnetic hosts like Fe, Co and Ni experience large magnetic hyperfine fields. Since then, the magnitude and the sign of these dilute impurity hyperfine fields have been measured on almost all the impurities for the iron host. These fields have been very useful in understanding a variety of solid state and nuclear physics phenomena. The hyperfine fields have proved to be very useful, as a diagnostic device in providing a local probe of the electronic state of an atom in metals. These large internal hyperfine fields, which are not otherwise available in the laboratory are extensively used in the study of the magnetic properties of very short-lived nuclear excited states [2].

Precise theoretical estimates of these fields are practically impossible, due to the complexity of the Hamiltonian and the many body techniques involved. The fact that these fields show a very regular systematic variation, when plotted as a function of impurity electronic configuration, prompted semi-theoretical approaches, to decode the basic mechanisms involved. The present status seems to be that we understand all the major mechanisms responsible for these fields [3-14], however a precise breakdown of their relative strengths is yet to be achieved.

The present chapter describes our studies on the systematics of these fields. Comparisons of the experimentally measured hyperfine fields, with the predictions of the various models are presented.

B. HOST MOMENT DEPENDENCE OF THE HYPERFINE FIELDS

For a detailed study of the host moment dependence and for the model comparisons, all the experimental data reported so far on the dilute impurity hyperfine fields in Fe, Co and Ni hosts was collected and collated [15]. From this tabulation, the 'best' experimental values were chosen, after a careful consideration of various factors like, the impurity concentration, the temperature of the measurement and the experimental technique employed. These values are tabulated in reference [16]. A plot of these values vs th

impurity electronic configuration is given in Figures (1-3).

The magnitudes of the hyperfine fields for an impurity in Fe, Co and Ni hosts are often assumed to be proportional to the magnetic moments of the respective host matrices ($\mu_{Fe} = 2.22\ \mu_B$, $\mu_{Co} = 1.72\ \mu_B$ and $\mu_{Ni} = 0.604\ \mu_B$). However, this assumption was investigated in greater detail. To examine this, the 'reduced fields' (H_{hf}/μ_h) for Fe, Co and Ni hosts were calculated. A plot of these ratios, i.e. $\{(H_{hf}/\mu_h)_{Co}/(H_{hf}/\mu_h)_{Fe}\}$ and $\{(H_{hf}/\mu_h)_{Ni}/(H_{hf}/\mu_h)_{Fe}\}$ vs the impurity electronic configuration is given in Fig.(4). It is clearly seen that the observed hyperfine fields are not strictly proportional to the host moments. The deviations are usually larger than 10%.

Such deviations are in fact expected, should we consider a detailed dependence of the hyperfine fields on the host and impurity moments. Thus, based on Kushida et al.'s discussion [17], we have,

$$(H_{hf})_{imp} = a^{core} \cdot \mu_i + a^{ns} \cdot \mu_i + a^{3d-4s} \cdot \mu_i + a_1^{core} \cdot \mu_h + a_1^{ns} \cdot \mu_h \qquad (1)$$

Where μ_i and μ_h are the impurity and the host moments respectively. a^{core} represents the contributions due to core-polarization of the impurity shells by the impurity moment. a^{ns} is the 'self' polarization of the conduction electrons, due to impurity moment, a^{3d-4s} represents the contributions

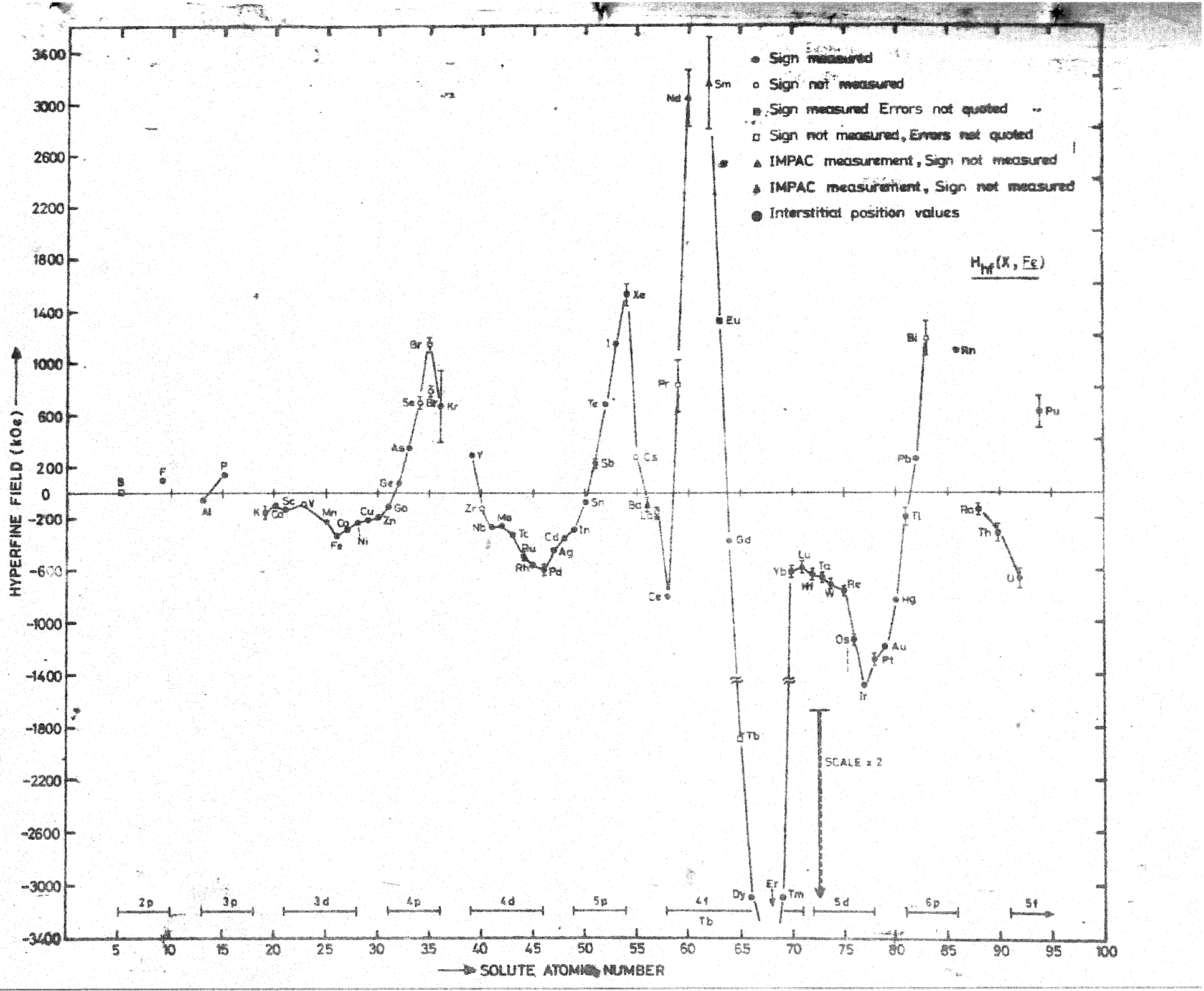
Sign measured
Sign not measured
Sign measured Errors not quoted
Sign not measured, Errors not quoted
IMPAC measurement, Sign not measured
IMPAC measurement, Sign not measured
Interstitial position values
$H_{hf}(X, Fe)$
HYPERFINE FIELD (kOe)
SOLUTE ATOMIC NUMBER
SCALE x 2
2p
3p
3d
4p
4d
5p
4f
Tb
5d
6p
5f
3400
3000
2600
2200
1800
1400
1000
600
200
0
-200
-600
-1000
-1400
-1800
-2200
-2600
-3000
-3400
5
10
15
20
25
30
35
40
45
50
55
60
65
70
75
80
85
90
95
100
B
F
P
Al
K
Ca
Sc
V
Mn
Co
Fe
Ni
Cu
Zn
Ga
Ge
As
Se
Br
Kr
Y
Zr
Nb
Mo
Tc
Ru
Rh
Pd
Ag
Cd
In
Sn
Sb
Te
I
Xe
Cs
Ba
La
Ce
Pr
Nd
Sm
Eu
Gd
Tb
Dy
Er
Tm
Yb
Lu
Hf
Ta
W
Re
Os
Ir
Pt
Au
Hg
Tl
Pb
Bi
Rn
Ra
Th
U
Pu

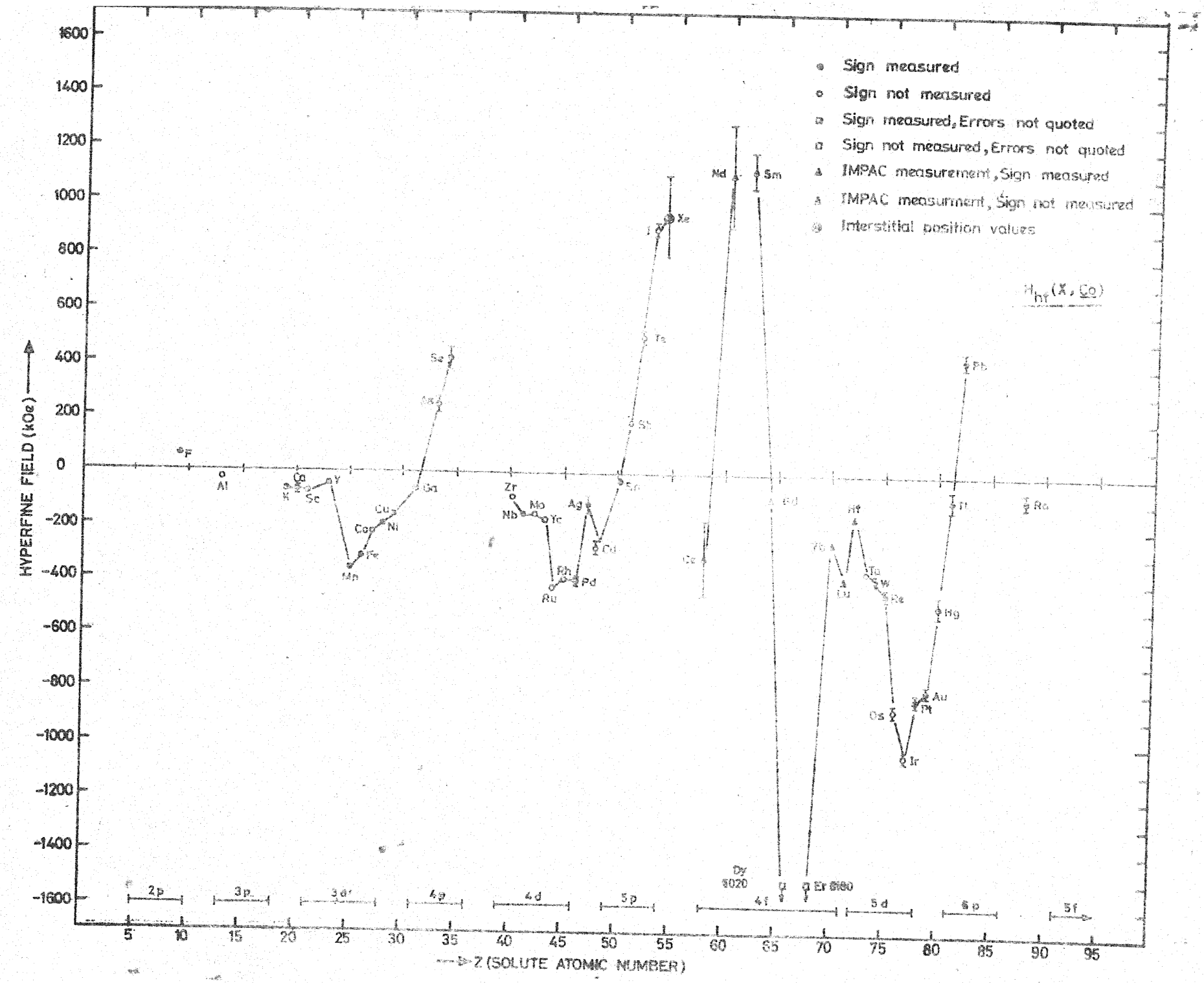
Sign measured
Sign not measured
Sign measured, Errors not quoted
Sign not measured, Errors not quoted
IMPAC measurement, Sign measured
IMPAC measurment, Sign not measured
Interstitial position values
$H_{hf}(X, Co)$
HYPERFINE FIELD (kOe)
Z (SOLUTE ATOMIC NUMBER)
1600
1400
1200
1000
800
600
400
200
0
-200
-400
-600
-800
-1000
-1200
-1400
-1600
5
10
15
20
25
30
35
40
45
50
55
60
65
70
75
80
85
90
95
2p
3p
3d'
4p
4d
5p
4f
5d
6p
5f
F
Al
Ca
K
Sc
Y
Se
As
Ga
Ti
V
Cr
Mn
Fe
Co
Ni
Cu
Zr
Nb
Mo
Tc
Ru
Rh
Pd
Ag
Cd
Sn
Sb
I
Xe
Nd
Sm
Ce
Dy
8020
Er 8180
Yb
Hf
Ta
W
Re
Os
Ir
Pt
Au
Hg
Pb
Th
Ra

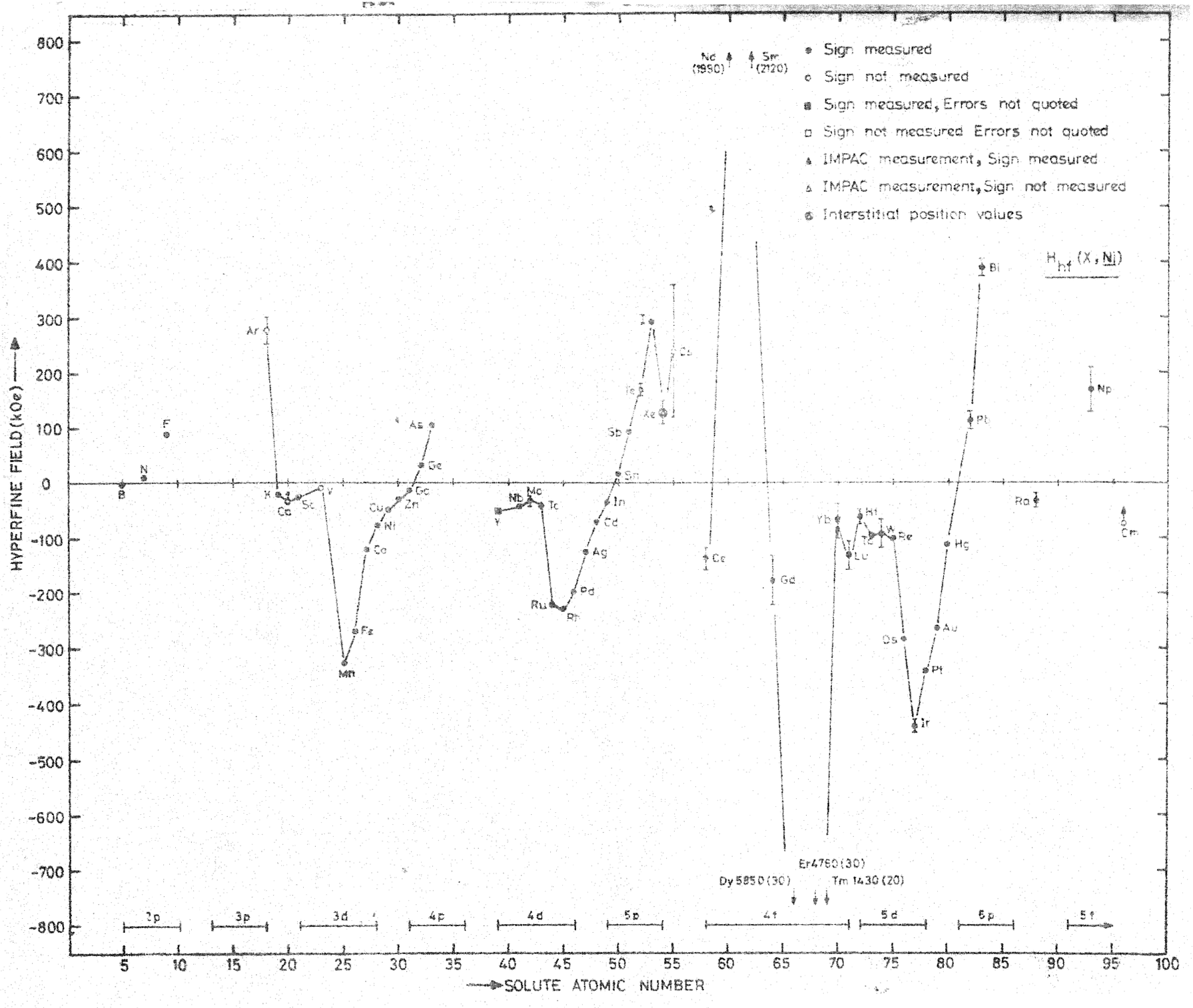
Nd (1990)
Sm (2120)
Sign measured
Sign not measured
Sign measured, Errors not quoted
Sign not measured Errors not quoted
IMPAC measurement, Sign measured
IMPAC measurement, Sign not measured
Interstitial position values
$H_{hf}(X, \underline{Ni})$
HYPERFINE FIELD (kOe)
SOLUTE ATOMIC NUMBER
Er4760(30)
Dy5850(30)
Tm 1430(20)
2p
3p
3d
4p
4d
5p
4f
5d
6p
5f

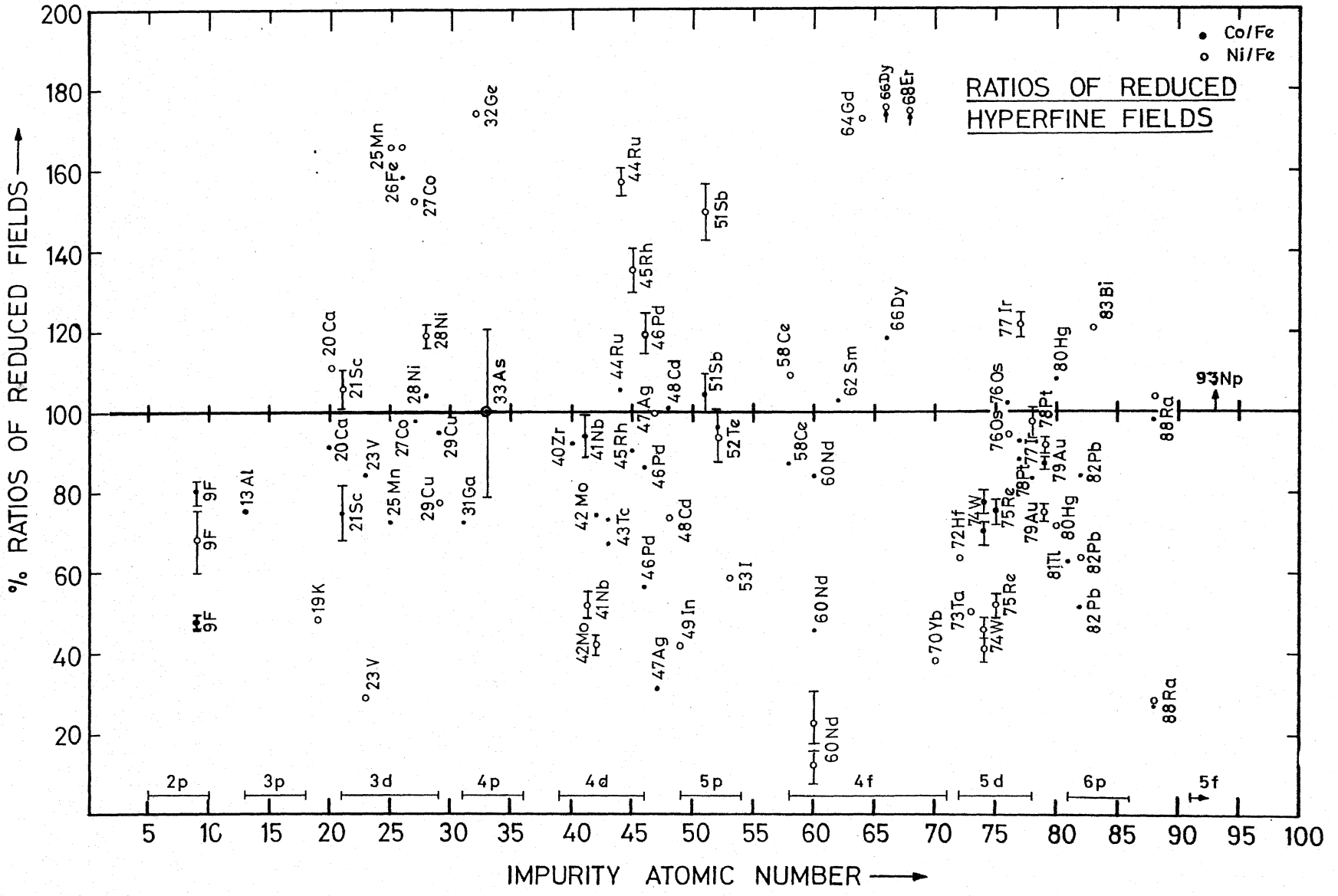
RATIOS OF REDUCED HYPERFINE FIELDS
Co/Fe
Ni/Fe
% RATIOS OF REDUCED FIELDS
IMPURITY ATOMIC NUMBER
2p
3p
3d
4p
4d
5p
4f
5d
6p
5f

FIG. 4

due to an admixture of 3d-4s wave functions. a_1^{core} represents core polarization due to host and a_1^{ns} is the conduction electron polarization due to the host moment. All these contributions are discussed in a somewhat greater detail in the following section. It can be very well realized that it is rather futile to expect any rigid proportionality with the host moment as has been very clearly evidenced in Fig. (4).

C. HYPERFINE FIELD MODELS : COMPARISON WITH EXPERIMENTAL VALUES

1. Hamiltonian

A general Hamiltonian for an impurity atom, characterized by the quantum numbers L, S, and J, embedded in a ferromagnetic host can be given as [4],

$$H = V_{cf} + 2\mu_B \vec{H}_{ex}.\vec{S} + \lambda \vec{L}.\vec{S} - \gamma_I \vec{H}_c \cdot \vec{I} + 2\mu_B \gamma_I \langle r^{-3} \rangle \{(-k)\, \vec{S}.\vec{I}\}$$
$$+ 2\mu_B \mu_I \sum_i \frac{\vec{I}_i \cdot \vec{I}}{r_i^3} + 2\mu_B \mu_I \sum_i \left[\frac{3(\vec{r}_i \cdot \vec{s}_i)(\vec{r}_i \cdot \vec{I})}{r_i^5} - \frac{\vec{s}_i \cdot \vec{I}}{r_i^3} \right] \qquad (2)$$

where μ_B is the Bohr magneton, $\gamma_I = g_I \mu_N$ is the nuclear g-factor and μ_N is the nuclear magneton. V_{cf} is the crystal field potential, describing the influence of surrounding atoms. $\vec{H}_{ex}$ is the magnetic exchange field due to host moments. $\lambda \vec{L} \cdot \vec{S}$ represents the electronic spin-orbit

interaction term. $\vec{H}_c$ represents the contributions from the spin polarization of the conduction electrons via a Fermi contact interaction [18], $k\vec{S}\cdot\vec{I}$ represents the core spin-polarization of the filled shells of the impurity atoms and this also generates a Fermi contact hyperfine field. k is a parameter measuring the extent of core polarization. $\vec{l}_i\cdot\vec{I}$ represents the hyperfine interaction between the magnetic field set up due to the orbital motion of the electrons, $\vec{l}_i$ being the angular momenta of the i^{th} electron with a position vector $\vec{r}_i$. The last term represents nuclear dipolar-electron spin dipolar interaction term, the external, demagnetizing and the Lorentz fields have been discussed in Chapter I.

The first three terms in the Hamiltonian are largest and thus determine the zeroth order wave function. The relative magnitudes of V_{cf} and $\lambda\vec{L}\cdot\vec{S}$ allow us to distinguish between two cases and accordingly a further discussion could be carried over under two subheadings:

2. Strong Crystal Fields - Non rare-earth Solutes ($\lambda\vec{L}\cdot\vec{S} \ll V_{cf}$)

3. Weak Crystal Fields - Rare-earth solutes ($\lambda L\cdot S \gg V_{cf}$)

2. Strong Crystal Fields - Non rare-earth Solutes ($\lambda\vec{L}\cdot\vec{S} \gg V_{cf}$)

For large crystal fields, the orbital angular momentum is almost quenched, i.e., $\langle L_z \rangle \simeq 0$. This is largely true for transition series solutes. For example, in iron series the

unquenched orbital angular momentum contribution is typically ~ 10 kOe, which is only a few percent of the free atomic hyperfine field. Such small residual values of angular momenta, arise essentially due to the distortion of the orbital wave function by the weak spin-orbit part. The Hamiltonian is further simplified as the dipolar term also vanishes, if the ferromagnetic host has a cubic symmetry (Dipolar terms vanish for S-state ions as well). Under such conditions, the Hamiltonian reduces to

$$\mathcal{H} = V_{cf} + 2\mu_B \vec{H}_{ex}\cdot\vec{S} - \gamma_I \vec{H}_c\cdot\vec{I} - 2\mu_B\gamma_I \langle r^{-3}\rangle (k)\, \vec{S}\cdot\vec{I} \quad (3)$$

Under these conditions, the crystal fields determine the zeroth order electron wave function. The exchange term can then be [4] used to get the spin expectation value of the ion in the lattice. The last two terms can be combined to define an effective hyperfine field at the nuclear site, i.e.,

$$\gamma_I \vec{H}_{eff}\cdot\vec{I} = \gamma_I \vec{H}_c\cdot\vec{I} + 2\mu_B\gamma_I \langle r^{-3}\rangle (k)\, \vec{S}\cdot\vec{I} \quad (4)$$

$$\text{i.e.} \quad \vec{H}_{eff} = \vec{H}_c + 2\mu_B \langle r^{-3}\rangle (k)\, \vec{S} \quad (5)$$

Hence the effective magnetic hyperfine field in non rare-earth solutes can then be thought to arise largely from

i. Conduction electron polarization : H_{CEP}
ii. Core polarization : H_{CP}, and
iii. Overlap polarization : H_v

i. Conduction electron polarization :

In this case, one considers that the magnetic centres act as spin dependent scattering potentials, that strongly perturb the spatial distribution and the energy of the free conduction electrons described by

$$\psi_{kr} = \vec{U}_k(r)\, e^{i\vec{k}\cdot\vec{r}}\, \phi(\sigma) \qquad (6)$$

The spin-dependent scattering potentials perturb the up and down spins differently and produce an oscillatory spin polarization. Such spin polarized conduction electrons, then generate hyperfine field at an impurity atom at a distance R via a Fermi contact term.

$$H_{CEP} = \frac{8\pi\mu_B}{3} < |U_k(R)|^2 > [|\psi_{\uparrow}(0)|^2_R - |\psi_{\downarrow}(0)|^2_R] \qquad (7)$$

Such an oscillatory spin polarization may arise from (a) (a) Friedal's charge perturbation [8-9], (b) the RKKY type moment perturbation [19] and (c) the s-d interband mixing [20].

The conduction electron polarization could be given as [12],

$$H_{CEP} = H_{\Sigma} + H_s \qquad (8)$$

where H_{Σ} represents a summed contribution to the conduction electron polarization by all the neighbours (transferred polarization) and H_s is the polarization induced by the

impurity atom (self-polarization) due to its local d(f) moment.

a. Daniel and Freidal model and Campbell extension

An impurity in a matrix is considered as a spherically symmetric potential V, the depth of which is adjusted to yield the right screening charge, which in turn is determined by Friedal's sum rules and the phase-shifts. In the first order,* this potential depth is determined by the charge difference ΔZ, between the impurity Z_i and the host Z_h (after properly taking care of the closed shells and d-screening). For iron $Z_h \sim 1$, [21], while for impurity it will be the number of valence electrons. The width of the potential is decided by the number of conduction electrons per atom.

The magnetic exchange coupling between the host moment and the conduction electrons spin splits the conduction

---

*A small correction to this valence difference was proposed by Blatt [22], who suggested that the introduction of a impurity results in an outward displacement of the host neighbour atoms, which in turn is equivalent to a removal of some fraction of ionic charge from the region occupied by the impurity, i.e.

$\Delta Z_{eff} = \Delta Z - \frac{\delta V}{\Omega}$ where $\frac{\delta V}{\Omega}$ is the fractional change in the size of the cell occupied by the impurity.

band resulting in a difference of energy for the two spins (up and down). Thus the conduction electrons with different spins (up or down) see different scattering potentials i.e.

$$V_{\uparrow} = V - \varepsilon; \quad V_{\downarrow} = V + \varepsilon \quad \text{and} \quad V_{\downarrow} - V_{\uparrow} = 2\varepsilon \qquad (9)$$

where ε is the s-d exchange energy. This results in an unequal scattering for the up and down spins. Such an unequal scattering results in a difference in the radial wave function of the two spin types ($\psi_{s\uparrow}$ and $\psi_{s\downarrow}$) leading to a net spin polarization. The conduction electron hyperfine field is then given by the proportionality,

$$H_{CEP} \alpha \int_{0}^{E_F} [\, |\psi_{\uparrow}(0)|^2 n_{\uparrow}(E) - |\psi_{\downarrow}(0)|^2 n_{\downarrow}(E) \,] \, dE \qquad (10)$$

Daniel and Friedal assumed, one s-type conduction electron per host-atom. A ferromagnetic coupling was assumed to explain the observed experimental data correctly. The model was quite successful because it could correctly predict the observed change in sign of the hyperfine fields in 'sp' solutes for $\Delta Z = 3$ (Sb-Sn).

Campbell [10] later improved the Daniel and Friedal's model. He showed that ~ 0.25 S-type conduction electrons/host atom is a more realistic number. This as shown in Fig. (5) resulted in very different estimates of CEP compared to Daniel and Friedal model. Campbell assumed an antiferromagnetic s-d coupling, whereas Daniel and Friedal model

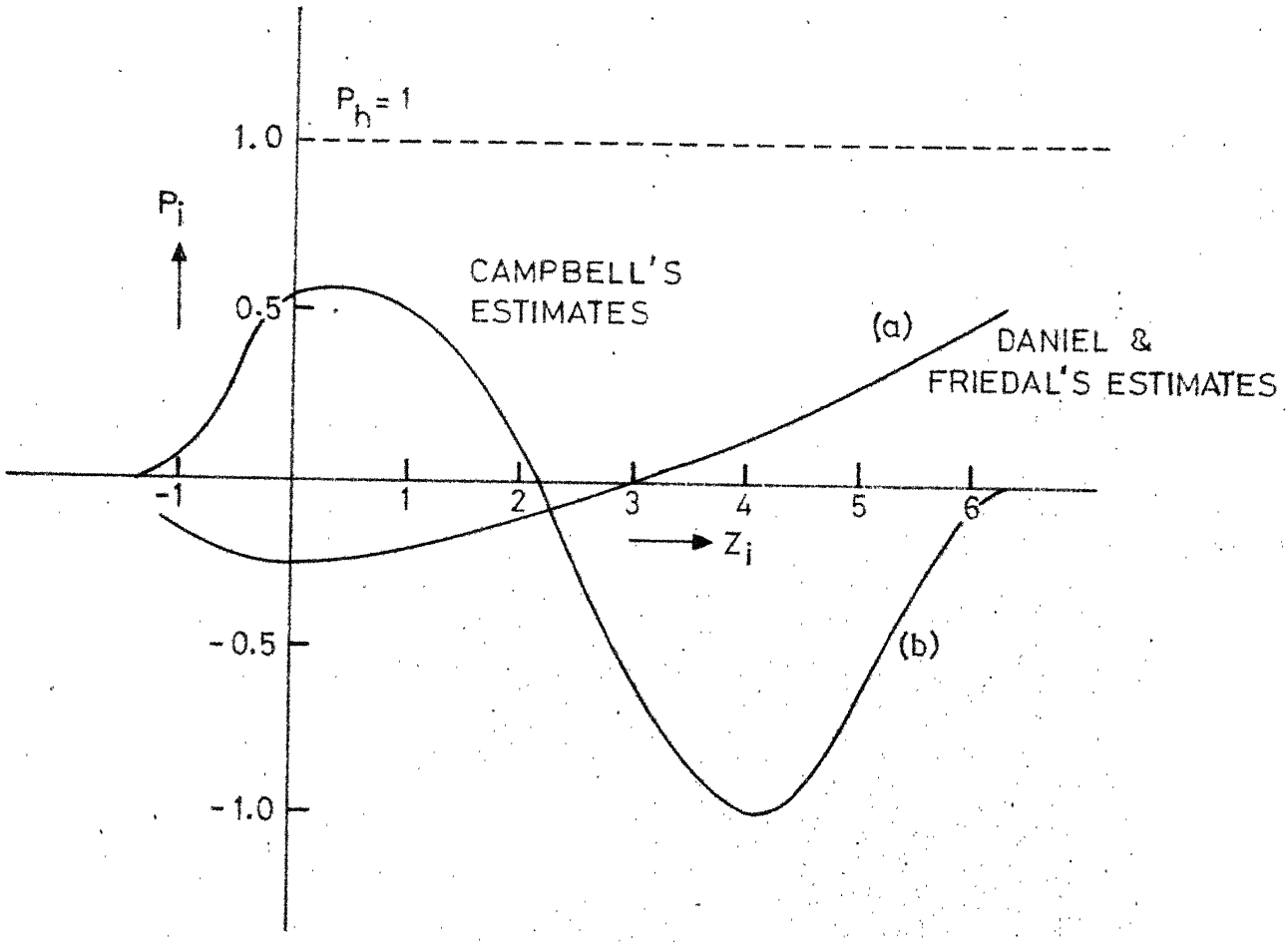

Fig. 5. Conduction electron polarization at the impurity site predicted by a) Daniel and Friedal's Model b) Campbell's model, plotted as a function of volume Z_i of impurity atom.

implies a ferromagnetic coupling. Campbell also calculated the self-polarization contribution for the transition impurities by modifying the impurity potential from,

$$V_{\uparrow} - V_{\downarrow} = -2\varepsilon$$

to a difference,

$$V_{\uparrow} - V_{\downarrow} = -2\varepsilon + J\mu_i \qquad (11)$$

where $J\mu_i$ appropriately modifies the potential to take care of impurity moment. Campbell got the conduction electron contribution as

$$H_{CEP} = A(z)P_i = A(z)\, P_h\, (0.6 + 0.4\ \mu_i/\mu_h) \qquad (12)$$

μ_i and μ_h being the impurity and host moments respectively. This model predicts a sharp decrease in the hyperfine field values with an increase in the charge difference. Further a large ΔZ results in $V >> \varepsilon$ (the s-d exchange energy) and accordingly one would expect $V_{\uparrow}$ and $V_{\downarrow}$ to be not too different and hence the resulting $\psi_{\uparrow}$ and $\psi_{\downarrow}$ are also similar. In these cases the field is largely decided by the mean spin polarization of the conduction band. On the other hand, when $V \simeq \varepsilon$ i.e. $\Delta Z \sim 0$, as is generally true for transition series solutes, the difference in spin up and spin down wave functions is significant and the resulting hyperfine field is therefore critically dependent on the s-d exchange energy and is opposite to the mean spin polarization.

Such a model though intituitively simple, however, suffers from a large handicap in providing exact 'numbers' especially due to a complicated band-structure and Fermi surfaces in alloys, and one has to rely heavily on some model dependent parameters and band structure calculations.

The other polarization mechanism is the RKKY [19] type interaction, where the oscillatory spin density of the conduction electron arises due to a coulomb exchange interaction between the localized d-electrons and the conduction electrons. Such an interaction always results in a net positive conduction electron polarization. Finally, s-d interband mixing arises due to the fact that in real transition metals, there is no clearcut distinction between the s- and d-electrons [20] and one therefore considers an effective exchange interaction J' through interband mixing of the conduction and the local moment electron orbits. Such an interaction in most cases leads to a negative CEP.

b. Model due to Shirley et al.

Another successful approach to estimate conduction electron polarization hyperfine field was initiated by Shirley and Westenbarger [3] and later improved upon by Shirley, Rosenblum and Matthias [4]. Without going into the detailed dynamics of the origin of these fields, these authors proposed that H_{CEP} would be a scaled fraction of the

free atom hyperfine field i.e. the hyperfine field generated by an unpaired outermost s-electron. The model however explicitly assumed a host moment proportionality. Thus,

$$H_{CEP} = p \cdot \mu_h \cdot H_{ns} \qquad (13)$$

where the factor p-absorbs all the host and solute dependent factors like say, the electron transfer in alloying and the difference in s-electron density at the nucleus in a free atom and in the metallic lattice. Inspite of the simplicity of the model, it has provided a reasonably reliable and an extremely simple way to calculate the conduction electron polarization.

The value of p is obtained from the experimental data for dilute impurities with a filled core, i.e. nd^{10} structure (Cu, Zn, Ag, Cd, Au, Hg), where the conduction electron contribution is expected to be predominant. Using more recent data, the values of p are recalculated and are tabulated in Table I. It may however be worthwhile to note that this model does not give any z-dependence of p, in contrast to Daniel-Friedal-Campbell's model, where the conduction electron contribution was found to be critically dependent on the electronic configuration of the impurity.

c. Stearns experiments: Scaling rules

Stearns [12] was able to measure the conduction electron polarization due to impurity neighbour shells (H_Σ)

Table I

Solute	H_{ns} (MOe)	Host Fe		Host Co		Host Ni	
		H_{hf}(kOe)	p	H_{hf}(kOe)	p	H_{hf}(kOe)	p
$3d^{10}Cu$	2.7	-213	0.078	-157	0.058	- 45	0.016
$4d^{10}Ag$	5.0	-447.2	0.089	-108	0.021	-122.4	0.024
$4d^{10}Cd$	6.5	-340	0.052	-268	0.041	- 68.6	0.013
$5d^{10}Au$	19.8	-1170	0.059	-797	0.042	-272	0.013
$5d^{10}Hg$	25.0	-440	0.017	-370	0.014	- 80	0.003
Average 'p'			0.059		0.035		0.013
μ_h			2.22 β		1.72 β		0.606 β
Ratio			0.027		0.021		0.230

in the Fe host. With a careful analysis of the Mossbauer and the pulsed NMR results on ordered Fe_3Si alloy, she was able to experimentally deduce the total conduction electron polarization of all the neighbour shells. Assuming the additivity of contributions of different shells, she gave,

$$H_{\Sigma}^{Fe} = \sum_{N=1}^{6} N_i \Delta H_i = -145 \text{ kOe} \qquad (14)$$

where N_i gives the number of iron atoms in the i^{th} shell, H_i is the hyperfine field contribution from an Fe atom in the i^{th} shell. Assuming that H_{Σ} is proportional to the host moments, one obtains, $H_{\Sigma}^{Co} = -120$ kOe and $H_{\Sigma}^{Ni} = -48$ kOe. These values could also be obtained independently through hyperfine field values of Cu, Au and Ag where CEP is expected to be dominant.

ii. Core polarization

The notion of core polarization was first invoked by Sternheimer [23], who used it to explain the observed large negative hyperfine fields on transition series solutes. The core electrons are paired and hence do not contribute to the hyperfine field in the first order. In the second order, the exchange interaction between the 3d-electrons of the solute and the solute core electrons results in an unequal spatial distortion of the radial wave function for the up and down spins, leaving a net spin density at the nuclear site. The usual convention is that the magnetic

hyperfine field is positive, when it is parallel to the direction of magnetization. Since positive field corresponds to a positive spin, the spins are said to be positive when antiparallel to the direction of external field. The 3d spin of the impurity orients opposite to the direction of the external magnetization. This in turn 'attracts' the core ns$\uparrow$ (n = 1,2,3) electrons and repel ns$\downarrow$ electrons. leaving thereby a net negative spin density at the nuclear site and hence a negative field. Figure (6) brings out this contention explicitly. Freeman and Watson [7] have employed unrestricted Hartree-Fock method to calculate the contribution to the hyperfine field from each of the core ns shells. Their calculations show that out of the core ns shells, the 2s shell's contribution is maximum. Freeman and Watson also calculated the core polarization hyperfine field/unpaired d-electron to be as -125 kOe/3d spin, -375 kOe/4d unpaired spin and -1200 kOe/5d unpaired spin. These fields/spin are expected to be constant throughout a transition series, which has been verified experimentally. Thus, in Shirley's model, the total field is given as,

$$H_{hf} = \mu_h p\, H_{ns} + 2 \langle S_z \rangle H_{nd} \qquad (15)$$

$$= H_{CEP} + H_{CP}$$

Thus a localized d-moment at the solute atom which in turn polarizes its own core ns shells, can give large negative core polarization fields. The neutron diffraction data [24]

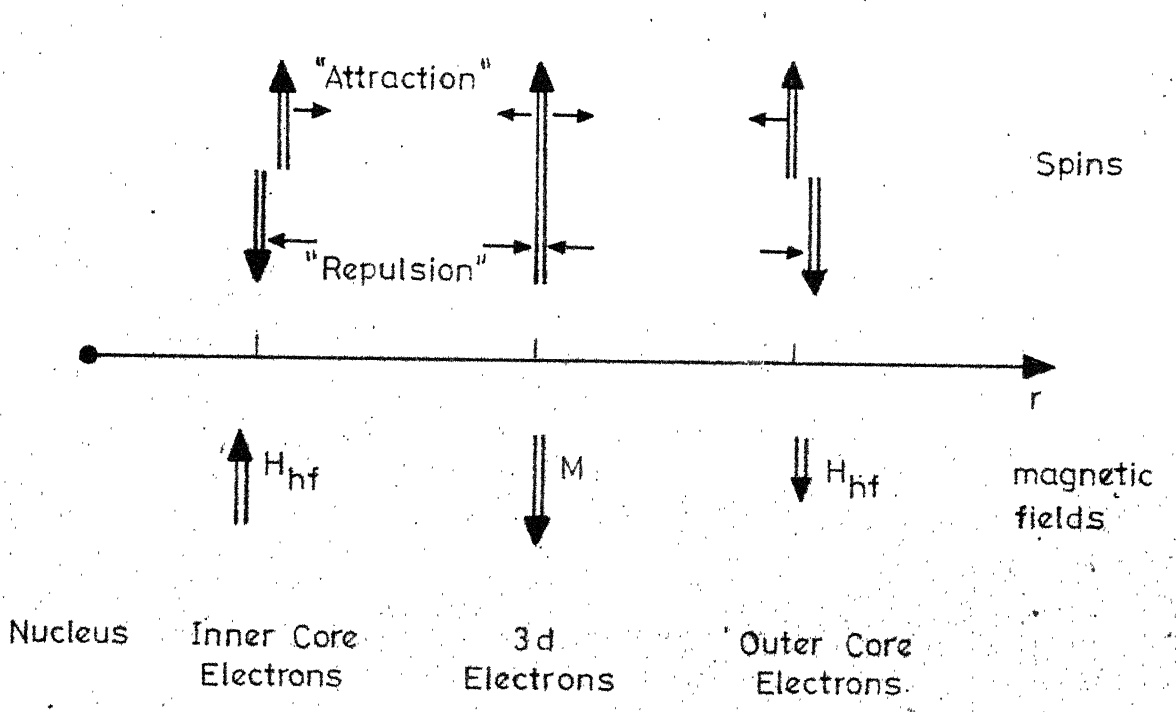

Fig. 6. Schematic representation of the spin polarization induced by the 3d electrons. The arrows indicate the average positions of the inner, outer and 3d electron spins and the effects of exchange interaction.

in fact has given adequate evidence for the existence of such local d-moments. Accordingly, the d-moments derived from equation (16), using the experimental hyperfine field data may be compared with the measured d-moment values from neutron diffraction experiments. For such a comparison, from the values of p given in Table I, the CEP estimates were calculated. The CEP estimates thus obtained were subtracted from the experimental hyperfine fields to get the core polarization contribution to the hyperfine field. From these estimates of the core polarization contributions, and using the calculations of Freeman and Watson [6,7] the localized d-moment values were calculated, and are tabulated in Table II and plotted in Fig. (7), along with the experimental values obtained from neutron diffraction measurements, wherever applicable.

Recently Cheng-jyi Song et al. [25] have reported a first direct measurement of the 2s-3s spin densities using Mossbauer effect with electron spectroscopy. Their experiment, to some extent, verify the calculations of Freeman and Watson [5-7], Duff and Das [26] and of Liu and Bagus [27]. The satisfactory predictions of the CP model in giving localized d-moments, as confirmed by diffuse neutron scattering data, along with Cheng-jyi Song's experimental confirmation of theoretical calculations do give us a reasonable amount of confidence to conclusively say that

Table II

Series	Element	Host Fe		Host Co		Host Ni	
		Calc.μ_B	Expt.μ_B	Calc.μ_B	Expt.μ_B	Calc.μ_B	Expt.μ_B
3d	Sc	0.4		0.2		0.1	
	Ti						
	V	0.2		0.1			
	Mn	1.0	0 $\pm$ 0.5	0.6		2.4	
	Fe	1.8	2.22	2.1		1.9	
	Co	1.3	2.1$\pm$0.3	1.2		0.8	
	Ni	0.7	1.2$\pm$0.3	0.2		0.7	
	Cu	0.4		0.5		0.1	
4d	Nb	0.3		0.3		0.0	
	Mo	0.2		0.2			
	Tc	0.4		0.4		0.0	
	Ru	0.8	0.7$\pm$0.4	0.8		0.5	
	Rh	0.9	0.5$\pm$0.3	0.7		0.4	
	Pd	0.9	0.3$\pm$0.3	0.3		0.4	
	Ag	0.4				0.1	
5d	Ta	0.2		0.1		0.0	
	W	0.1		0.1			
	Re	0.1		0.0			
	Os	0.3	0.1$\pm$0.3	0.4		0.1	
	Ir	0.4	0.2$\pm$0.3	0.4		0.2	
	Pt	0.2	0.1$\pm$0.3	0.2		0.1	
	Au			0.1		0.1	

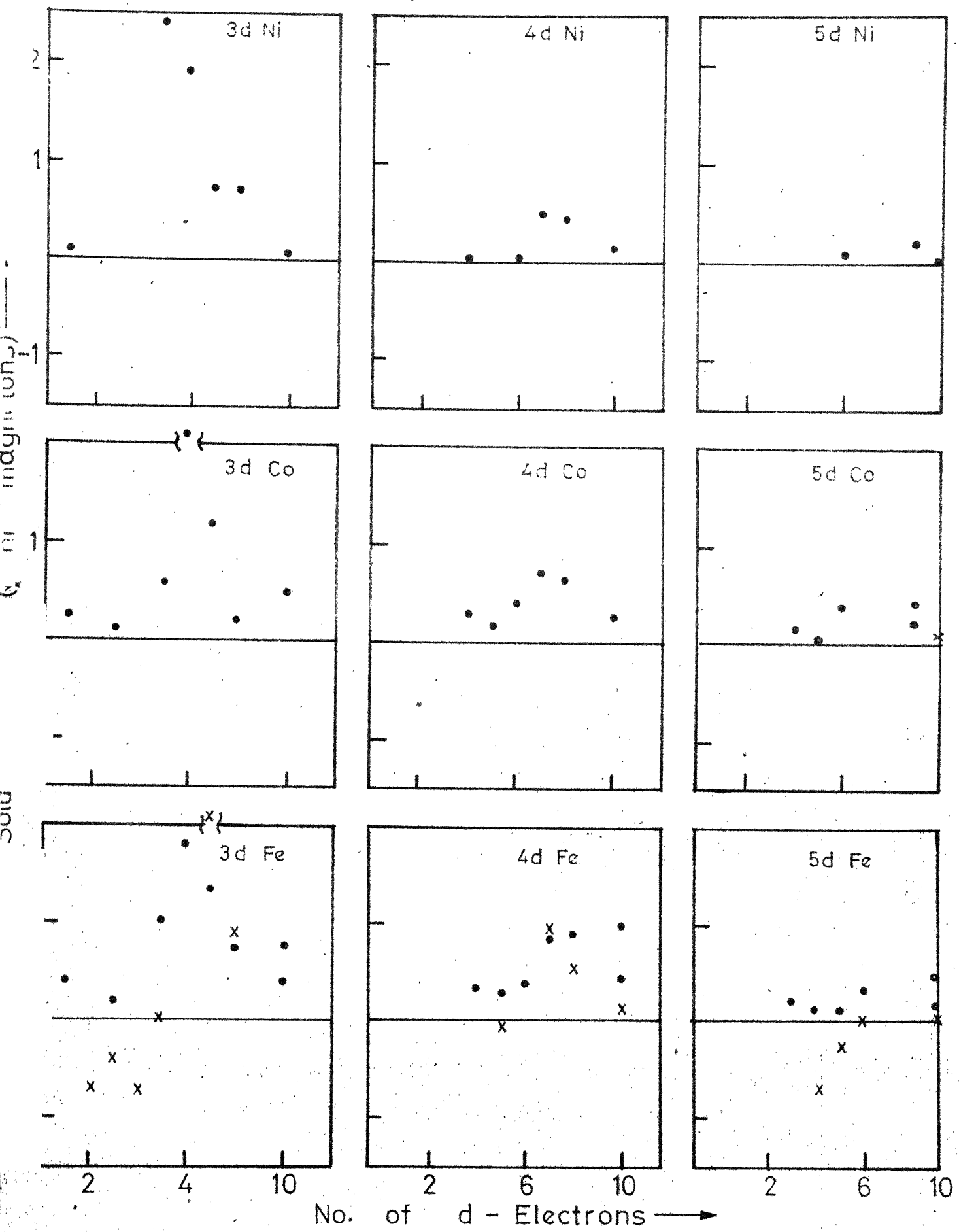

7. The local d-moments derived using Shirley et al.'s model. Experimental values are indicated by (X) wherever applicable.

the CP is a dominant contribution in the transition series solutes. Such a model further strengthens Shirley's model and his predictions vis a vis CEP estimates.

iii. Overlap polarization

The other approaches in calculating transferred hyperfine fields is the chemical bonding approach [13]. In this the impurity atom is treated as a ligand coordinated to its nearest magnetic neighbours. As a result of overlap and/or covalency, the ligand's outermost electrons get spin polarized, subsequently generating a hyperfine field via a Fermi contact interaction. Following such an approach Stearns [12], suggested the possibility of a volume overlap term and Shirley [13] tried to explain the fields especially on $d^{10}s^{2}p^{n}$ solutes by calculating the overlap of 3d host and 5s impurity wavefunctions. The contact field resulting due to an overlap polarization is essentially positive [7].

a. Stearns Volume Overlap Model

This model postulates a misfit volume overlap contribution due to valence ns-like electrons, which remain bound to the impurity site. Such an overlap polarization, therefore, occurs only if the volume of the impurity exceeds the effective volume available to it in the host matrix. Thus, when $V_{imp} > V_{host}$, the valence ns-like electrons, overlap with the

host matrix and get positively polarized by an amount proportional to the volume misfit of the volume of the solute atom. Stearns gave a simple linear relation for such a polarization, i.e.,

$$p_v(z) = C(V_z - V_o) \qquad (16)$$

where C is a constant characteristic of the host, V_z is the volume of the solute and V_o is the effective volume available to the impurity on removing one host atom. The predictions of this model were calculated both by using equation (17) and by using the experimental data as described below. Using Stearn's estimates of $H_\Sigma^{Fe} = -145$ kOe, $H_\Sigma^{Co} = -117$ kOe and $H_\Sigma^{Ni} = -44$ kOe and the scaling rules given by her, i.e.

$$H_\Sigma^{z} = \frac{H_z^{ns}}{H_{4s}^{Fe}} H_\Sigma^{Fe} \qquad (17)$$

the conduction electron polarization contribution was calculated. These values were then subtracted from the experimental hyperfine field values of the solutes, which do not develop a moment (i.e., non transition and non rare earth series solutes) to get volume overlap contribution. It is thus implicitly assumed that the total contribution to hyperfine fields in such solutes ($d^{10}s^2p^n$ type) arises predominantly from the conduction electron polarization and the volume overlap polarization. The volume part H_v so obtained was then divided by the appropriate free atomic

hyperfine field to get the experimental volume overlap polarization values $p_v^{(z)}$. These are plotted as a function of the impurity volume (V_z) in Fig. (8). A least squares fit of these values to the equation (16) gave both the effective volume V_o and the constant C, for the three hosts as shown in Fig. (8). These least square fitted values were then used to calculate the predictions of the model using the relation (16). The impurity volumes were taken from Ref. [12,28]. The calculated volume overlap polarization p_v values are plotted along with the experimental values as a function of impurity Z, in figure (9) and are tabulated in Table III. The general gross features for the non-transition series solutes may be reproduced by this model. As expected, the overlap of the solute s-electrons with the polarized d-electrons of the host can give significant contributions to the hyperfine field. This contribution may be to a crude approximation given by the volume overlap effect. Although the gross features may be explained by this model, as one would expect there are large deviations in some cases and these deviations may probably be explained by invoking the microscopic structure of the ion.

b. Shirley's Overlap Model

Outlining the limitations and the inadequacies of the Daniel and Friedal's model for large values of solute valency ($d^{10}s^2p^n, \Delta Z >>$), Shirley [13] suggested that the

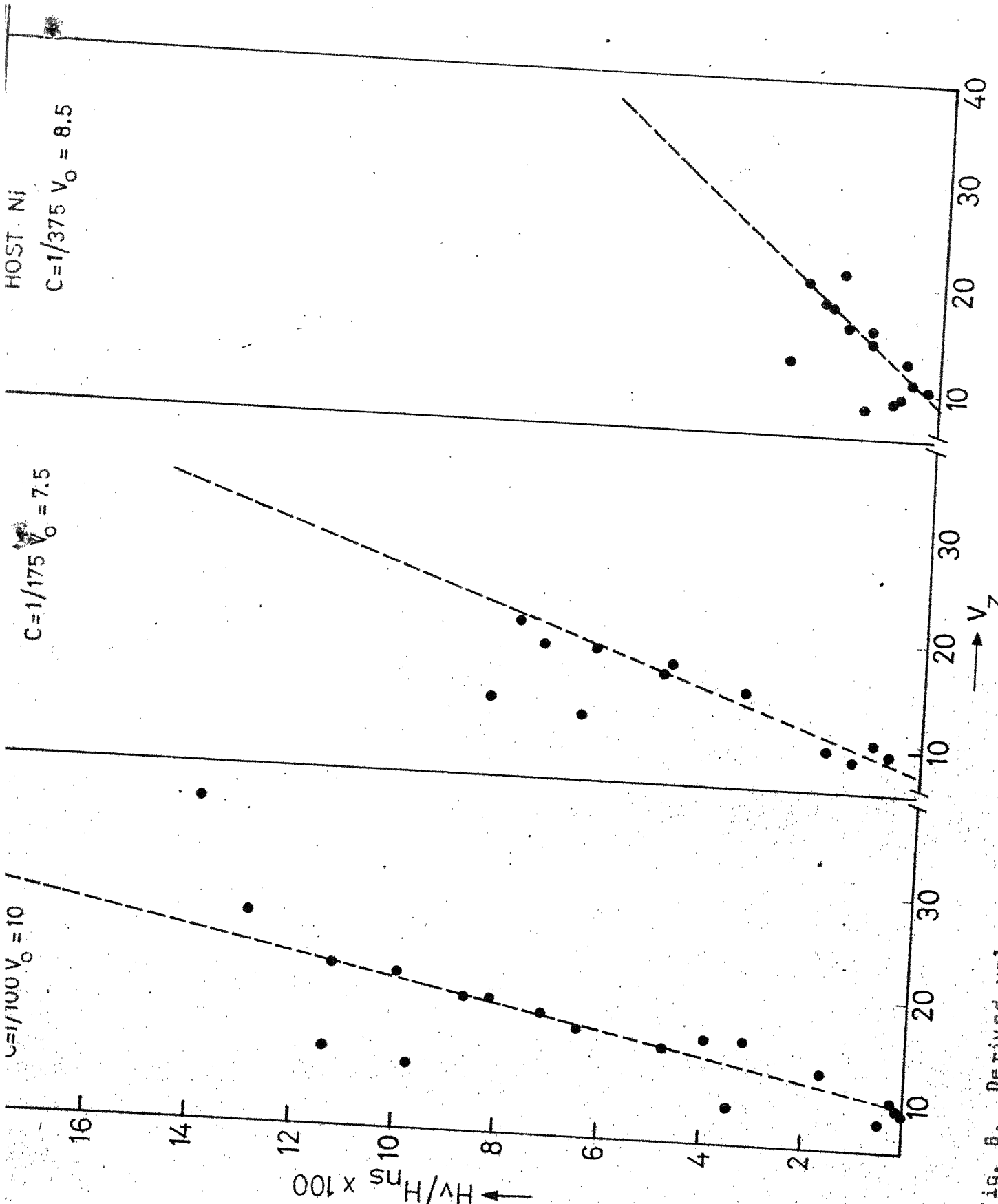

Fig. 8. Derived volume overlar[illegible] ization obtained using Stearns scaling rules plotted vs. V_z, th volume.

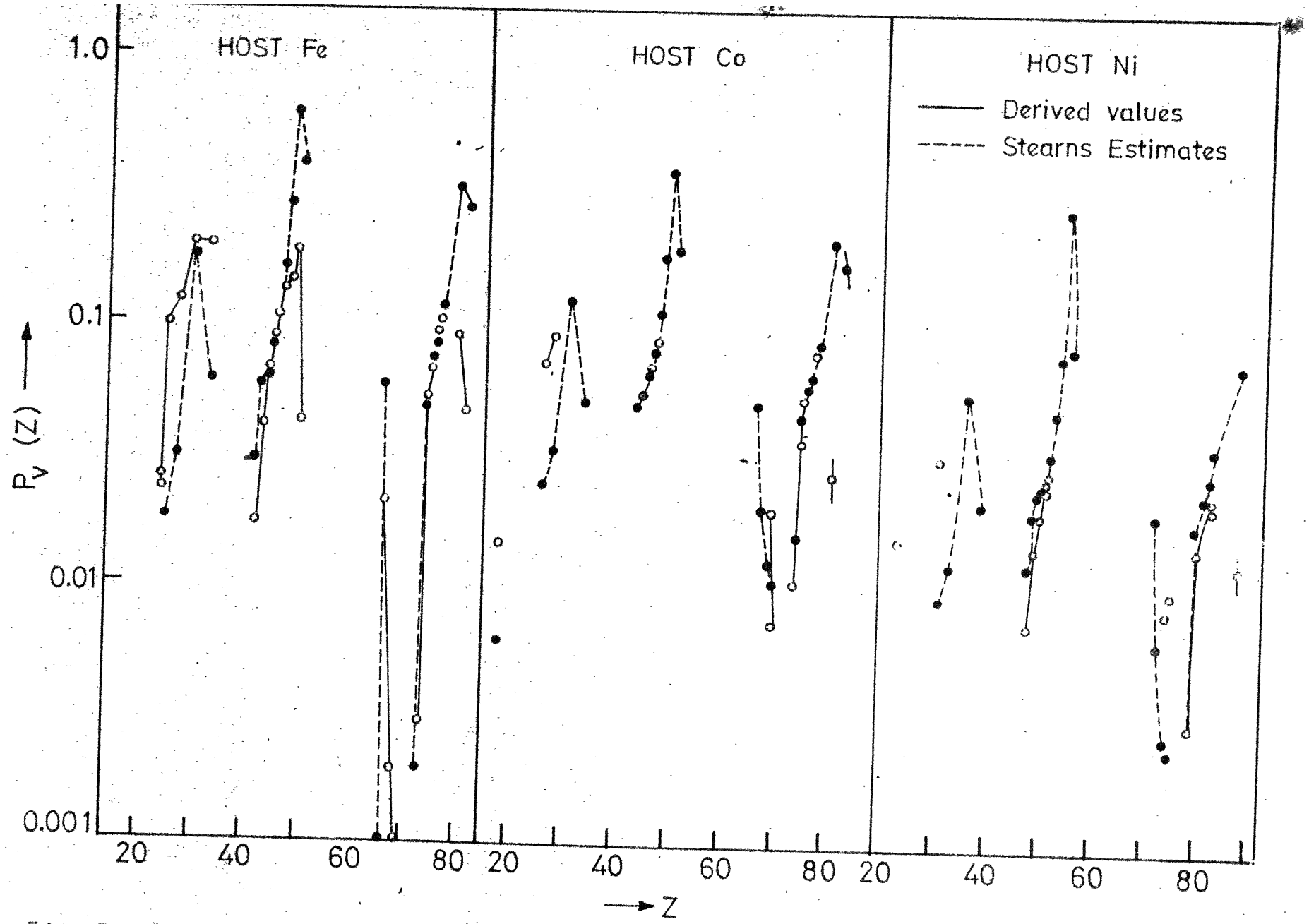

Fig. 9. Derived and the predicted values overlap polarization obtained using Stearns model. The points and the solid curve represent the derived polarization. The dashed curve represents the predicted polarization.

Table III

Z, El	Host Fe							Host Co					Host Ni				
	H_{ns}^{Z} (MG)	V_Z	H_Z (kOe)	$-H_{\Sigma}^{Z}$ (kOe)	H_v (kOe)	H_v/H_{ns}	p_v^Z	H_Z	$-H_{\Sigma}^{Z}$	H_v	H_v/H_{ns}	p_v^Z	H_Z	$-H_{\Sigma}^{Z}$	H_v	H_v/H_{ns}	p_v^Z
23V	1.4	8.5	- -87	101.5	7.5	0.005	0.00	48	74.46	20.4	0.014	0.006	7.5	25.7	+16.2	0.015	0.000
30Zr	3.0	9.17	105	217.5	105.5	0.035	0.00										0.000
31Ga	4.0	11.8	110	290	393	0.098	0.018	62	212	268	0.067	0.024					0.009
33As	7.5	13.1	+ 319	543.9	855.9	0.114	0.031	+294	398.9	641.9	0.085	0.032	+ 88	137.5	223.5	0.029	0.012
																0.03	
36Kr	13.0	27.82	1500	942.3	2435.3	0.19	0.178					0.116					0.053
39Y	24	16.1	+ 286	174	453	0.19	0.06					0.049					0.02
48Cd	6.4	13.0	- 348	464	109	0.017	0.03						- 69	117.3	46.3	0.007	0.012
49In	9.1	15.7	- 288	659.7	364.7	0.040	0.057					0.047	- 33	166.8	131.8	0.014	0.019
50Sn	12.0	16.2	- 81	870	782	0.065	0.062	- 20	638	621	0.051	0.050	+ 18	220	236	0.019	0.023
51Sb	15	18.4	+ 230	1087	1310	0.087	0.084	187	797	978.9	0.065	0.062	+ 94	275	367	0.024	0.026
52Te	20	20.5	+ 620	1450	2063	0.10	0.105	550	1063	1607	0.08	0.075	+195	366.3	559.3	0.027	0.032
53I	19	25.7	1170	1377.5	2540	0.13	0.157					0.104					0.046
54Xe	22	36.81	1400		2990	0.14	0.268					0.167					0.075
55Cs	2.4	70	273	174	447	0.18	0.600					0.357					0.264
56Ba	3.0	39	- 85	217.5	125.5	0.041	0.39					0.180					0.08
72Hf	7.7	15.7	- 300	558.2	251.2	0.032	0.057					0.047					0.019
			606														

Table III (...Contd.)

Z, El	H^Z_{ns} (MG)	Host Fe						Host Co					Host Ni				
		V_Z	H_Z (kOe)	$-H^Z_\Sigma$ (kOe)	H_v (kOe)	H_v/H_{ns}	p^Z_v	H_Z	$-H^Z_\Sigma$	H_v	H_v/H_{ns}	p^Z_v	H_Z	$-H^Z_\Sigma$	H_v	H_v/H_{ns}	p^Z_v
73Ta	8.3	10.9	- 656	601.7	- 61.3							0.019	- 98	2152.5	+54.3	0.006	0.0064
74W	9.3	9.53	- 643	674.2	24.2	0.002	0.000	-388	494.6	101.6	0.019	0.012	- 90	170.5	78.5	0.008	0.003
75Re	10.8	9.3	- 760	782.9	15.9	0.001	0.000	491	574.4	79.4	0.007	0.010	-100	198	96	0.009	0.003
79Au	18.5	10.2	-1280	1342	55	0.003	0.002	-797	984	181	0.0097	0.015	-294	339	43	0.003	0.003
80Hg	21.5	14.8	- 440	1559	1112	0.0517	0.048	-370	1145	769	0.035	0.042	- 86	394.2	306.2	0.0142	0.017
81Tl	26.0	17.24	- 185	1885	1693	0.065	0.072	- 90	1385	1289	0.050	0.055					
82Pb	33	18.27	+ 660	2392	3045	0.092	0.082	+430	1755	2179	0.066	0.060	+115	605	718	0.0217	0.026
			+ 280	2392	2665	0.081		+280		2666	0.081		125		728	0.022	
			+ 260	2392		0.081			1755								
83Bi	42	21.3	1180	3045	4218	0.100	0.113					0.079	325	770	1093	0.02	0.034
86Rn	60	42	900	4350	5250	0.088	0.32					0.197					
88Ra	4.7	36.5	- 120	340.7	213.7	0.045	0.265	-100	250	144	0.036	0.16	- 30	86.18	34.18	0.0119	0.07

large fields in these solutes arise due to 5s shell polarization by the host 3d-spins. Such a polarization could come either via a Pauli-distortion effect and/or by a covalency term. Orthogonalization of the host 3d spins and the impurity 5s spins lead to an admixture of the 3d-character into 5s-orbital with spin parallel to the 3d spin. This results in a Fermi contact hyperfine field s.t.

$$H_{hf} = |\langle 3d \mid 5s \rangle|^2 H_{5s} \qquad (18)$$

The amplitude $\langle 3d|5s\rangle$ gives the extent of overlap. Such an overlap of atomic wave functions is shown to explain the observed trends of the hyperfine fields in 5sp solutes.

iv. Balabanov and Delygin's model

Balabanov and Delyagin [14] studied the dependence of the magnetic hyperfine fields on the number of electrons in the outer shells of the impurity atom (i.e., on the total number of (n-1)d electrons, ns electrons and np electrons where n = 4,5 and 6 respectively for the elements of the period IV, V, VI). They approximated the observed regularity by means of a parabola, that is symmetrical about the middle of the period, i.e.,

$$H_{hf} = a + b\,(\nu - 9)^2 \qquad (19)$$

where ν is the number of outer electrons and a and b are constants. The model assumes that the electrons in the outer

shell polarizes the inner filled shell to give rise to a negative hyperfine field on the impurity. The positive contribution predominates when $|\nu - 9| \geq 5$. The magnitude of the positive contribution is also determined by the polarization of the internal shells, but does not depend on the value of the effective magnetic moment of the outer electrons of the impurity. Such a polarization is caused by a direct interaction of the electrons in the filled shells and the polarized electrons of the conduction band of the matrix.

Obviously enough, the predictions of this model depends on how best the experimental data could be fitted to a parabola. Also the assumption that the maximum negative field is obtained for minimum value of $|\nu - 9|^2$, i.e., in the middle of the period is not tenable, as the maximum is obtained for three different impurities for the three hosts (Figs. 1-3).

This model unfortunately does not offer any microscopic explanation of the polarization except that the outer shell electrons contribute to the hyperfine field. The experimental data presented in Figs. (1-3), show that the data can only be approximately represented by means of a parabola. In Fig.(10), the least squares fitted curve obtained from this model (fitted to equation (19)) along with the experimental data is given. The predictions of

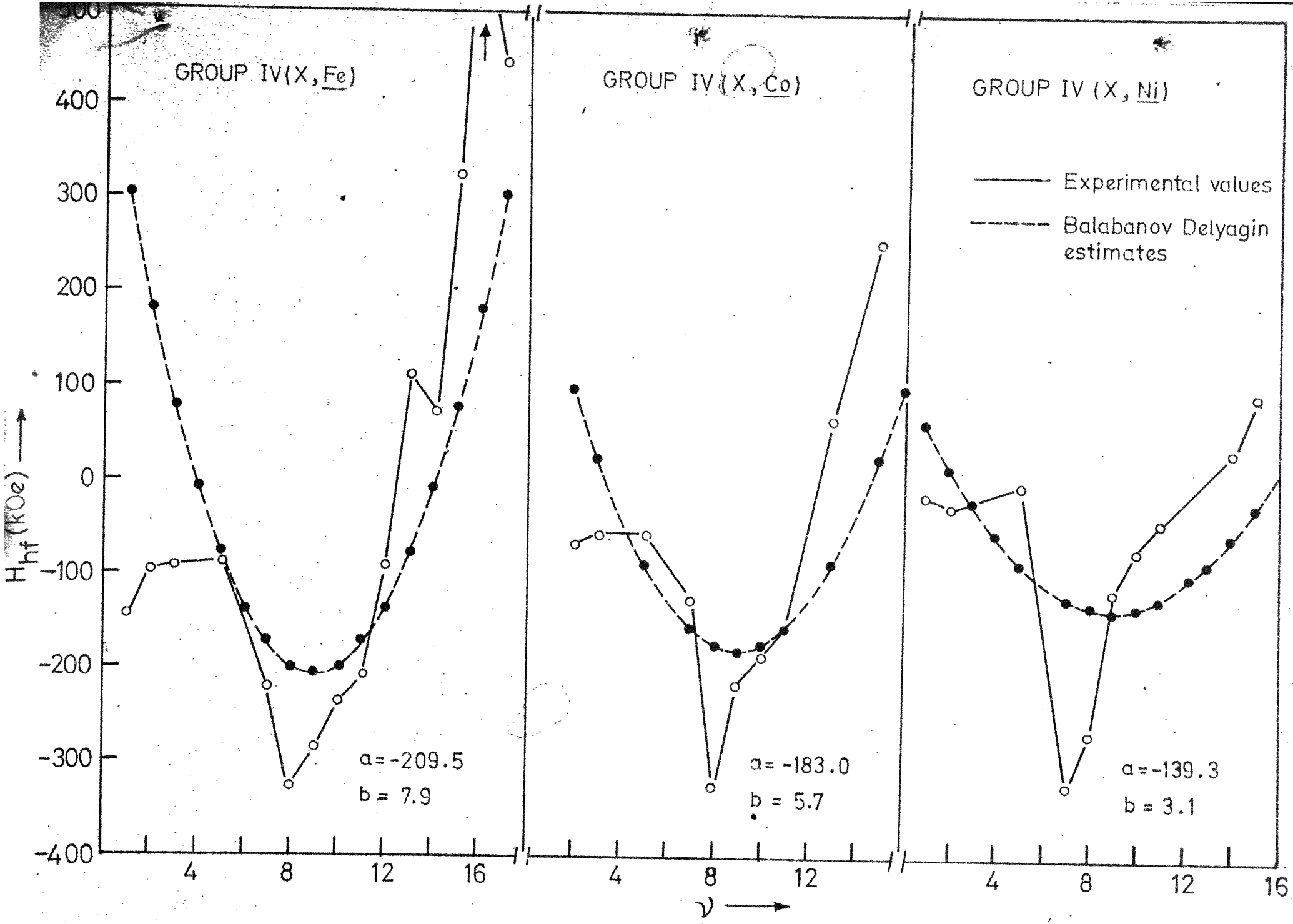

Fig. 10. Comparison of the hyperfine fields predicted by Balabanov and Delyagin model, with the experimental values for IV group solutes in Fe, Co and Ni hosts.

this model were compared with the experimental values for the fourth group in Fe, Co and Ni hosts and in 20 cases, the deviation is more than 20%. In some cases, the sign of the field predicted by this model is also not in agreement with the reported experimental sign. The host moment proportionality assumed by the model, has already been seen to have a limited validity. Further, many of the systematic trends of the observed hyperfine fields are not explained by this model [16].

3. Weak Crystal Fields-Rare Earth Solutes ($\vec{\lambda L}\cdot\vec{S} >> V_{cf}$)

For weak crystal fields the Hamiltonian reduces to the form,

$$\vec{H}_{hf} = \vec{H}_{exch.} + \lambda \vec{L}\cdot\vec{S} - \gamma_I \vec{H}_c\cdot\vec{I} + 2\mu_B\cdot\gamma_I \langle r^{-3}\rangle (-k)\vec{S}\cdot\vec{I}$$

$$+ 2\mu_B\gamma_I \sum_i \frac{\vec{l}_i\cdot\vec{I}}{r_i^3} - 2\mu_B\gamma_I \sum_i$$

$$\left[\left(\frac{\bar{s}_i\cdot\bar{I}}{r_i^3} - \frac{3(\bar{r}_i\cdot\bar{s}_i)(\bar{r}_i\cdot\bar{I})}{r_i^5}\right)\right]$$

Symbolically,

$$\vec{H}_{hf} = \vec{H}_{spin\text{-}orbit} + \vec{H}_{exch} + \vec{H}_{orb} + \vec{H}_{core} + \vec{H}_{cond} + \vec{H}_{spin\text{-}dipolar} \qquad (20)$$

Further discussion could be carried out for Lanthenide (4f) and Actinide (5f) solutes separately.

i. Lanthenide solutes

a. Orbital contribution

The 4f solutes retain much of their free ion character due to a very effective shielding of the 4f electrons by the 5s and 5p shells and accordingly the magnitudes of the observed field is primarily decided by the large unquenched orbital angular momenta of the 4f shell. The contribution due to the 4f electron orbital momenta is practically an order of magnitude larger than other contributions. The orbital contribution is expressed as,

$$H_{4f}^{orb} = 2\mu_B \langle 4f | r^{-3} | 4f \rangle \langle J \| N \| J \rangle \vec{J} \qquad (21)$$

The reduced matrix elements $\langle J \| N \| J \rangle$ are tabulated by Elliot and Stevenson [29] and the $\langle 4f | r^{-3} | 4f \rangle$ values have been determined both [30] by theory and experiment.

b. Core polarization contribution

The mechanism of core polarization in the rare earths is the same as in the transition series solutes, discussed earlier except for the fact that here the 4f electrons are responsible for core polarization. Assuming core polarization to be constant, within the 4f series, Freeman and Watson [7] gave an empirical relation based on available data, that the core contribution could be given as

$$H_{core} = 90 (g_J - 1) J \text{ (kOe)} \qquad (21)$$

However with a closer scrutiny and more accurate calculations by the same authors indicated that the field/unpaired spin was not constant and did vary considerably within the 4f series.

c. Conduction electron polarization

An estimate of conduction electron polarization could be obtained by Shirley's model. This contribution is however expected to be small owing to smaller 6s densities at the nucleus.

Thus the fields on rare earth (4f) solutes is primarily decided by the orbital part, which more or less keep their free atomic like character. The other contributions are in most cases an order of magnitude smaller. The sign of the field (especially a change in the sign near the middle of the 4f shell) can be qualitatively understood assuming an antiferromagnetic coupling between the 3d electron spins and the 4f spin, which in turn, align antiparallel (parallel) to the angular momenta in the first (second) half of the 4f shell[6b].

ii. Actinide solutes

In actinides [31] as compared to the lanthenides the 5f electrons are not that well shielded as the 4f electrons and in these elements, the spin orbit and crystal fields

are of comparable magnitudes resulting in partial quenching of the angular momenta. Further due to a significant overlap of 5f wave function with 6d, 6s, 7s wave function and accordingly configuration mixing effects become important for such solutes. Under such conditions, the core polarization effects become more important. Dunlop [32] has given on the basis of experimental data, an empirical relation for core contribution as,

$$H_{core} = -(560 \pm 100)\ (g_J - 1)\ J\ (kOe) \qquad (22)$$

The experimental hyperfine field measurements for actinides have been quite limited. The reasons being experimental difficulties arising due to: 1) α-decay after effects, 2) existence of more than one charge states, and 3) the daughter nuclei are also radioactive.

With limited data available, no studies on systematics could be undertaken.

D. CONCLUSIONS

From the plots of the best experimental dilute impurity hyperfine fields for Fe, Co and Ni matrices, many interesting systematic trends could be seen. Comparison of the 'reduced hyperfine field' values for Fe, Co and Ni hosts showed that the usual assumption, that the impurity hyperfine field values are proportional to the host moments,

is found to be not strictly valid and the deviations are usually larger than 10%. Because of the complexity of the Hamiltonian and the many body techniques involved, the detailed calculations to obtain the dilute impurity hyperfine fields in ferromagnetic hosts do not seem to be feasible in the near future. Therefore, most of the existing models for the dilute impurity hyperfine fields are semiempirical and are derived from meagre theoretical estimates and from the observed systematics of the fields. From the present comparisons of the experimental hyperfine field values with the predictions of the various existing models, it is concluded that the core-polarization and the conduction electron polarization model suggested by Shirley et al. is reasonably satisfactory for the transition series solutes. The volume overlap model due to Stearns can give the general gross features and crude estimates for the nsp solutes. The model due to Balabanov and Delyagin also gives the general trends.

Thus, the dilute impurity hyperfine fields is one area, where the experiments are far ahead of the theoretical calculations. More systematic and rigorous microscopic calculations for the different possible contributions are necessary to further understand the mechanisms involved regarding the origin of the dilute impurity hyperfine fields.

E. REFERENCES

1 B. N. Samoilov, V. V. Sklyarevskii and E. P. Stepanov, Z. Experim. i. Teor. Fiz. 36, 644 (1959) Sov. Phys. JETP, 36, 448 (1959) .

2 L. Grodzins, Ann. Rev. Nucl. Sci. 18, 291 (1968).

3 D. A. Shirley and G. A. Westenbarger, Phys. Revs. 138A, 170 (1965).

4 D. A. Shirley, S. S. Rosenblum and E. Matthias, Phys. Revs. 170, 363 (1968).

5 R. E. Watson and A. J. Freeman, Phys. Rev. 123, 2027 (1967).

6 (a) R. E. Watson and A. J. Freeman, in Magnetism IIA, Eds. G. T. Rado and H. Suhl (Academic, 1965) p. 167.

(b) R. E. Watson and A. J. Freeman, Phys. Rev. Lett. 6, 277 (1961).

7 (a) A. J. Freeman, in Hyperfine Interaction and Nuclear Radiation, Eds. E. Matthias and D. A. Shirley (North Holland, 1968), p. 447.

(b) A. J. Freeman and R. E. Watson in Hyperfine Interaction, Eds. A. J. Freeman and R. B. Frankel (Academic, 1967) p. 53.

8 E. Daniel and J. Friedal, J. Phys. Chem. Sol. 24, 1601 (1963).

9 E. Daniel, in Hyperfine Interactions, Eds. A. J. Freeman and R. B. Frankel (Academic, 1967) p. 712.

10 I. A. Campbell, J. Phys. C2, 1338 (1969).

11 D. A. Shirley, Ann. Rev. Nucl. Sci. 16, 89 (1966).

12 (a) M. B. Stearns, Phys. Rev. B1, 4383, 1973;
(b) ibid. B4, 4081 (1971);
(c) ibid. B6, 3326 (1972);
(d) ibid. B4, 4096 (1971);
(e) Phys. Lett. 34A, 146 (1971), and
M. Pasternak in Mossbauer Spectroscopy and its Applications, International Atomic Energy Agency, Vienna, 1972, p. 197.

13 D. A. Shirley, Phys. Lett. 25A, 129 (1967).

14 A. E. Balabanov and N. N. Delyagin, Z. E Ksperim. i. Teor. Fiz. 27, 1402 (1968) Sov. Phys. JETP, 27, 752 (1968)

15 * G. N. Rao and D. N. Sanwal, IIT/K Tech. Rep. Phys. 8/73.

16 G. N. Rao and A. K. Singhvi, IIT/K Tech. Rep. Phys. 3/74.

17 T. Kushida, A. H. Silver, Y. Koi and A. Tsujimura, J. Appl. Phys. (Suppl.) 33, 1079 (1962).

18 E. Fermi, Z. Physik. 60, 320 (1930).

19. (a) M. A. Rudermann and C. Kittel, Phys. Rev. 96, 99 (1954).
(b) T. Kasuya, Prog. Theor. Phys. (Kyotp), 16, 45 (1956).
(c) K. Yoshida, Phys. Rev. 106, 893 (1957).

20 (a) P. W. Anderson, Phys. Rev. 124, 41 (1961),
(b) A. J. Freeman, Phys. Rev. 139, A167 (1963).

21 N. Mott, Adv. Phys. 13, 325 (1964).

22 F. J. Blatt, Phys. Rev. 108, 285 (1957).

23 R. M. Sternheimer, Phys. Rev. 86, 316 (1952).

24 (a) M. F. Collins and G. C. Low, Proc. Phys. Soc. (London), 86, 535 (1965).
(b) J. W. Cabble, E. O. Wollen and W. C. Koehler, Phys. Revs. 138, 755 (1965).
(c) J. B. Comely, T. M. Holden and G. C. Low, Proc. Phys. Soc. C1, 458 (1968).

25 Cheng-jyi Song, J. Trooster and N. Benczer-Koller, Phys. Rev. B9, 3854 (1974).

26 K. S. Duff and T. P. Dass, Phys. Rev. B3, 2294 (1971).

27 P. S. Bagus and B. Liu, Phys. Rev. 148, 79 (1966).

28 Metals Handbook, p. 29 (Amer. Soc. for Metals, Cleveland, 1948) cited by Stearns in ref. 12(a).

---

* For a more recent tabulation, see, G. N. Rao, Table of Hyperfine Fields (to be published in Hyperfine Interactions).

29 R. J. Elliot and K. W. H. Stevenson, Proc. Roy. Soc. (London), A218 533 (1953).

30 P. Inia, Ph.D. Thesis (Groningen University, 1971).

31 G. M. Kalvius in Mossbauer Spectroscopy and Its Applications (IAEA, Vienna, 1972) p. 169.

32 B. D. Dunlop in Mossbauer Effect Methodology, Eds. I. J. Gruverman, Vol. 7 (Academic, 1971) p. 123.

VITAE

Born in Jodhpur, Rajasthan on November 2, 1950, the author studied in Sardar Higher Secondary School, Jodhpur. He graduated from University of Jodhpur in 1968 and obtained his M.Sc. degree in Physics in 1970 from University of Jodhpur. Since then he has been working as a research scholar in the Department of Physics, Indian Institute of Technology, Kanpur. He was awarded University of Jodhpur merit scholarship during August '68-August 70. He has held Junior Research Fellowship, India (September 1970 to October 1972) and Department of Atomic Energy (DAE), Government of India, Senior Research Fellowship (A) (October 1972 - January 1975). Presently, he is working as a Senior Research Fellow (B), DAE, in the Department of Physics, Indian Institute of Technology, Kanpur.

PUBLICATIONS

1. Hyperfine Fields Measurements on Sc in Fe and Re in Ni:
   D. K. Gupta, A. K. Singhvi, D. N. Sanwal and G.N. Rao,
   Phys. Rev. 7B, 2942 (1973).

2. Hyperfine Field Measurements on Dilute Scandium in Cobalt Matrix:
   A. K. Singhvi and G. N. Rao,
   Phys. Lett. 47A, 319 (1974).

3. Dilute Impurity Hyperfine Fields in Ferromagnetic Fe, Co and Ni Hosts:
   G. N. Rao and A. K. Singhvi,
   I.I.T. Kanpur, Technical Report, Phys. 3/74.
   (An updated version to appear in Hyperfine Interactions; Presented by G. N. Rao as an invited talk at the International meeting on Hyperfine Interaction, Leuven), September 1975.

4. Time Resolution of a Ge(Li) Detector:
   A. K. Singhvi, D. K. Gupta and G. N. Rao,
   J. Phys. 7E, 719 (1973).

5. Mossbauer Spectra of Ilmenites from Primary and Secondary Sources:
   A. K. Singhvi, D. K. Gupta, K.V.G.K. Gokhale and G. N. Rao,
   Phys. Stat. Sol. 23a, 321 (1974).

6. Decay of ^{189}W (11 min) and ^{49}Cr (42 min):
   B. V. N. Rao, A. K. Singhvi and G. N. Rao,
   Solid State and Nuclear Physics Symposium,
   Chandigarh (India), Vol. 15B, 1972 (Abstract only).

Under Preparation

Hyperfine Field Measurements on ^{181}Ta in Cobalt and Nickel Matrices.